N84-34765

A COMPARISON OF EXPERIMENTAL AND THEORETICAL RESULTS FOR LEAKAGE, PRESSURE DISTRIBUTION, AND ROTORDYNAMIC COEFFICIENTS FOR ANNULAR GAS SEALS

PROGRESS REPORT
NASA CONTRACT NAS8-33716

Prepared by
COLBY ORAN NICKS

Principal Investigator
Dara W. Childs, Ph.D, P.E.

September 1984

ABSTRACT

A Comparison of Experimental and Theoretical Results for Leakage, Pressure Distribution, and Rotordynamic Coefficients for Annular Gas Seals. (December 1984)

Colby Oran Nicks, B.S., Virginia Polytechnic Institute and State University

Chairman of Advisory Committee: Dr. Dara Childs

This thesis concerns a study of annular gas seals which is currently in progress at Texas A&M University. A brief discussion of the importance of seal behavior in rotordynamics is presented, as is a review of current annular seal theory. An outline of Nelson's analytical-computational method for determining rotordynamic coefficients for this type of compressible-flow seal is included. Various means for the experimental identification of the dynamic coefficients are outlined, and the method employed at the TAMU test facility is explained. The TAMU test apparatus is described, and the test procedures are discussed. Experimental results, including leakage, entrance-loss coefficients, pressure distributions, and rotordynamic coefficients for a smooth and a honeycomb constant-clearance seal are presented and compared to theoretical results from Nelson's analysis. The results for both seals show little sensitivity to the running speed over the test range. Agreement between test results and theory for leakage through the seal is satisfactory. Test results for direct stiffness show a greater sensitivity to fluid prerotation than predicted. Test results show that the deliberately-roughened surface of the honeycomb seal provides improved stability versus the smooth seal.

Preceding Page Blank

DEDICATION

This thesis is dedicated to my wife Robin. Her love, support, and sacrifices have made it all possible.

ACKNOWLEDGEMENTS

It is appropriate to acknowledge the contributions that my co-workers have made to this project. Thanks go to Keith Hale and Dean Nunez for their dedication to making the apparatus and facility operate as smoothly as it has. Also, my gratitude goes out to Joe Scharrer and David Moyer for their assistance in the computational aspects of the program. I would also like to express my appreciation to David Elrod for his help in reducing the data to a manageable form, and to Ann Owens for her assistance with the written thesis work. Dr. Clay Nelson should not be overlooked for the contribution of his analytical model. Finally, thanks go to my advisor, Dr. Dara Childs, for his patience and guidance on this project.

TABLE OF CONTENTS

CHAPTER		Page
I	INTRODUCTION	1
II	ANNULAR SEAL ANALYSIS REVIEW	4
III	NELSON'S ANALYSIS	8
IV	TEST CONCEPTS	13
V	TEST APPARATUS OVERVIEW	22
VI	TEST HARDWARE	23
	Static Displacement Control	23
	Dynamic Displacement Control	26
	Pressure Ratio	28
	Inlet Circumferential Velocity Control	28
	Seal Configuration	30
	Rotational Speed	30
VII	INSTRUMENTATION	38
	Rotor Motion Measurements	38
	Reaction-Force Measurements	38
	Fluid Flow Measurements	39
VIII	DATA ACQUISITION AND REDUCTION	42
IX	TEST PROCEDURES	47
X	RESULTS	49
	Static Results	53
	Dynamic Results	65
	Dynamic Results-Smooth Seal	73
	Dynamic Results-Honeycomb Seal	76
XI	CONCLUSIONS	86
XII	REFERENCES	88
XIII	VITA	90

LIST OF TABLES

Page

Table 1. Test seal specifications. 50

Table 2. Friction-factor data. 52

Table 3. Theory versus experiment leakage comparison. . . . 56

LIST OF FIGURES

		Page
Fig. 1	Small motion of a seal rotor about an eccentric position.	5
Fig. 2	Small motion of a seal rotor about a centered position.	5
Fig. 3	Empirical entrance-loss relationship used in Nelson's analysis.	10
Fig. 4	Static displacement method used for stiffness determination.	14
Fig. 5	Synchronous rotation and precession method used for equivalent coefficient identification.	15
Fig. 6	Independent rotation and precession method used for coefficient identification.	17
Fig. 7	External shaker method used for coefficient identification.	19
Fig. 8	Components used for static and dynamic displacement of seal rotor.	24
Fig. 9	Test apparatus.	25
Fig. 10	Shaking motion used for rotordynamic coefficient identification.	27
Fig. 11	Inlet guide vane detail.	29
Fig. 12	Cross-sectional view of test section showing smooth stator.	31
Fig. 13	Detail of smooth stator.	32
Fig. 14	Cross-sectional view of test section showing honeycomb stator.	33
Fig. 15	Detail of honeycomb stator.	34
Fig. 16	Test apparatus assembly.	36
Fig. 17	Exploded view of test apparatus.	37
Fig. 18	Signal conditioning schematic for data acquisition.	43
Fig. 19	Honeycomb stator insert detail.	51

Page

Fig. 20 Smooth seal leakage. 54

Fig. 21 Honeycomb seal leakage. 55

Fig. 22 Axial pressure gradient in smooth seal with no prerotation, unchoked flow, ten running speeds. . . . 57

Fig. 23 Axial pressure gradient in smooth seal with prerotation in the direction of rotor rotation. . . . 59

Fig. 24 Axial pressure gradient in smooth seal with no prerotation. 60

Fig. 25 Axial pressure gradient in smooth seal with prerotation opposing rotor rotation. 61

Fig. 26 Axial pressure gradient in honeycomb seal with prerotation in the direction of rotor rotation. . . . 62

Fig. 27 Axial pressure gradient in honeycomb seal with no prerotation. 63

Fig. 28 Axial pressure gradient in honeycomb seal with prerotation opposing rotor rotation. 64

Fig. 29 Entrance-loss for smooth seal, prerotation in direction of rotor rotation. 66

Fig. 30 Entrance-loss for smooth seal, no prerotation. . . . 67

Fig. 31 Entrance-loss for smooth seal, prerotation opposing rotation. 68

Fig. 32 Entrance-loss for honeycomb seal, prerotation in direction of rotor rotation. 69

Fig. 33 Entrance-loss for honeycomb seal, no prerotation. . . 70

Fig. 34 Entrance-loss for honeycomb seal, prerotation opposing rotor rotation. 71

Fig. 35 Relative transfer function of test apparatus. 72

Fig. 36 Direct stiffness of smooth seal. 74

Fig. 37 Cross-coupled stiffness of smooth seal. 75

Fig. 38 Direct damping of smooth seal. 77

Fig. 39 Cross-coupled damping of smooth seal. 78

Page

Fig. 40 Direct stiffness of honeycomb seal. 79

Fig. 41 Cross-coupled stiffness of honeycomb seal. 80

Fig. 42 Direct damping of honeycomb seal. 82

Fig. 43 Cross-coupled damping of honeycomb seal. 83

Fig. 44 Whirl frequency ratio for smooth and honeycomb seals. 84

NOMENCLATURE

A,B = Fourier coefficients for rotor motion

C,c = direct and cross-coupled stiffness coefficients (FT/L)

e_o = displacement of seal rotor from centered position (L)

K,k = direct and cross-coupled stiffness coefficients (F/L)

$\bar{k}$ = entrance-loss coefficient

M,m = direct and cross-coupled added-mass coefficients (M)

m = fluid mass flow rate (M/T)

ns,ms = stator Hirs coefficients

nr,mr = rotor Hirs coefficients

p = fluid pressure (F/L^2)

R = seal radius (L)

R_a = $2\rho UC/\mu$ = nominal axial Reynolds number

U = mean fluid flow velocity (L/T)

X,Y = radial seal displacements (L)

γ = ratio of specific heats for air

ε_o = e_o / C_r = equilibrium eccentricity ratio

ρ = fluid density (M/L^3)

λ = Fanning friction-factor

τ = fluid shear stress (F/L^2)

ω = shaft angular velocity (1/T)

Ω = shaft precessional velocity (1/T)

μ = fluid viscosity (FT/L^2)

INTRODUCTION

With turbomachinery design trends tending toward increased speeds and loadings, lighter weight, and reduced clearances between rotating and stationary parts, considerable concern with instability and synchronous response has arisen. Synchronous response refers to vibration of the turbomachine rotor assembly at a frequency coincident with the rotational speed. Characteristically, the vibration amplitude increases to a maximum at each critical speed (coincidence of the running speed with a rotor's damped natural frequency), and then decreases to a relatively steady level. Operation of turbomachines at rotational speeds above any of the critical speeds requires the rotor to traverse them during start-up and shut-down. Therefore, in order to limit the peak synchronous vibration levels, the machine designer aspires to introduce damping into the rotor system.

In contrast to synchronous vibration, "unstable" or "self-excited" motion is typically subsynchronous. This motion takes the form of whirling of the rotor shaft at a natural frequency less than the rotational speed. The exciting force for this whirling motion is a tangential force acting on the rotor due to some fluid or friction mechanism. This vibration often occurs with large amplitudes which sustain or grow as running speed increases. At best, this self-excited whirling prevents further speed increases; at worst, it results in damage to or catastrophic failure of the equipment. One of the rotordynamic force mechanisms which plays a role in self-excited rotor motion and synchronous response is that of the forces developed by

annular seals. Until recently, most investigations of annular seals in turbomachinery have been concerned with reducing the leakage of the working fluid through the seal (i.e., improving the sealing effect). However, recent experiences have shown that forces developed by these seals can have considerable influence on the stability and synchronous response of rotating machinery. Black et al. [1-3] have demonstrated the critical effects that forces developed by neck-ring and interstage seals have on the rotordynamic behavior of pumps. Also, stability difficulties with the Space Shuttle Main Engine (SSME) high-pressure fuel turbopump [4] have prompted further research into these forces developed by liquid seals.

Experiences have shown that various gas seal configurations can have similar influences on the rotordynamic behavior of turbomachinery. In the high-pressure oxygen turbopump of the SSME, for example, initial vibration problems were remedied by changing the turbine interstage seal from a stepped-labyrinth configuration to a convergent taper seal with a honeycomb stator and a smooth rotor[5]. A lack of experimental data to completely explain this and other gas seal behavior makes obvious the need for research in this area.

The purpose of this report is twofold. It describes the test facility and initial test program developed to experimentally measure the fluid forces induced by annular gas seals, and it provides a comparison of theoretically predicted and experimentally obtained data for smooth and honeycomb seals. The leakage of the working fluid through the seal, the pressure gradient along the seal length, entrance pressure-loss data, and rotordynamic coefficients provide a basis for comparison. A short discussion on seal theory is included, and various

rotordynamic coefficient identification schemes are described. The work presented herein is intended to add to the rapidly expanding database on seal forces, and to determine the validity of one theoretical analysis for predicting those forces.

ANNULAR SEAL ANALYSIS REVIEW

As related to rotordynamics, seal analysis has the objective of determining the reaction forces acting on the rotor arising from shaft motion within the seal. Due to similarities between plain journal bearings and annular seals, seal analysis is generally based on governing equations which have previously been developed for bearings.

Annular seals and plain bearings are geometrically similar, but seals typically have radial clearance-to-radius ratios on the order of 0.005, versus C_r/R ratios of 0.001 for bearings. Due to seal clearances and pressure differentials, fully-developed turbulent flow normally exists. Also, seals are nominally designed to operate in a centered position. Journal bearings, on the other hand, have operating eccentricities which vary with running speed and load. Therefore, most of the rotordynamic work for bearings has been done to determine dynamic coefficient versus eccentricity relationships.

Two linearized seal models, expressed in terms of dynamic coefficients, have been suggested for the motion/reaction-force relationship. For small motions of the rotor about an arbitrary position in the seal, as shown in Fig.1, the relation can be written

$$-\begin{Bmatrix} F_X \\ F_Y \end{Bmatrix} = \begin{bmatrix} K_{XX}(\varepsilon_o) & K_{XY}(\varepsilon_o) \\ K_{YX}(\varepsilon_o) & K_{YY}(\varepsilon_o) \end{bmatrix} \begin{Bmatrix} X \\ Y \end{Bmatrix} + \begin{bmatrix} C_{XX}(\varepsilon_o) & C_{XY}(\varepsilon_o) \\ C_{YX}(\varepsilon_o) & C_{YY}(\varepsilon_o) \end{bmatrix} \begin{Bmatrix} \dot{X} \\ \dot{Y} \end{Bmatrix} + \begin{bmatrix} M_{XX}(\varepsilon_o) & M_{XY}(\varepsilon_o) \\ M_{YX}(\varepsilon_o) & M_{YY}(\varepsilon_o) \end{bmatrix} \begin{Bmatrix} \ddot{X} \\ \ddot{Y} \end{Bmatrix} \quad (1)$$

where the dynamic coefficients {KXX, KYY, CXX, CYY, MXX, MYY} and {KXY, KYX, CXY, CYX, MXY, MYX} represent the "direct" and "cross-coupled" stiffness, damping, and added-mass terms, respectively. These

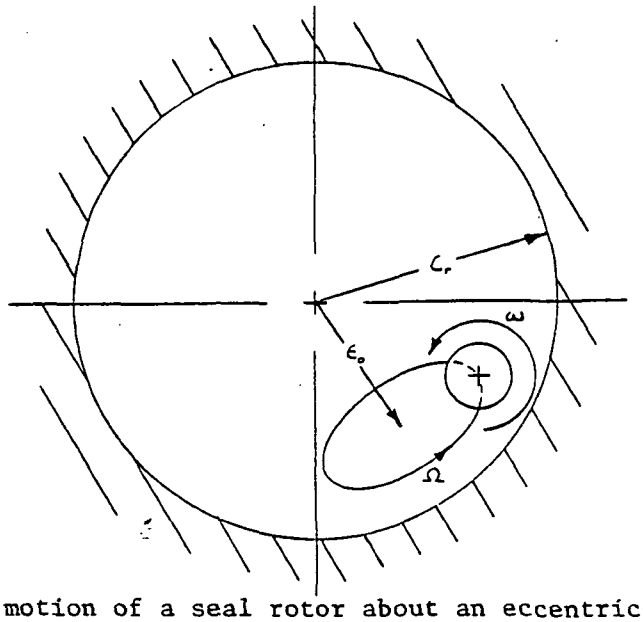

Fig. 1 Small motion of a seal rotor about an eccentric position; ω is the rotor spin speed, Ω is the precessional orbit frequency.

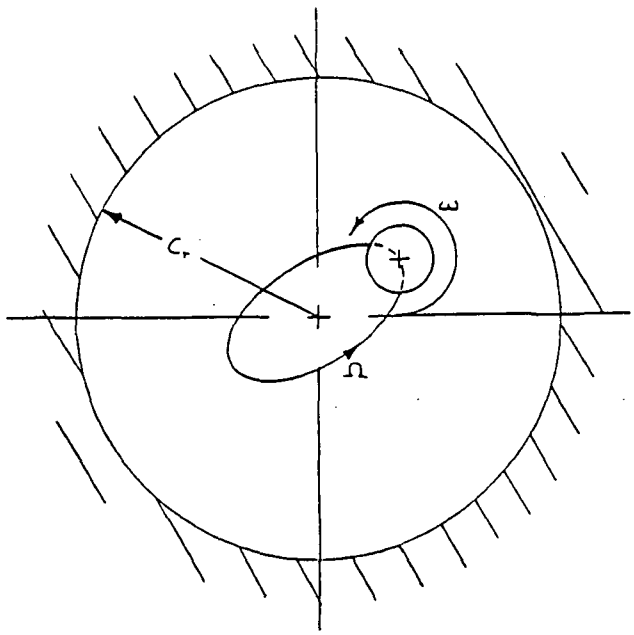

Fig. 2 Small motion of a seal rotor about a centered position; ω is the rotor spin speed, Ω is the precessional orbit frequency.

coefficients are functions of the equilibrium eccentricity ratio $\varepsilon_o = e_o / C_r$, where the eccentricity ratio ε_o equals the displacement (e_o) of the rotor from the centered position divided by the nominal radial clearance (C_r). The term "cross-coupled" refers to the coupling effect exhibited by the off-diagonal terms; specifically, motion in one plane introduces reaction forces in an orthogonal one. These cross-coupled terms arise from the fluid's circumferential velocity component, and show a strong dependency on both the magnitude and direction (with respect to rotor rotation) of the velocity. This circumferential velocity component may arise from the prerotation of the fluid as it enters the seal due to some rotating element upstream, or it may develop as the fluid passes through the seal, with rotor shear forces "dragging" the viscous fluid around its periphery. The cross-coupled stiffness term usually produces a destabilizing force component, and therefore is of considerable interest. The cross-coupled damping and added-mass terms are generally much less influential than the cross-coupled stiffness term with respect to stability. For no fluid rotation, these cross-coupled terms are zero.

The second linearized seal model applies for small motions of the rotor about a centered position in the seal, as shown in Fig. 2 . This model can be expressed

$$-\begin{Bmatrix} F_X \\ F_Y \end{Bmatrix} = \begin{bmatrix} K & k \\ -k & K \end{bmatrix} \begin{Bmatrix} X \\ Y \end{Bmatrix} + \begin{bmatrix} C & c \\ -c & C \end{bmatrix} \begin{Bmatrix} \dot{X} \\ \dot{Y} \end{Bmatrix} + \begin{bmatrix} M & m \\ -m & M \end{bmatrix} \begin{Bmatrix} \ddot{X} \\ \ddot{Y} \end{Bmatrix} \quad (2)$$

where the dynamic coefficient matrices are skew-symmetric.

Theoretical work on annular seals has been done for both incompressible and compressible fluids. Black et al. [6] have developed

analytical "short-seal" solutions for incompressible seals, which account for circumferential fluid flow due to wall shear stresses but not pressure perturbations. The analysis employs a bulk-flow assumption and accounts for fluid prerotation as is enters the seal. Childs' [7] incompressible seal analysis provides "finite-length " solutions, in which both shear and pressure-induced flow are included. Childs' utilizes Hirs' [8] turbulent bulk-flow model, and accounts for inlet swirl as well as perturbations in axial and circumferential Reynolds numbers due to clearance perturbations.

Compressible flow in seals has been analyzed by Fleming [9, 10] and Nelson[11, 12]. Fleming presents a short seal solution for the leakage, direct stiffness, and direct damping coefficients for straight and tapered, smooth, annular gas seals, but does not include the cross-coupled damping terms. Nelson, whose analysis is used for comparison in this report, analyzes both smooth and surface-roughened annular seals in the straight and tapered configurations. An outline of Nelson's analysis is included in the section that follows.

NELSON'S ANALYSIS

Nelson [11, 12] has developed an analysis which provides both static and dynamic results for annular gas seals. The static results include fluid leakage through the seal, pressure gradient along the seal axis, and the fluid axial and circumferential velocities through the seal. Dynamic data provided by the analysis consists of the rotordynamic coefficients (direct and cross-coupled stiffness and damping terms) for small rotor motion about a centered position (equation(2)). Nelson assumes that the added-mass terms are negligible for gas seals, and, hence, equation(2) is written

$$-\begin{Bmatrix} F_X \\ F_Y \end{Bmatrix} = \begin{bmatrix} K & k \\ -k & K \end{bmatrix} \begin{Bmatrix} X \\ Y \end{Bmatrix} + \begin{bmatrix} C & c \\ -c & C \end{bmatrix} \begin{Bmatrix} \dot{X} \\ \dot{Y} \end{Bmatrix} \tag{3}$$

Nelson utilizes a modified Hirs' [8] turbulent bulk-flow fluid model to develop governing axial and circumferential momentum equations, and his model is completed by the continuity and energy equations. Hirs' model defines the wall shear stress τ_w as

$$\tau_w = 1/2\ \rho U_m^2\ no(2\rho U_m H\ /\ \mu)^{mo} = 1/2\ \rho U_m^2\ noR_a^{mo} \tag{4}$$

where U_m is the mean flow velocity relative to the surface upon which the shear stress acts, and H is the local seal clearance. Hirs' formulation assumes that the surface roughness is the same on the rotor and stator. However, if the bulk-flow velocities relative to the rotor and stator are substituted in equation (4), the shear stresses at the rotor and stator are, respectively,

$$\tau_r = 1/2\ \rho U_r^2\ nr(2\rho U_r H\ /\ \mu)^{mr}$$
$$\tau_s = 1/2\ \rho U_s^2\ ns(2\rho U_s H\ /\ \mu)^{ms} \qquad (5)$$

Hence, different surface roughnesses in the seal elements can be accounted for via the empirical coefficients mr, nr and ms,ns for the rotor and stator surfaces. These coefficients may be calculated from static-pressure-gradient test data, and are then provided as input parameters for Nelson's analysis.

Assuming small motion of the rotor about a centered position, Nelson uses a perturbation analysis similar to that employed by Childs [7] to develop zeroth and first-order perturbation equations. The zeroth-order solution represents a zero-eccentricity flow condition, with rotor rotation but without precession. This solution is iterative and yields the mass-leakage flow rate, and the axial distribution of pressure, axial velocity, density, and circumferential velocity.

An iterative solution scheme is employed, using initial guesses for the zeroth-order seal entrance Mach number and entrance pressure-loss coefficient. The entrance-loss relationship is defined by

$$p_o(0) = 1\ /\ \{1 + [(\gamma-1)(\bar{k}+1)M_o^2(0)]\ /\ 2\}^{\gamma/(\gamma-1)} \qquad (6)$$

where $p_o(0)$ is the seal entrance/reservoir pressure ratio and $M_o(0)$ is the entrance Mach number. The entrance Mach number is iteratively adjusted, and the loss coefficient $\bar{k}$ is recalculated according to a curve fit by Deissler [13]

$$\bar{k} + 1 = \sqrt{5.3\ /\ \log_{10} R_a} \qquad (7)$$

which is plotted in Fig. 3. At axial Reynolds numbers above 200,000, $\bar{k}$ is equated to zero. The iterative solution procedure for $M_o(0)$ and $\bar{k}$ continues until either:

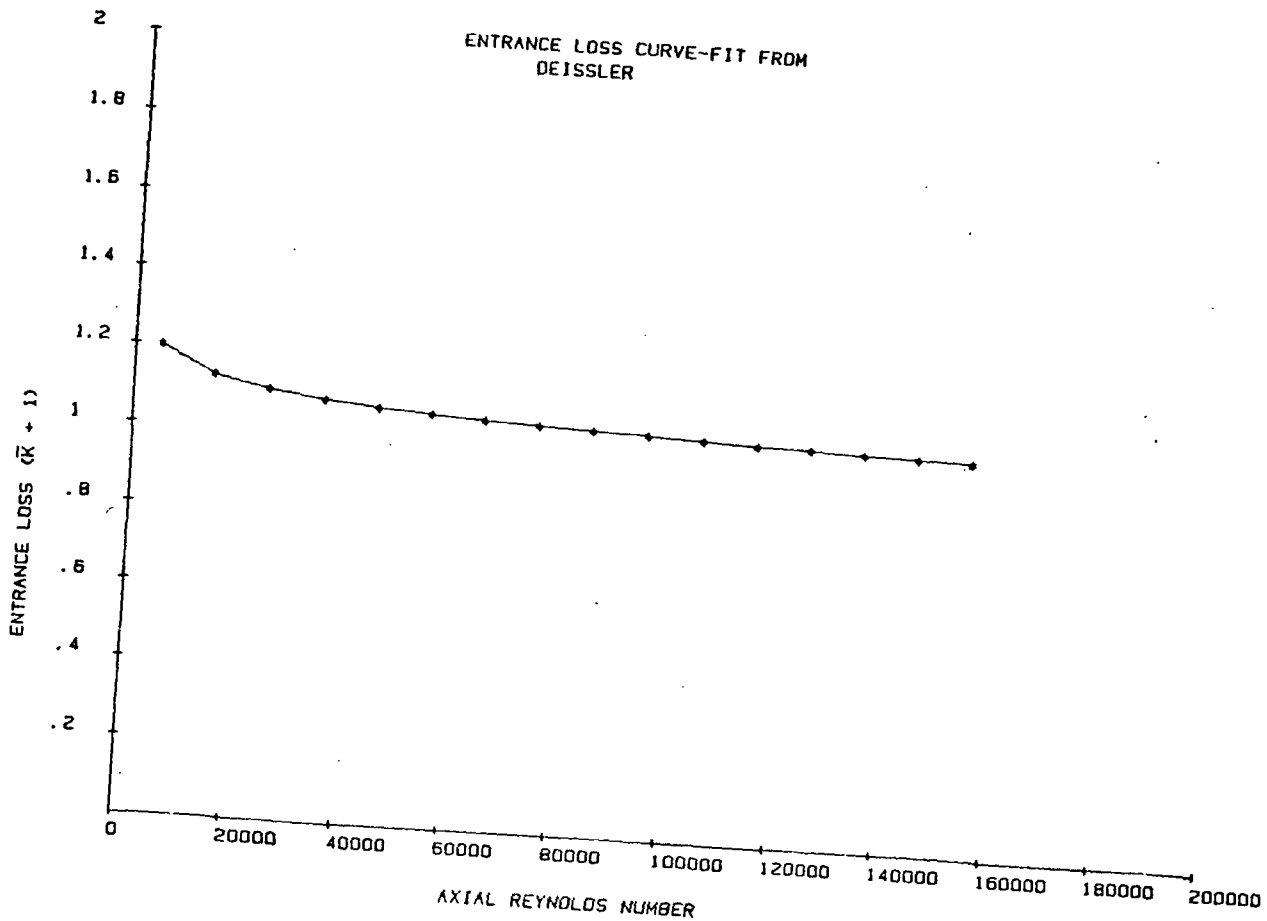

Fig. 3 Empirical entrance loss-relationship used in Nelson's analysis.

1) the Mach number at the exit reaches unity and the exit pressure is greater than the sump pressure (choked flow), or
2) the exit pressure equals the sump pressure and the exit Mach number is less than unity (unchoked flow).

The pressure, density, and velocity distribution and their derivatives which are determined in the zeroth-order solution are used in defining coefficients of the first-order perturbation equations. These equations define the pressure, density, and axial and circumferential velocity perturbations due to rotor motion, and are transformed to sixteen ordinary differential equations in the axial coordinate z. The four physical boundary conditions required for the solution of these equations depend on the perturbation conditions that are specified at the seal entrance and exit. The inlet circumferential velocity perturbation is zero. Expansion of the entrance pressure-loss relationship of equation (6) yields a second boundary condition. For choked flow, the first-order perturbation in the exit Mach number is zero, while for unchoked flow, the first-order perturbation in the exit pressure is zero.

Application of these boundary conditions and numerical integration of the ordinary differential equations provides the first-order solution. Integration of the first-order pressure solution along and around the seal periphery yields the direct and cross-coupled stiffness and damping coefficients, K, k, C, and c, respectively.

The input parameters which can be varied in Nelson's analysis include:

1) reservoir pressure and temperature,
2) sump pressure,

3) seal geometry (i.e. radius, length, clearances),

4) rotor rotational speed and precession rate,

5) entrance circumferential velocity of fluid,

6) rotor and stator surface roughness (Hirs constants),

7) empirical entrance-loss relationship, e.g., Deissler's, equation (16), and

8) fluid viscosity, gas constant, and ratio of specific heats.

It is apparent that a large amount of theoretical data can be generated to determine the influence that these various parameters have on the fluid forces in annular gas seals. However, there is a lack of experimental data with which to compare the results of Nelson's analysis. Currently, test results due to Wachter and Benckert [14] exist for labyrinth seals, a special class of non-contacting seals which have stepped surfaces or "teeth" on the rotor, stator, or both. Experimental results for smooth and/or surface-roughened gas seals are limited to data for honeycomb seals also published by Wachter and Benckert. Hence, the need for a test apparatus which can be used to study the effects of the same variables provided for in Nelson's analysis is obvious. The experimental data generated by such an apparatus would be valuable for comparison to both Nelson's theories and others which may be developed in the future.

TEST CONCEPTS

A number of test programs have been implemented to measure the stabilizing and destabilizing fluid forces which are developed by turbomachinery elements. Some are concerned mainly with the study of seal forces, while others examine the forces developed by centrifugal pump impellers. In each case, reaction force and relative motion measurements are used for rotordynamic coefficient identification. Four general approaches have been employed, and will be reviewed here.

Wachter and Benckert [14] employ a static displacement method for determining stiffness coefficients. In this method, as shown in Fig. 4, the rotor is displaced statically to some measured eccentric position while a pressure differential forces the working fluid past the seal. By measuring the reaction force components which are parallel and perpendicular to the static displacement vector, the direct and cross-coupled stiffnesses can be determined. Referring to equation (2) for small rotor motion about a centered position, a static rotor displacement in the X-direction yields

$$K = -F_X/e_o \ , \ k = F_Y/e_o \tag{8}$$

Since this static displacement method has no dynamic motion, no damping or added-mass terms can be evaluated.

A second approach to rotordynamic coefficient identification is utilized by Childs[15]. Depicted in Fig.5, this method uses a circular orbit of the rotor within the seal. The rotor is mounted eccentrically on a shaft which rotates. Thus, the rotor precesses in a circular orbit at the same rate and direction as shaft rotation. This synchronous precession provides for the determination of the radial and tangential

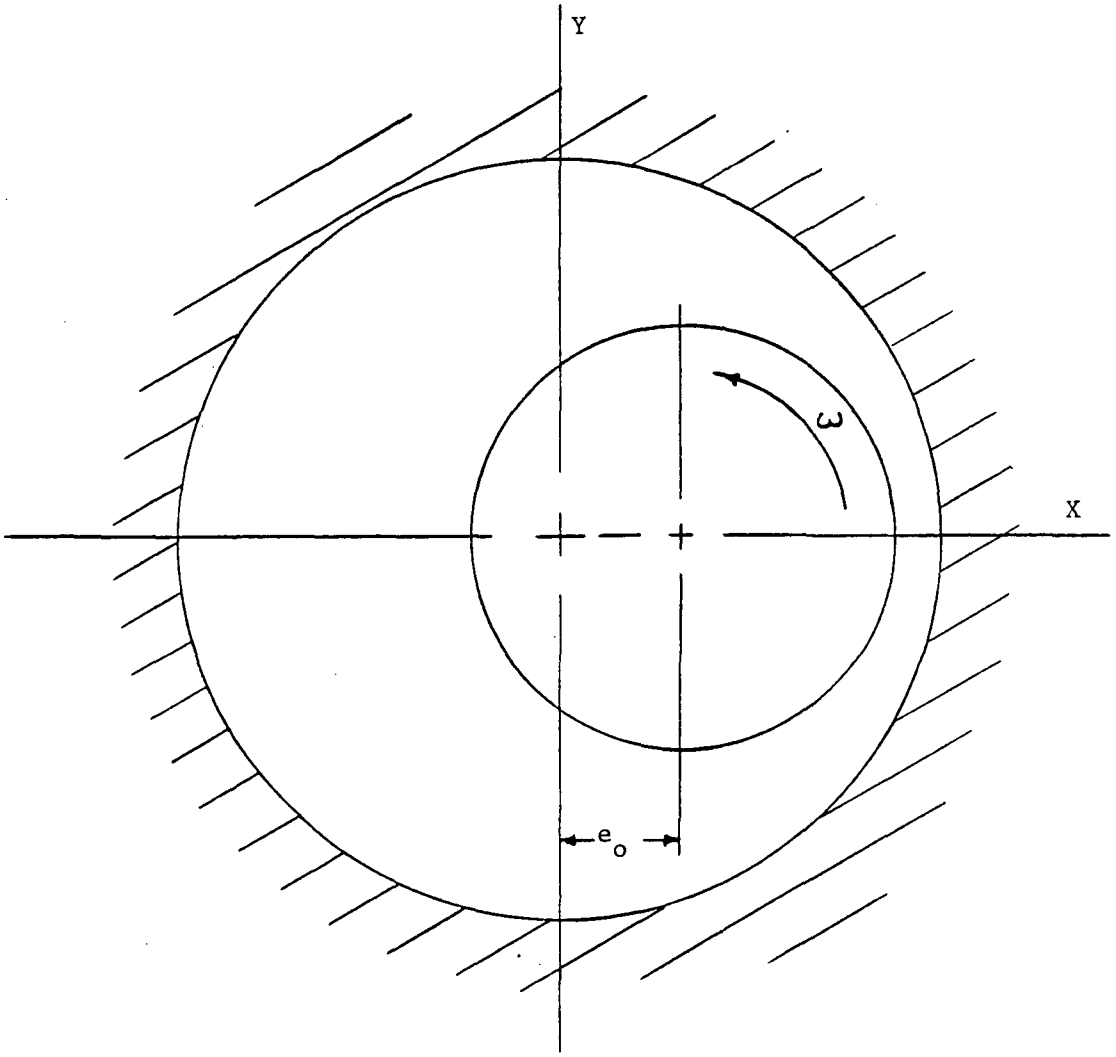

Fig. 4 Static displacement method used for stiffness determination.

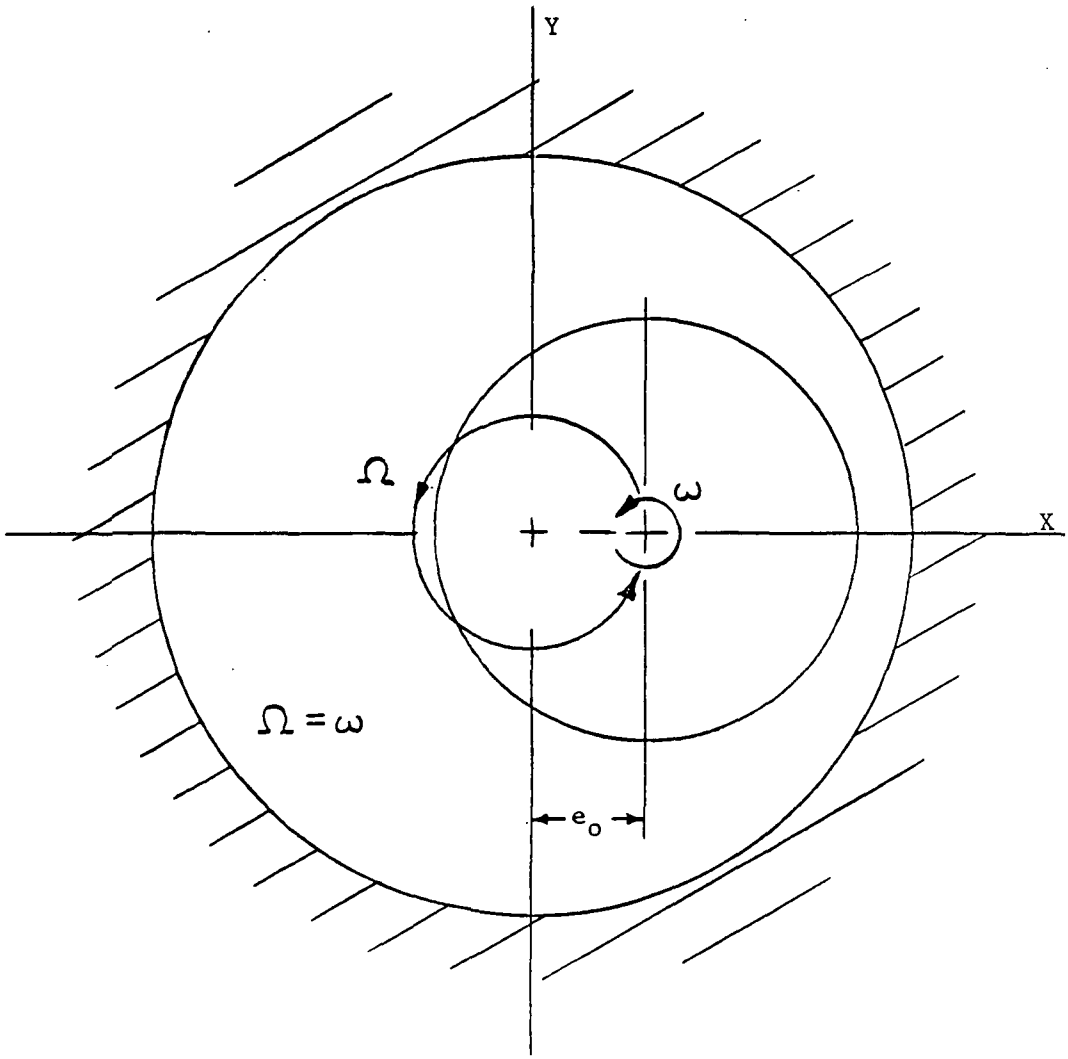

Fig. 5 Synchronous rotation and precession method used for equivalent coefficient identification.

components of the seal reaction force. The F_r and F components are obtained through integration of the measured pressure distribution along and around the seal periphery. Expressing measured rotor motion as

$$X = e_o \cos(\omega t)$$
$$Y = e_o \sin(\omega t) \tag{9}$$

for small circular orbit of radius e_o and precessional frequency $\omega=\Omega$, and substituting into equation (2) yields the radial and tangential force coefficcient definitions

$$F_r / e_o = M\omega^2 - c\omega - K = -K_{ef} + M_{ef}.\omega^2$$
$$F / e_o = k - C\omega = -C_{ef}.\omega \tag{10}$$

where the cross-coupled mass coefficient is assumed negligible with respect to the influence of k and C. Because the cross-coupled coefficients k and c are linear functions of ω, identification of the individual dynamic coefficients is not possible in this method. However, equivalent direct stiffness, damping, and added-mass coefficients can be calculated as indicated in equation (10).

Independent rotation and precession control, as shown in Fig. 6, is a third testing method which is currently employed both in impeller and seal studies [16], [17], [18]. Various means are used to produce a circular orbit (precession) of the rotor or impeller at a rate different from its rotational speed. For a small circular orbit of radius e_o and precessional frequency Ω , the measured precessional motion of the rotor is

$$X = e_o \cos(\Omega t)$$
$$Y = e_o \sin(\Omega t)$$

The F_X and F_Y reaction force components are measured and can be

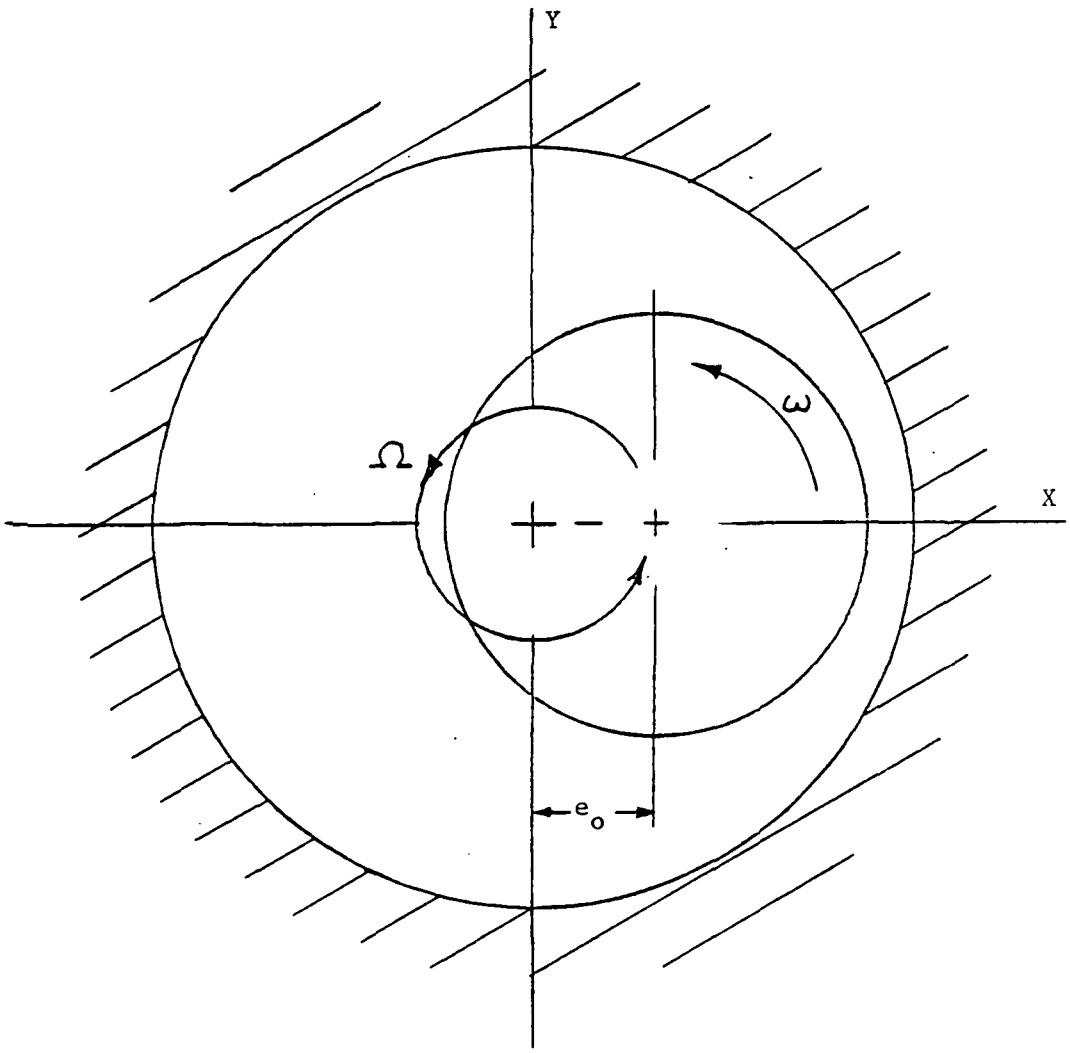

Fig. 6 Independent rotation and precession method used for coefficient identification.

expressed

$$F_X = F_{XS} \sin(\Omega t) + F_{XC} \cos(\Omega t)$$
$$F_Y = F_{YS} \sin(\Omega t) + F_{YC} \cos(\Omega t) \tag{11}$$

By substituting these expressions into equation (2) and equating coefficients of sine and cosine terms, the following equations are obtained

$$- F_{XC} / e_o = K + c\Omega - M\Omega^2 \qquad - F_{YC} / e_o = -k + C\Omega + m\Omega^2$$
$$- F_{XS} / e_o = k - C\Omega - m\Omega^2 \qquad - F_{YS} / e_o = K + c\Omega + M\Omega^2 \tag{12}$$

Hence, by measuring the reaction force components and rotor motion at two different precession frequencies, eight equations in six unknowns are obtained, and the rotordynamic coefficients can be calculated.

A fourth testing method has been used by Iino and Kaneko [19] for determining dynamic coefficients, and this same method is employed at the TAMU gas seal test facility. An external hydraulic shaker is used to impart translatory harmonic motion to the rotating seal, and rotor motion relative to the stator and the reaction force components acting on the stator are measured.

Fig. 7 shows the manner in which the rotor could be positioned and oscillated in order to identify the dynamic coefficients of the seal for small motion about e_o. If the added-mass terms are assumed negligible, equation (1) is rewritten

$$- \begin{Bmatrix} F_X \\ F_Y \end{Bmatrix} = \begin{bmatrix} K_{XX}(\varepsilon_o) & K_{XY}(\varepsilon_o) \\ K_{YX}(\varepsilon_o) & K_{YY}(\varepsilon_o) \end{bmatrix} \begin{Bmatrix} X \\ Y \end{Bmatrix} + \begin{bmatrix} C_{XX}(\varepsilon_o) & C_{XY}(\varepsilon_o) \\ C_{YX}(\varepsilon_o) & C_{YY}(\varepsilon_o) \end{bmatrix} \begin{Bmatrix} \dot{X} \\ \dot{Y} \end{Bmatrix} \tag{13}$$

First, harmonic horizontal motion of the rotor is assumed, where

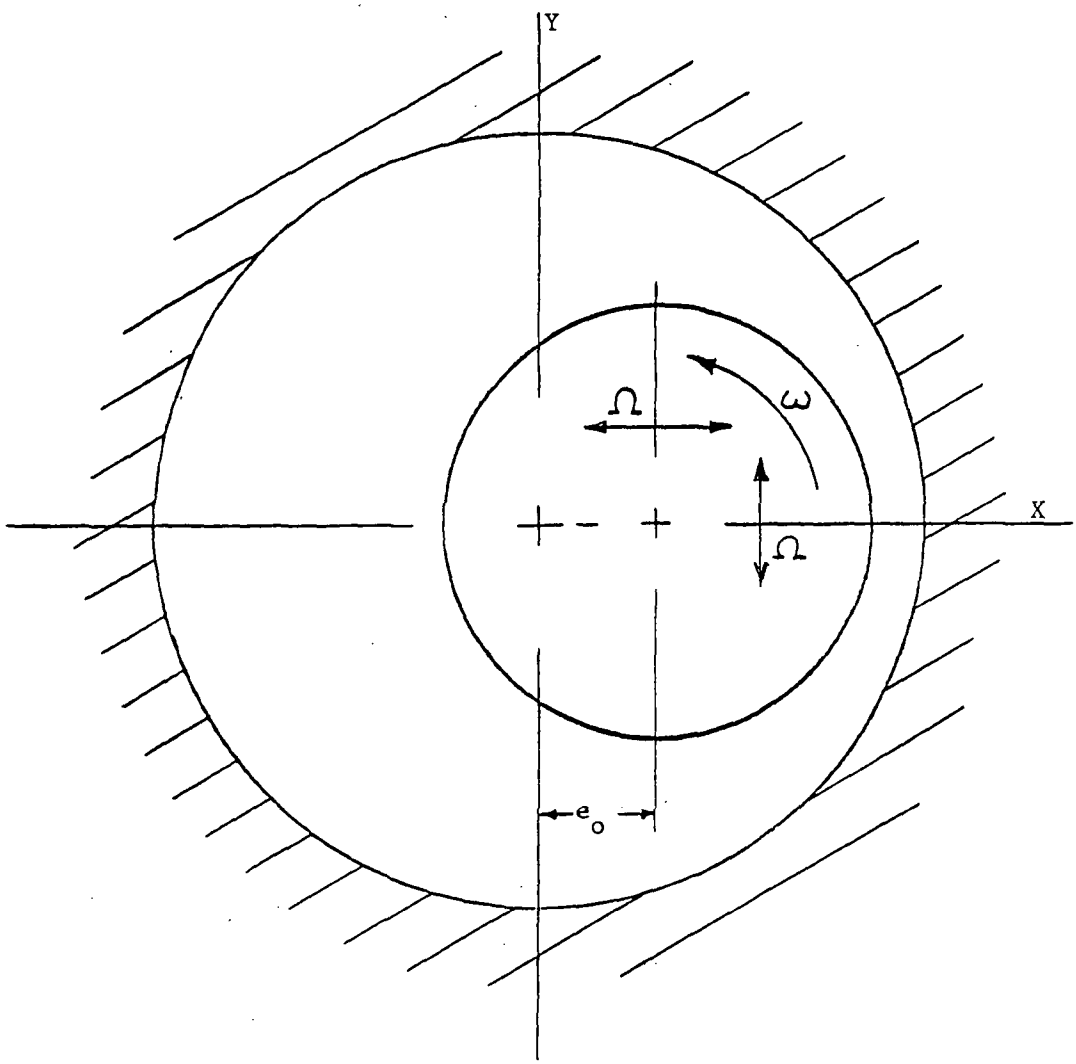

Fig. 7 External shaker method used for coefficient identification.

$$X = e_o + A \sin(\Omega t) + B \cos(\Omega t)$$

$$\dot{X} = A\Omega \cos(\Omega t) - B\Omega \sin(\Omega t)$$

$$Y = \dot{Y} = 0$$

This yields small motion parallel to the static eccentricity vector, where Ω is the shaking frequency. In a similar fashion, the X and Y-direction force components can be expressed

$$\begin{aligned} F_X &= F_{XS} \sin(\Omega t) + F_{XC} \cos(\Omega t) \\ F_Y &= F_{YS} \sin(\Omega t) + F_{YC} \cos(\Omega t) \end{aligned} \tag{14}$$

Substituting these expressions into equation (13) and equating coefficients of sine and cosine terms yields the following four equations

$$\begin{aligned} F_{XS} &= K_{XX} A - C_{XX} B \\ F_{XC} &= K_{XX} B + C_{XX} A \\ F_{YS} &= K_{YX} A - C_{YX} B \\ F_{YC} &= K_{YX} B + C_{YX} A \end{aligned} \tag{15}$$

Solving this system of four equations in four unknowns defines the dynamic coefficients as

$$\begin{aligned} K_{XX}(\varepsilon_o) &= (F_{XC} B + F_{XS} A) / (A^2 + B^2) \\ K_{YX}(\varepsilon_o) &= (F_{YS} A + F_{YC} B) / (A^2 + B^2) \\ C_{XX}(\varepsilon_o) &= (F_{XC} A - F_{XS} B) / \Omega(A^2 + B^2) \\ C_{YX}(\varepsilon_o) &= (F_{YC} A - F_{YS} B) / \Omega(A^2 + B^2) \end{aligned} \tag{16}$$

Therefore, by measuring the reaction forces due to known rotor motion, determining the Fourier coefficients (A, B, F_{XS}, F_{XC}, F_{YS}, F_{YC}), and substituting into the above definitions, the indicated dynamic coefficients can be identified. If the rotor is shaken about a centered position, then the process is complete. Since the linearized model has skew-symmetric stiffness and damping matrices, all of the coefficients

are identified. If, however, the rotor is shaken about an eccentric position as initially postulated, then it must be shaken vertically about that same point in order to complete the identification process.

Assuming harmonic vertical motion of the rotor, as defined by

$$X = e_o, \dot{X} = 0,$$

$$Y = A \sin(\Omega t) + B \cos(\Omega t), \text{ and}$$

$$\dot{Y} = A\Omega \cos(\Omega t) - B\Omega \sin(\Omega t),$$

yields oscillatory motion that is perpendicular to the assumed static eccentricity vector. A similar process as before results in the coefficient definitions

$$\begin{aligned} K_{YY}(\varepsilon_o) &= (F_{XS} A + F_{XC} B) / (A^2 + B^2) \\ K_{XY}(\varepsilon_o) &= -(F_{YC} B + F_{YS} A) / (A^2 + B^2) \\ C_{YY}(\varepsilon_o) &= (F_{XC} A - F_{XS} B) / \Omega(A^2 + B^2) \\ C_{XY}(\varepsilon_o) &= (F_{YS} B - F_{YC} A) / \Omega(A^2 + B^2) \end{aligned} \tag{17}$$

All eight dynamic coefficients are thus determined by alternately shaking the rotor at one frequency Ω in directions which are parallel and perpendicular to the static eccentricity vector.

TEST APPARATUS OVERVIEW

Detailed design of the TAMU gas seal apparatus was carried out by J.B. Dressman of the University of Louisville. It is of the external shaker configuration, and the dynamic coefficient identification process is as described in the latter part of the preceding section.

Considering both the coefficient identification process and Nelson's analysis, some objectives for the design of the test apparatus are apparent. First, in order to determine the dynamic coefficients, the apparatus must provide for the necessary rotor motion within the seal, and measurement of the reaction-force components due to this motion must be possible. Secondly, it would be advantageous (for purposes of comparison) if the apparatus could provide the same variable seal parameters afforded by Nelson's analysis (i.e., pressures, seal geometry, rotor rotational speed, fluid prerotation, and rotor/stator surface roughness). With this capability, the influence of each independent parameter could be examined and compared for correlation between theoretical predictions and experimental results.

With these design objectives in mind, the discussion of the test apparatus is presented in three sections. The first section, Test Hardware, describes how the various seal parameters are physically executed and controlled. For example, the manner in which the dynamic "shaking" motion of the seal rotor is achieved and controlled is described in this section. The second section, Instrumentation, describes how these controlled parameters, such as rotor motion, are measured. Finally, the Data Acquisition and Reduction section explains how these measurements are used to provide the desired information.

TEST HARDWARE

This section deals only with the mechanical components and operation of the test apparatus. It is intended to provide answers to the following questions:

1) How is the static position of the seal rotor controlled?
2) How is the dynamic motion of the rotor executed and controlled?
3) How is compressed air obtained and supplied to the apparatus, and how is the pressure ratio across the seal controlled?
4) How is the incoming air prerotated before it enters the seal?
5) How are the seal rotor and stator mounted and replaced?
6) How is the seal rotor driven (rotated)?

Recalling the rotordynamic coefficient identification process described earlier, the external shaker method requires that the seal rotor be set in some static position and then be oscillated about that point. The test apparatus meets those requirements by providing independent static and dynamic displacement control, which are described below.

Static Displacement Control. The test apparatus is designed to provide control over the static eccentricity position both horizontally and vertically within the seal. The rotor shaft is suspended pendulum-fashion from an upper, rigidly mounted pivot shaft, as shown in Figs. 8 and 9. This arrangement allows a side-to-side (horizontal) motion of the rotor, and a cam within the pivot shaft allows vertical positioning of the rotor.

The cam which controls the vertical position of the rotor is driven

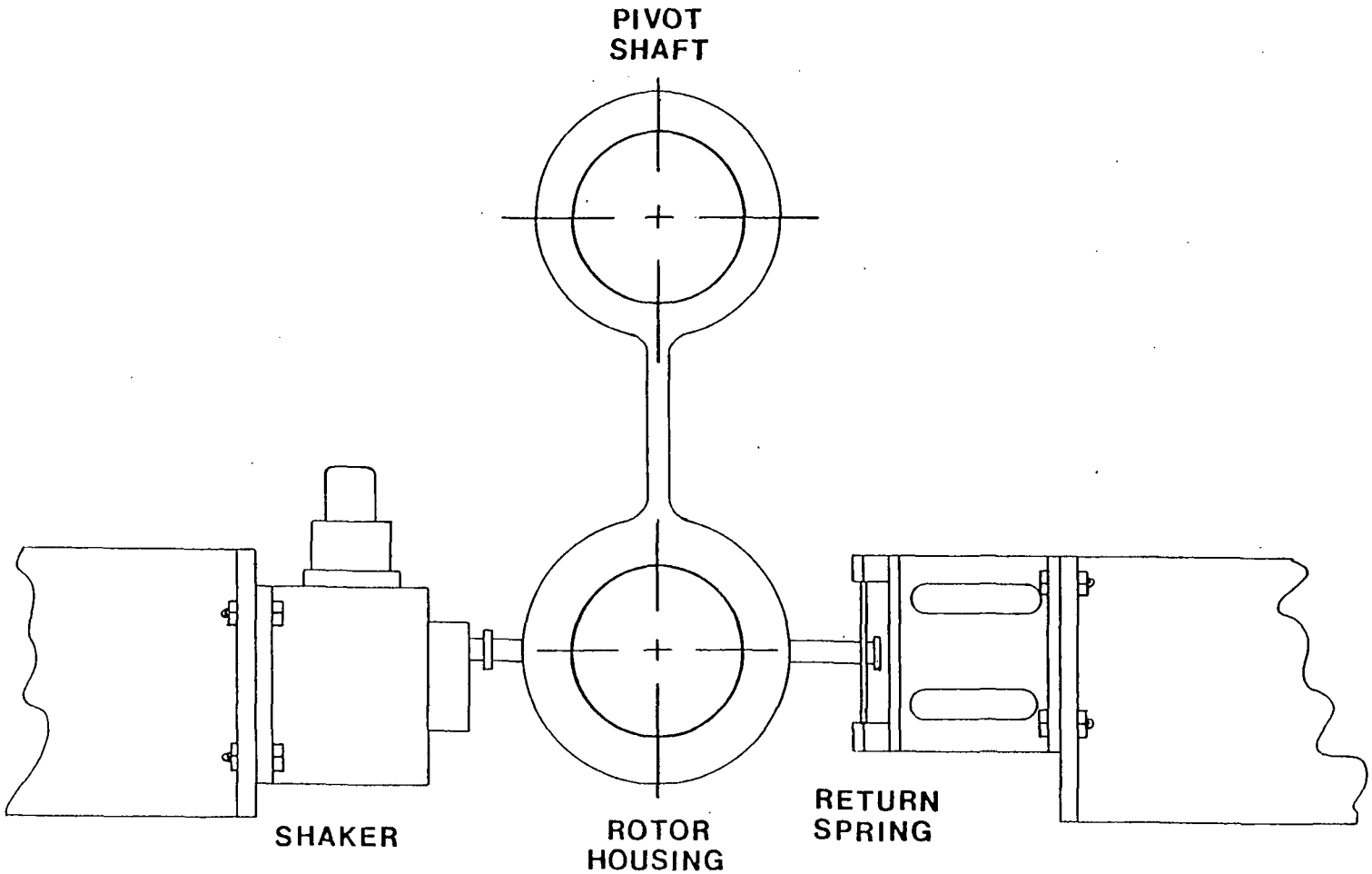

Fig. 8 Components used for static and dynamic displacement of seal rotor.

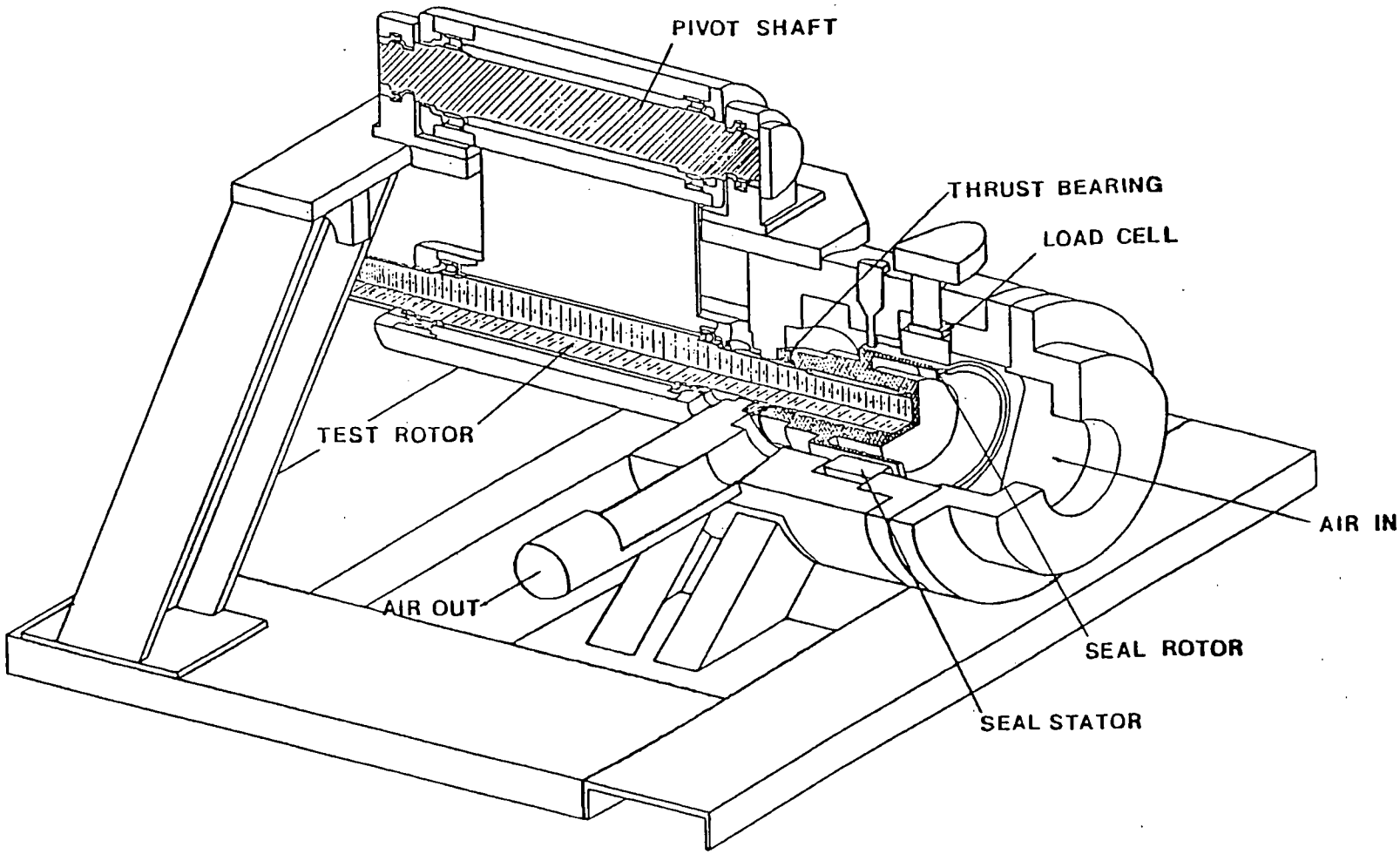

Fig. 9 Test apparatus.

by a remotely-operated DC gearhead motor, allowing accurate positioning of the rotor during testing. Horizontal positioning of the rotor is accomplished by a Zonic hydraulic shaker head and master controller, which provide independent static and dynamic displacement or force control. The shaker head is mounted on an I-beam support structure, and can supply up to 4450 N (1000 lbf) static and 4450 N dynamic force. As illustrated in Fig. 8, the shaker head output shaft acts on the rotor shaft bearing housing, and works against a return spring mounted on the opposite side of the bearing housing. The return spring maintains contact between the shaker head shaft and the bearing housing, thereby preventing hammering of the shaker shaft and the resulting loss of control over the horizontal motion of the rotor.

Dynamic Displacement Control. The dynamic motion of the seal rotor within the stator is horizontal. In addition to controlling the static horizontal position of the rotor, the Zonic shaker head moves the rotor through horizontal harmonic oscillations as the test is run. A Wavetek function generator provides the sinusoidal input signal to the Zonic controller, and both the amplitude and frequency of the rotor oscillations are controlled.

Although the test rig design provides for dynamic motion of the rotor only in the horizontal X-direction, all of the coefficients for either seal model (equation (3) or (13)) can still be determined. As Fig. 10 shows, the required rotor motion perpendicular to the static eccentricity vector can be accomplished in an equivalent manner by statically displacing it the same amount (e_o) in the vertical direction and continuing to shake horizontally.

In addition to providing control over the rotor's static position

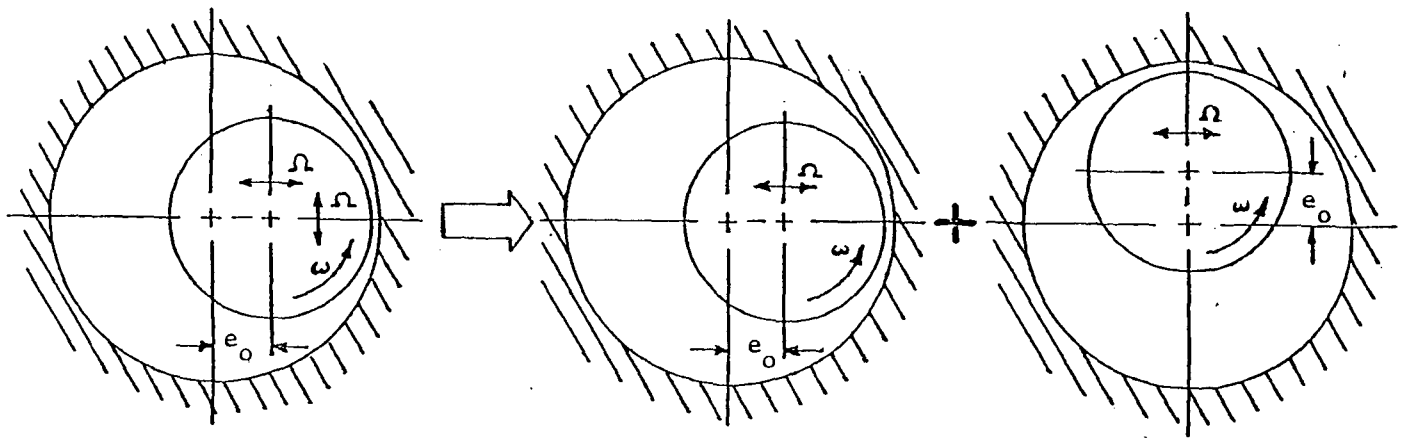

Fig. 10 Shaking motion used for rotordynamic coefficient identification.

and dynamic motion, the test apparatus allows other seal parameters to be controlled independently, providing insight into the influence these parameters have on seal behavior. These parameters coincide with the variable input parameters for Nelson's analysis, and they include:

1) pressure ratio across the seal,
2) prerotation of the incoming fluid,
3) seal configuration, and
4) rotor rotational speed.

Pressure Ratio. The inlet air pressure and attendant mass flow rate through the seal are controlled by an electric-over-pneumatically actuated Masoneilan Camflex II flow control valve located upstream of the test section. An Ingersoll-Rand SSR-2000 single stage screw compressor rated at 34 m^3/min @ 929 kPa (1200 scfm @ 120 psig) provides compressed air, which is then filtered and dried before entering a surge tank. Losses through the dryers, filters, and piping result in an actual maximum inlet pressure to the test section of approximately 722 kPa (90 psig) and a maximum flow rate of 27 m^3/min (950 scfm). A four-inch inlet pipe from the surge tank supplies the test rig, and after passing through the seal, the air exhausts to atmosphere through a manifold with muffler.

Inlet Circumferential Velocity Control. In order to determine the effects of fluid rotation on the rotordynamic coefficients, the test rig design also allows for prerotation of the incoming air as it enters the seal. This prerotation introduces a circumferential component to the air flow direction, and is accomplished by guide vanes which direct and accelerate the flow towards the annulus of the seal. The vanes are machined from brass disks, and Fig. 11 illustrates the vane

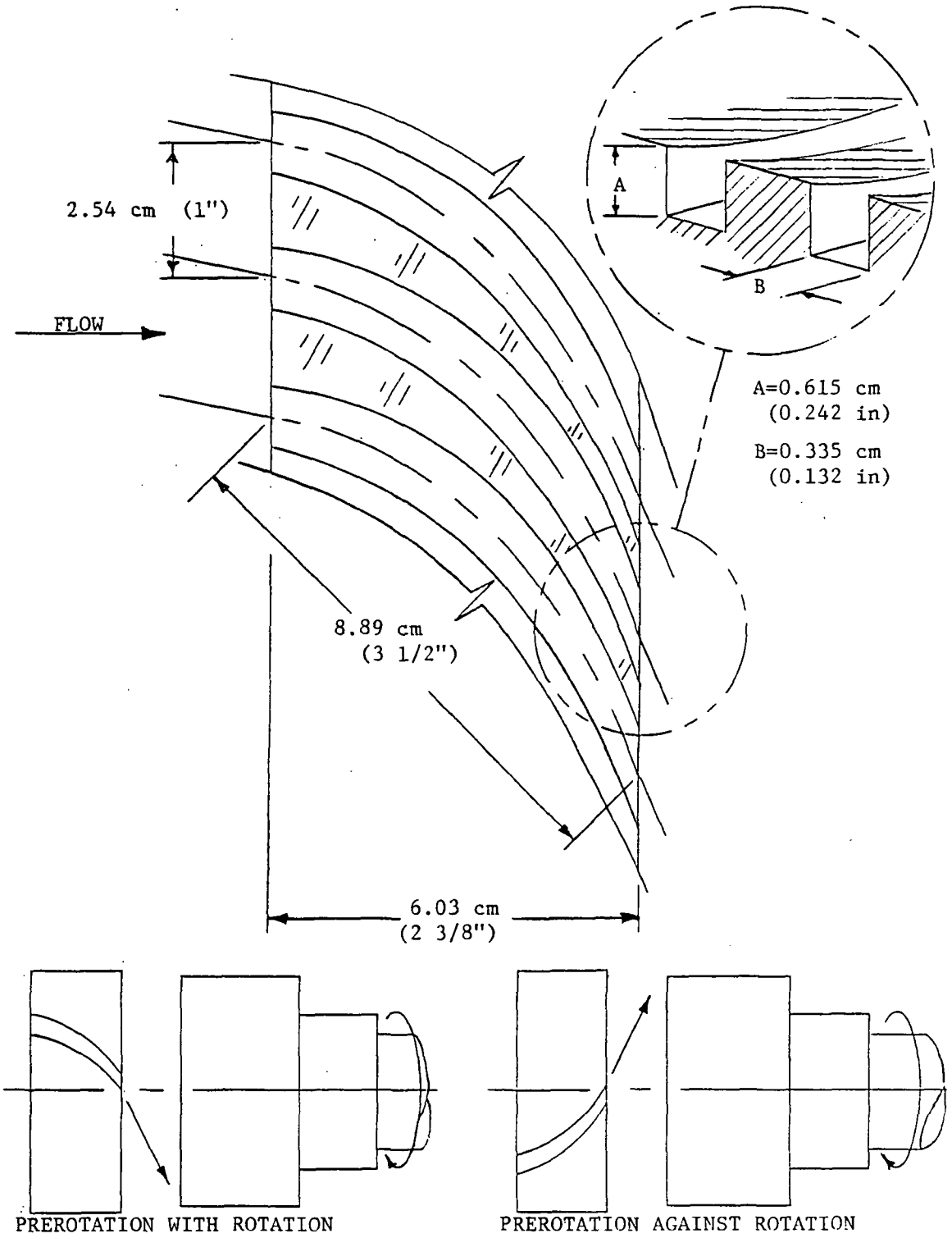

Fig. 11 Inlet guide vane detail.

configuration. Three sets of guide vanes are available; one rotates the flow in the direction of rotor rotation, another introduces no fluid rotation, and the third rotates the flow opposite the direction of rotor rotation.

Seal Configuration. The design of the test rig permits the installation of various rotor/stator combinations. As shown in Figs.12-15, the stator is supported in the test section housing by three Kistler quartz load cells in a trihedral configuration. Figs.12 and 13 show the smooth-rotor/smooth-stator seal, while the smooth-rotor/honeycomb-stator seal is illustrated in Figs.14 and 15. The seal rotor is press-fitted and secured axially by a bolt circle to the rotor shaft. Seals with different geometries (i.e., clearances, tapers, lengths) can be tested, as well as seals with different surface roughnesses. The replacement of these rotor/stator combinations can be accomplished with minimal downtime.

Rotational Speed. A Westinghouse 50-hp variable-speed electric motor drives the rotor shaft through a belt-driven jackshaft arrangement. This shaft is supported by two sets of Torrington hollow-roller bearings [20]. These bearings are extremely precise, radially preloaded, and have a predictable and repeatable radial stiffness. Axial thrust due to the pressure differential across the seal is absorbed by a flat, roller-type, caged thrust bearing at the rear of the rotor. Both the shaft and thrust bearings are lubricated by a positive-displacement gear-type oil pump.

Different jackshaft drive-pulleys can be fitted to provide up to a 4:1 speed increase from motor to rotor shaft, which would result in a rotor shaft speed range of 0-21,200 cpm. Current design limitations,

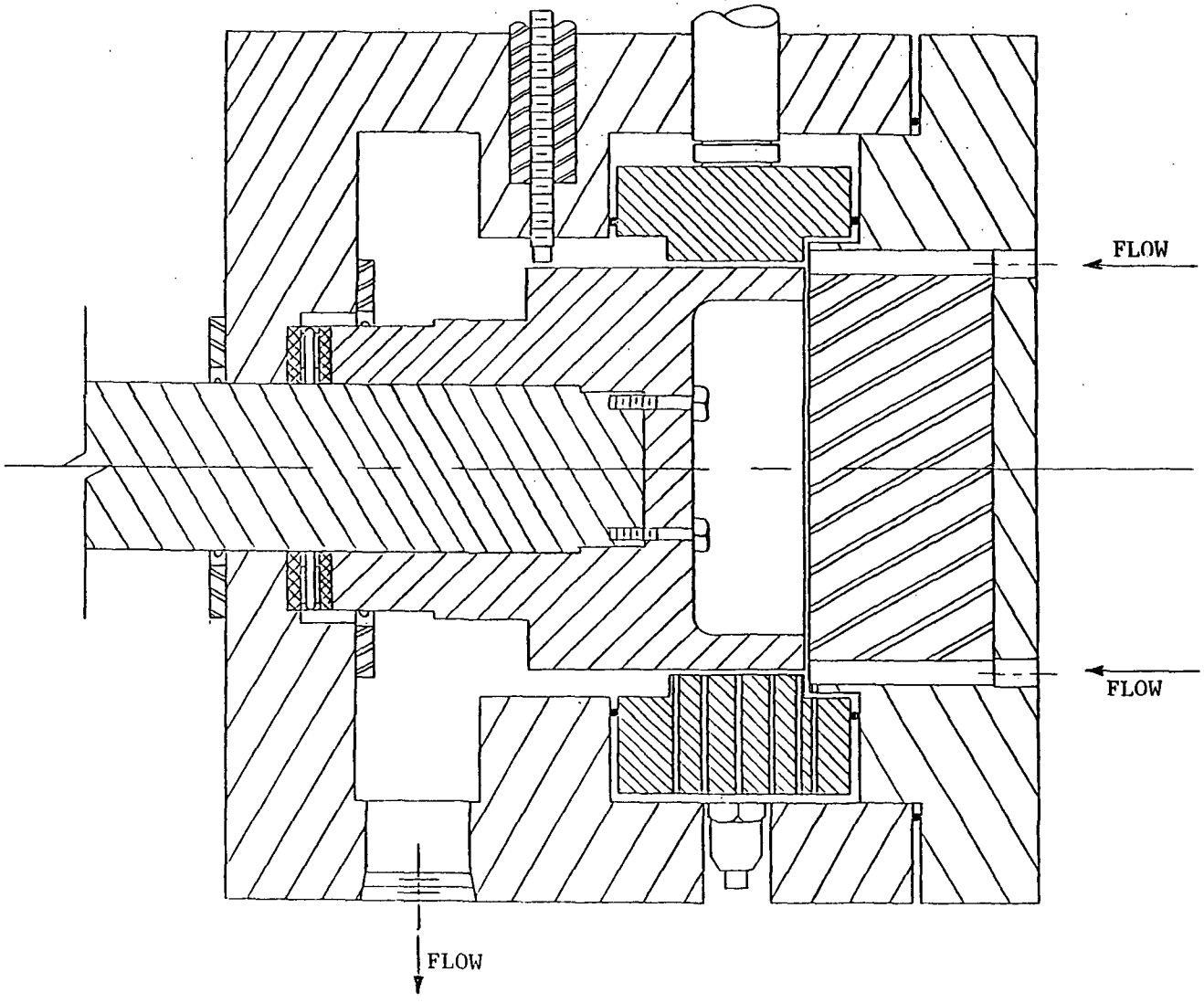

Fig. 12 Cross-sectional view of test section showing smooth stator.

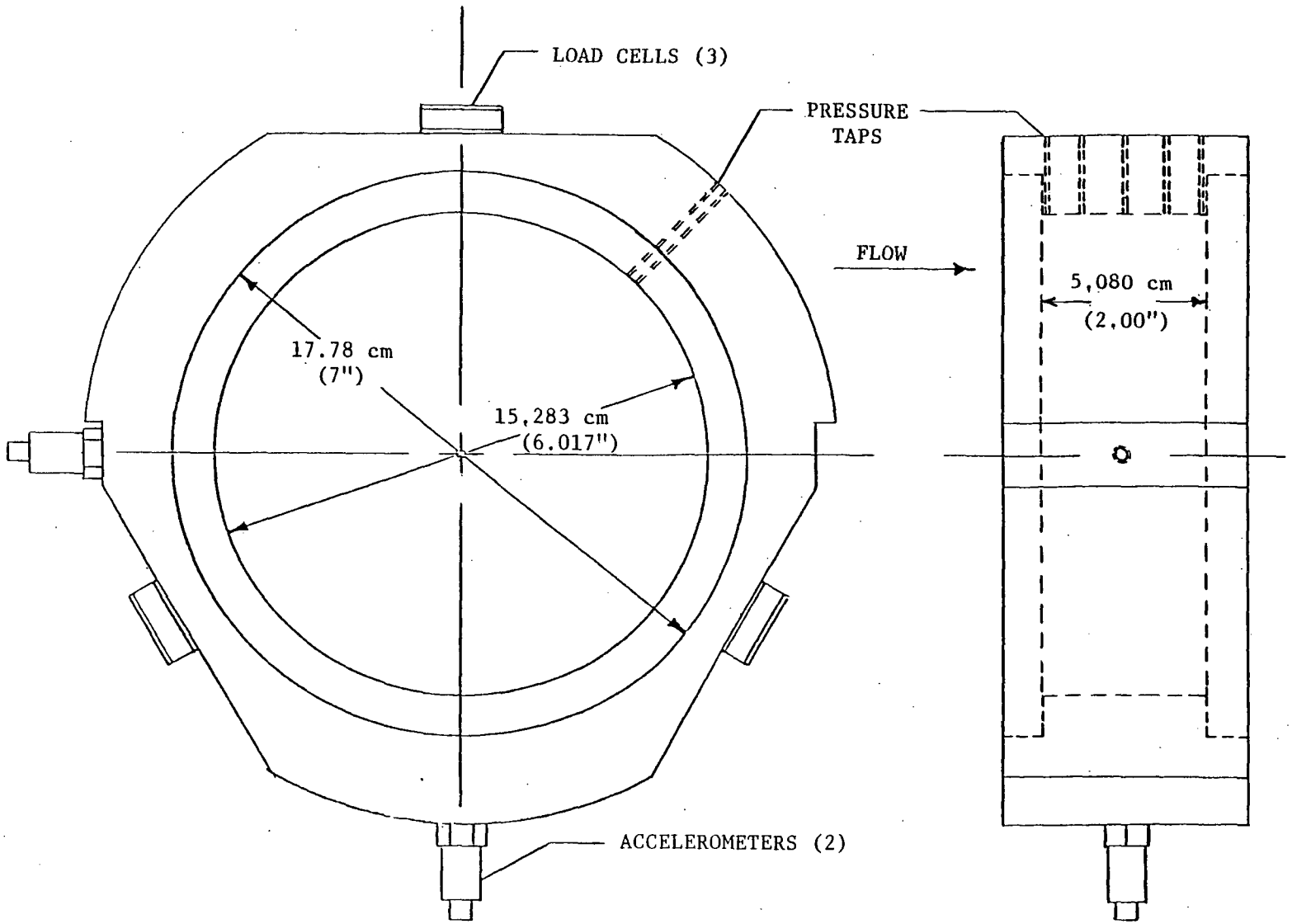

Fig. 13 Detail of smooth stator.

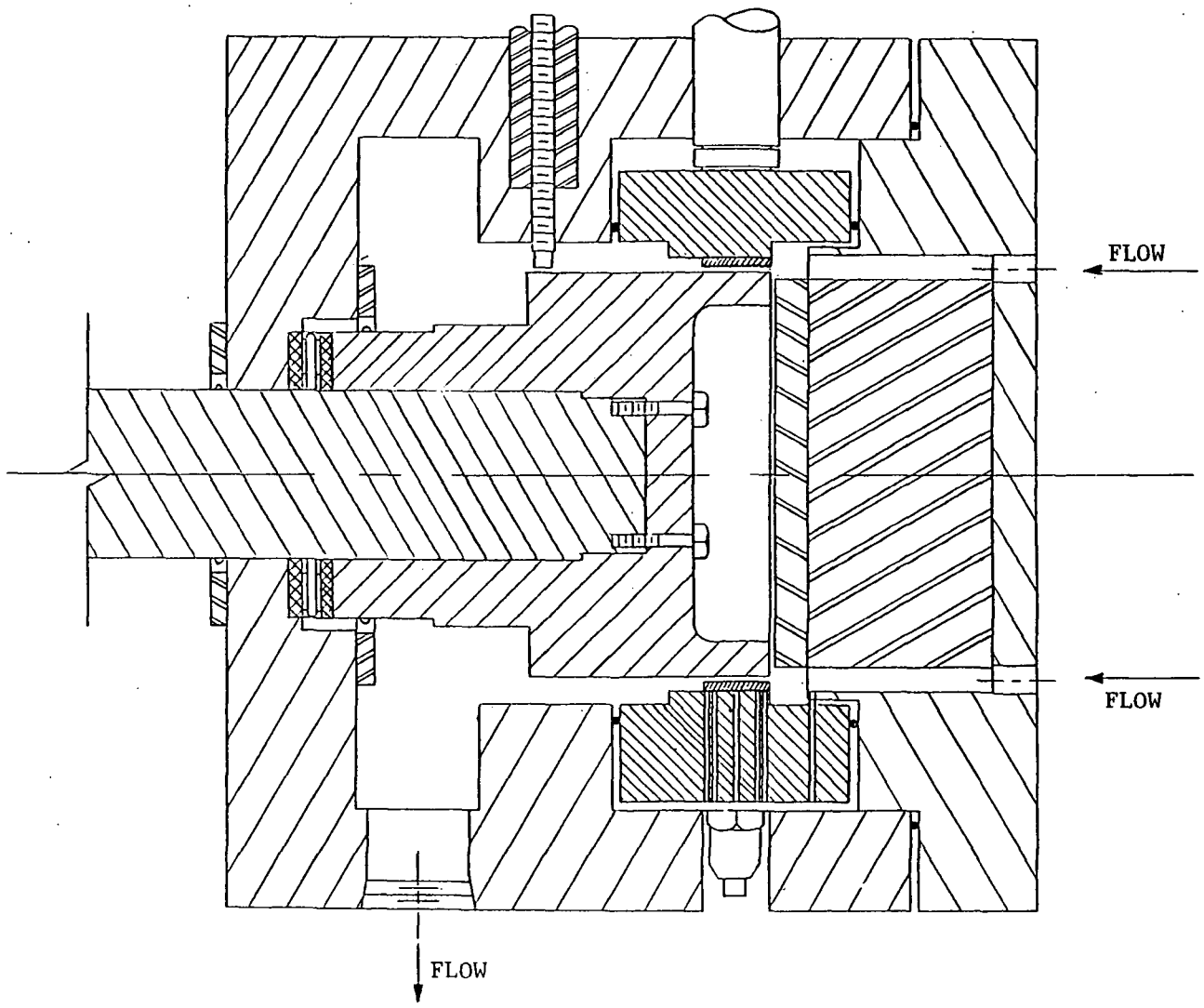

Fig. 14 Cross-sectional view of test section showing honeycomb stator.

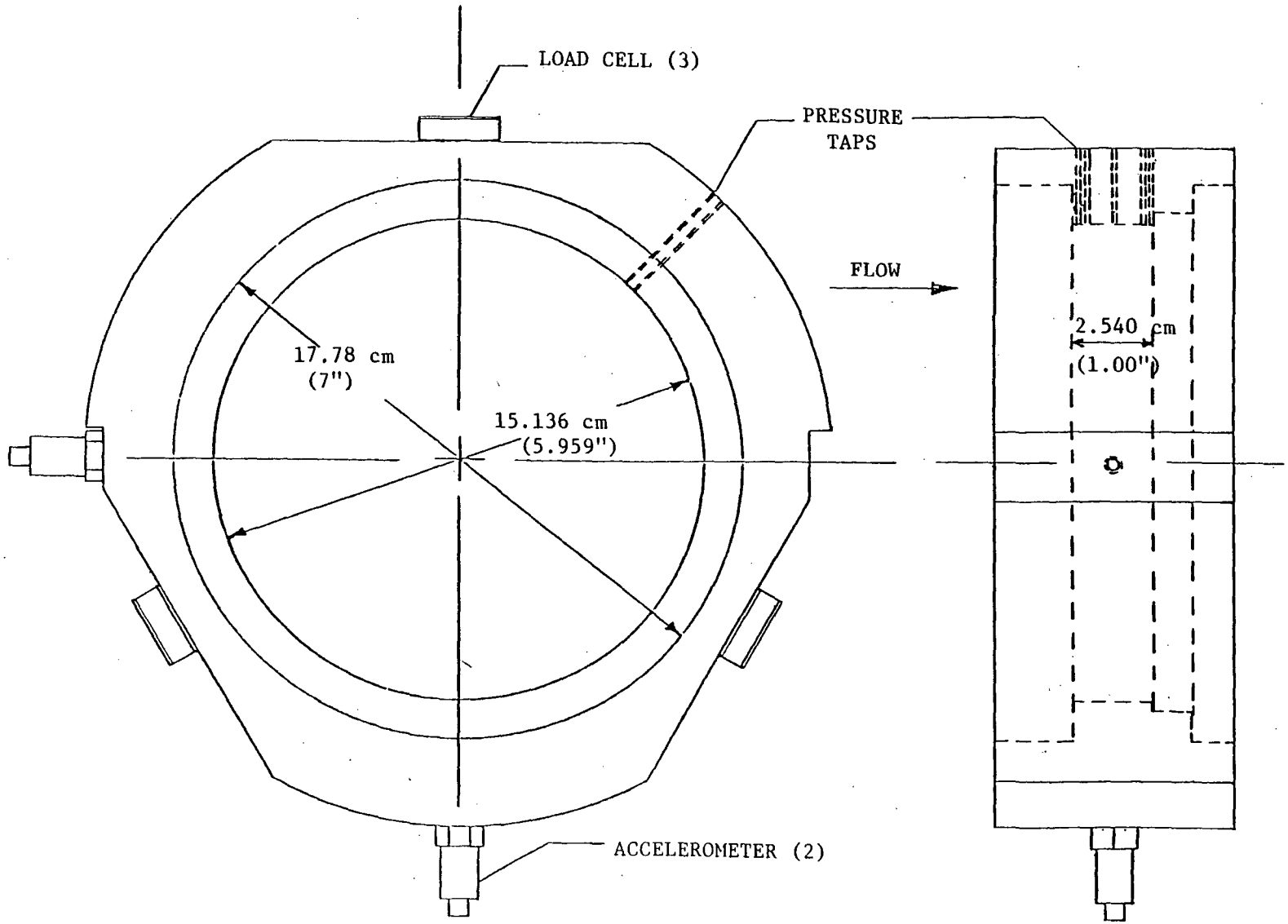

Fig. 15 Detail of honeycomb stator.

however, prevent the attainment of this upper rotational speed. High bearing temperatures, reduction of interference in the rotor-rotor shaft fitment due to inertia-induced radial growth of the rotor inside diameter, and excessive stresses in the drive-pulleys have served to limit shaft speed. The highest rotational speed attained at the time of this writing is 8500 cpm, although design modifications to allow higher speeds are under investigation.

To conclude this discussion of the test hardware, two views of the complete test apparatus are included. Fig. 16 shows the assembled rig, while an exploded view is provided in Fig. 17.

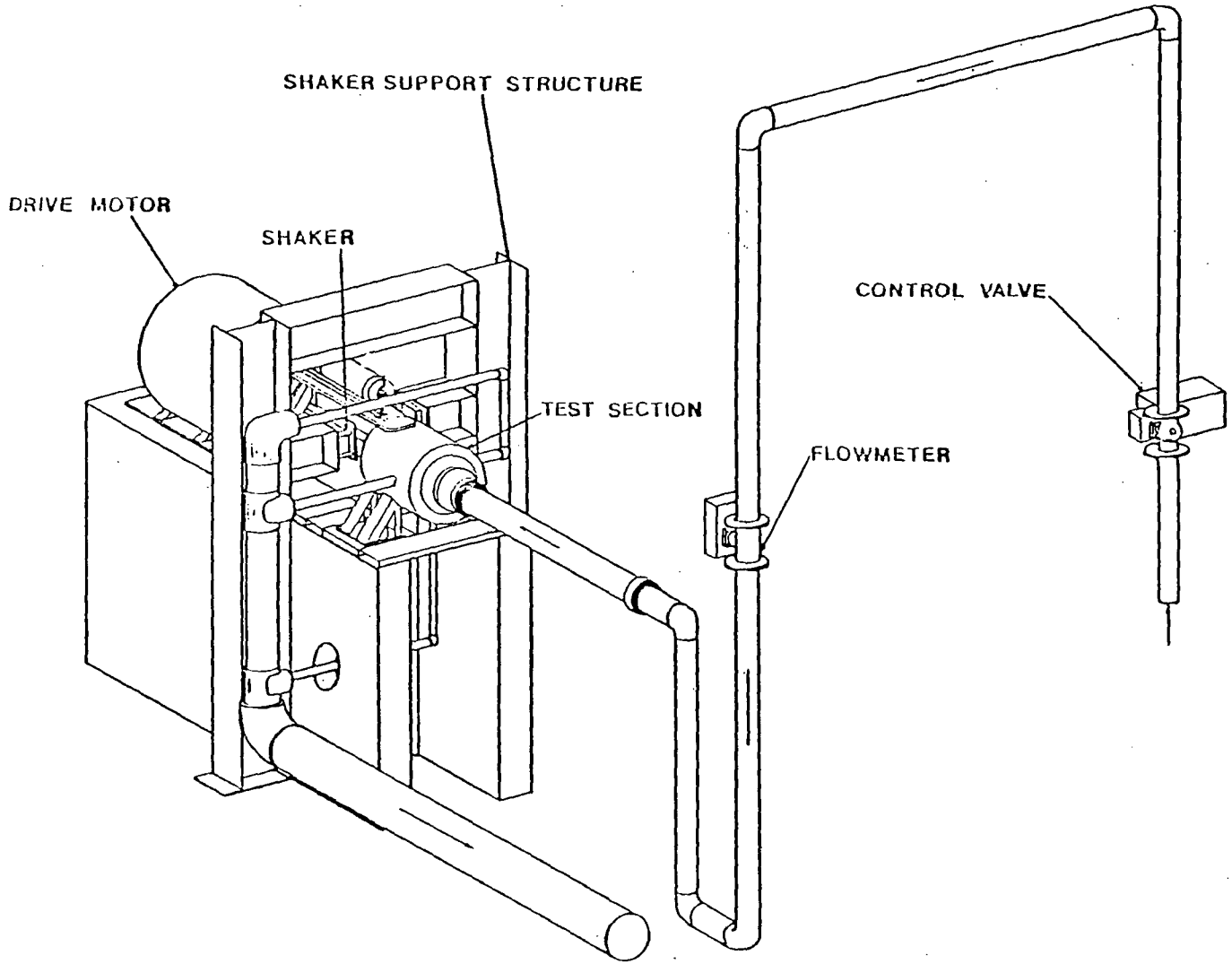

Fig. 16 Test apparatus assembly.

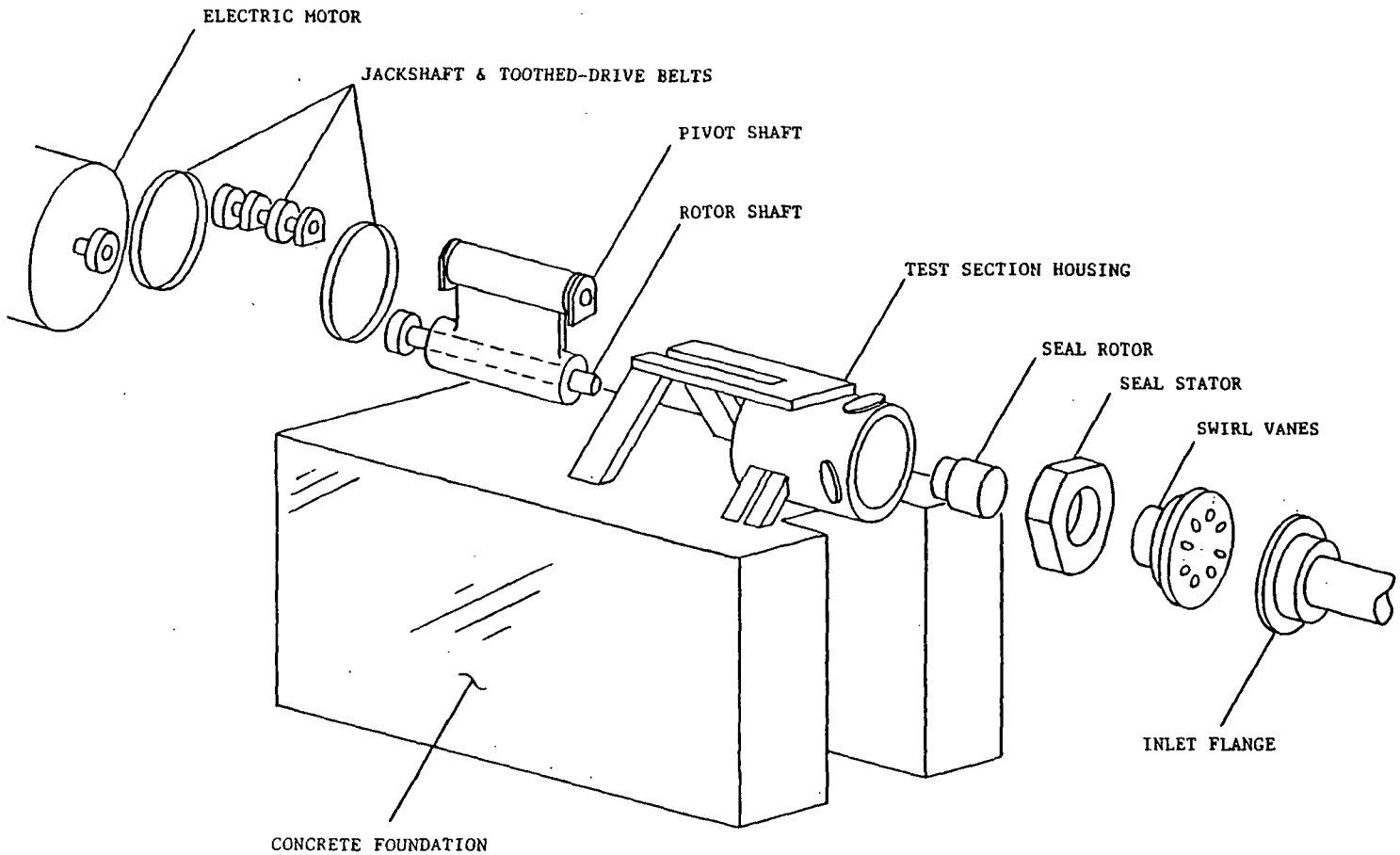

Fig. 17 Exploded view of test apparatus.

INSTRUMENTATION

Having discussed what seal parameters can be varied, and how the variations are implemented, the measurement of their respective effects can now be described. The types of measurements which are made can be grouped into three categories:

1) rotor motion,
2) reaction-force measurements, and
3) fluid flow measurements.

These categories are described individually in the sections that follow.

Rotor Motion Measurements. The position of the seal rotor within the stator is monitored by two Bently-Nevada eddy-current proximity probes, mounted in the test section housing. These probes are located 90 degrees apart, and correspond to the X and Y- directions. The proximity probes are used to determine the static position and dynamic motion of the rotor, and their resolution is 0.0025 mm (0.1 mil).

Reaction-Force Measurements. Reaction forces arise due to the static position and dynamic motion of the seal rotor within the stator. The reaction forces (F_X, F_Y) exerted on the stator are measured by the three Kistler quartz load cells which support the stator in the test section housing. When the rotor is shaken, vibration is transmitted to the test section housing, both through the thrust bearing and through the housing mounts. The acceleration of the housing and stator generates unwanted inertial "ma" forces which are sensed by the load cells, in addition to those pressure forces developed by the relative motion of the seal rotor and stator. For this reason, PCB piezoelectric accelerometers with integral amplifiers are mounted in the X and Y-directions on the stator,

as shown in Figs. 13 and 15. These accels allow a (stator mass) x (stator acceleration) subtraction to the forces (F_X, F_Y) indicated by the load cells. With this correction, which is described more fully in the next section, only the pressure forces due to relative seal motion are measured.

Force measurement resolution is a function of the stator mass and the resolution of the load cells and accelerometers. Accelerometer resolution is 0.005 g, which must be multiplied by the stator mass in order to obtain an equivalent force resolution. The masses of the stators used in the test program reported here are 11.4 kg(25.2 lb) and 3.94 kg(8.69 lb), corresponding to the smooth and honeycomb stators, respectively. Hence, force resolution for the accelerometers is 0.560 N (0.126 lb) and 0.191 N (0.043 lb), for each stator, respectively. Resolution of the load cells is 0.089 N(0.02 lb). Therefore, the resolution of the force measurement is limited by the accelerometers. With a stator with less mass, and/or accelerometers with greater sensitivity, force resolution could be improved.

Fluid Flow Measurements. Fluid flow measurements include the leakage (mass flow rate) of air through the seal, the pressure gradient along the seal axis, the inlet fluid circumferential velocity, and the entrance pressure loss.

Leakage is measured with a Fischer & Porter vortex flowmeter located in the piping upstream of the test section. Resolution of the flowmeter is 0.0014 m^3 (0.05 acf), and pressures and temperatures up and downstream of the meter are measured for mass flow rate determination.

For measurement of the axial pressure gradient, the stator has pressure taps drilled along the length of the seal in the axial

direction. These pressures, as well as all others, are measured with a 0-1.034 MPa (0-150 psig) Scanivalve differential-type pressure transducer through a 48 port, remotely-controlled Scanivalve model J scanner. Transducer resolution is 0.552 kPa (0.08 psi).

In order to determine the circumferential velocity of the air as it enters the seal, the static pressure at the guide vane exit is measured. This pressure, in conjunction with the measured flowrate and inlet air temperature, is used to calculate a guide vane exit Mach number. A compressible flow continuity equation

$$\dot{m} = p_{ex} A_{ex} M_{ex} [(\gamma/R_g T_t) (1 + (\gamma-1)M_{ex}^2 / 2)]^{1/2} \quad (18)$$

is rearranged to provide a quadratic equation for Mex

$$M_{ex}^2 = \{-1 + 1 + 4((\gamma-1)/2\gamma) (m R_g T_t / p_{ex} A_{ex})^2 \} / (\gamma-1) \quad (19)$$

where γ is the ratio of specific heats and R_g is the gas constant for air, T_t is the stagnation temperature of the air, p_{ex} is the static pressure at the vane exit, and A_{ex} is the total exit area of the guide vanes. Since all of the variables in the equation are either known or measured, the vane exit Mach number, and therefore the velocity, can be found.

In order to determine the circumferential component of this inlet velocity, a flow turning angle correction, in accordance with Cohen[21], is employed. The correction has been developed from guide vane cascade tests, and accounts for the fact that the fluid generally is not turned through the full angle provided by the shape of the guide vanes. With this flow deviation angle calculation, the actual flow direction of the air leaving the vanes (and entering the seal) can be determined. Hence, the magnitude and direction of the inlet velocity is known, and the appropriate component is the measured inlet circumferential velocity.

The entrance pressure-loss coefficient, defined in equation (6), is determined from the measured pressures just upstream of and just inside the seal. An entrance Mach number is calculated in the same manner as outlined previously, using the measured pressure immediately inside the seal and the annular area between the rotor and stator. This entrance Mach number, and the ratio of the seal entrance/guide vane exit pressures are substituted into equation (6), and the entrance loss coefficient, $\bar{k}$, is determined.

DATA ACQUISITION AND REDUCTION

With the preceding explanations of how the seal parameters are varied, and how these parameters are measured, the discussion of how the raw data is processed and implemented can begin. Data acquisition is directed from a Hewlett-Packard 9816 (16-bit) computer with disk drive and 9.8 megabyte hard disk. The computer controls an H-P 6940B multiprogrammer which has 12-bit A/D and D/A converter boards and transfers control commands to and test data from the instrumentation.

As was previously stated, the major data groups are seal motion/reaction force data and fluid flow data. The motion/reaction force data are used for dynamic coefficient identification. The hardware involved includes the load cells, accelerometers, X-direction motion probe, a Sensotec analog filter unit, a tunable bandpass filter, and the A/D converter. The operation of these components is illustrated in Fig.18, and their outputs are used in a serial sampling scheme which provides the computer with the desired data for reduction. Recalling the discussion of the reaction force measurements in the preceding section, a (stator mass) x (stator acceleration) subtraction from the indicated load cell forces is necessitated due to vibration of the stator and test section housing. This subtraction is performed with an analog circuit, and results in corrected F_X and F_Y force components due to relative seal motion.

The forced oscillatory shaking motion of the seal rotor is the key to the operation of the serial synchronous sampling (SSS) routine which is employed. The frequency of the rotor oscillation is set by a function generator, and rotor motion is sensed by the X-direction motion probe.

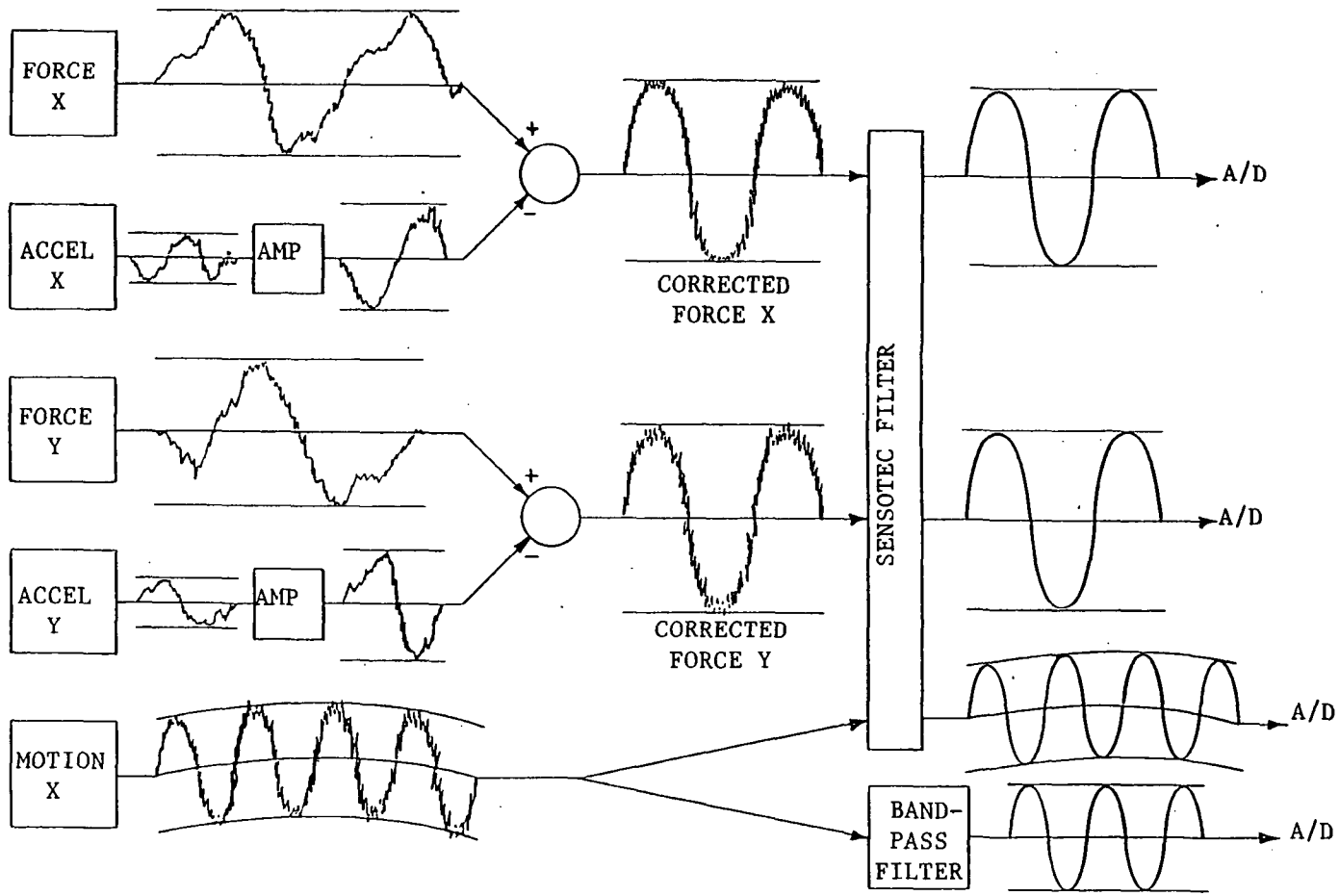

Fig. 18 Signal conditioning schematic for data acquisition.

The motion signal is filtered by the narrow bandpass filter, and is used as a trigger signal for the SSS routine. Upon the operator's command, the SSS routine is enabled, and the next positive-to- negative crossing of the filtered motion signal triggers a quartz crystal clock/timer. Ten cycles of the corrected $F_X(t)$ signal are sampled, at a rate of 100 samples/cycle. The second positive-to-negative crossing of the filtered motion signal triggers the timer and initiates the sampling of ten cycles of the $F_X(t)$ signal. Finally, the third positive-to-negative crossing triggers the timer again, and ten cycles of the corrected X(t) signal are sampled. Thus, at every test condition, 1000 data points are obtained for $F_X(t_i)$,$F_Y(t_i)$, and $X(t_i)$, and the data arrays are stored in computer memory.

Some important points need to be stressed concerning this force/motion data acquisition. First, the bandpass filter is used only to provide a steady signal to trigger the timer/clock. Any modulation of the motion signal due to rotor runout is eliminated by this filter, as long as the rotational frequency and shaking frequency do not coincide. Therefore, the shaking frequencies are selected to avoid coincidence with running speeds. However, the rotor motion and corrected force signals which are sampled and captured for coefficient identification are filtered only by a low-pass filter (500 Hz cutoff), and the effects of runout as well as shaking motion are present in the recorded data. A second point worth noting is that the sample rate is directly dependent on the shaking frequency. As the shaking frequency is increased, the sample rate (samples/second) also increases. In order to get the desired 100 samples/cycle, shaking frequencies must be chosen to correspond to discrete sample rates which are available. Hence, the

frequency at which the rotor is shaken is carefully chosen to provide the desired sampling rate and a steady trigger signal.

Most of the fluid flow data are used for the input parameters required by Nelson's analysis. The upstream (reservoir) pressure and temperature, downstream (sump) pressure, and the inlet circumferential velocity (determined as outlined earlier) are provided directly. The friction-factor values of the rotor and stator are supplied in the form of Hirs coefficients, which are obtained from the pressure distribution data in the manner described below.

Recalling the discussion of Hirs' turbulent bulk-flow fluid model, the model assumes that the wall shear stresses can be written as in equation (4). For the gas seals discussed here, an adiabatic, compressible flow with friction analysis is employed, and the measured pressure gradient and mass flow rate (leakage) data are used to calculate a friction factor coefficient, λ, for each test condition. From the λ versus R_a and ω data, the Hirs coefficients mr, nr of the friction factor formula

$$\lambda = nr\ R_a^{mr}\ [\ 1 + 1\ /\ 4b^2]^{(1+mr)/2}\ ,\quad b = U\ /\ R\omega \tag{20}$$

are calculated on a least-square basis. For the smooth-rotor/smooth-stator combination, the values are assumed to apply for both the rotor and stator. Hence, for this case, mr=ms and nr=ns.

For the smooth-rotor/honeycomb-stator combination, a combined λ is measured, which is related to the rotor λ_r and (honeycomb) stator λ_s by

$$\lambda_c = (\lambda_r + \lambda_s)\ /\ 2 \tag{21}$$

and hence,

$$\lambda_s = 2\lambda_c - \lambda_r \tag{22}$$

Therefore, λ_s is determined from measured data for λ_c and a calculated value for λ_r from Equation (21) with experimentally determined values for mr and nr. Then, as before, the λ_s versus R_a and ω data are used to calculate the Hirs coefficients for the honeycomb stator.

As stated previously, the Hirs coefficients for the seal rotor and stator are required input parameters for Nelson's analysis, as are the fluid flow conditions up and downstream of the seal and the rotational speed of the rotor. The appropriate input parameters for each specific test case can be provided for Nelson's analysis from static test results and measurements. In this manner, a point-by-point comparison of theoretical predictions to experimental results can be made for leakage through the seal, axial - pressure distribution, entrance - loss coefficient, and rotordynamic coefficients.

TEST PROCEDURES

At the start of each day's testing, the force, pressure, and flowmeter systems are calibrated. The total system, from transducer to computer, is calibrated for each of these variables. The force system calibration utilizes a system of pulleys and known weights applied in the X and Y-directions. An air-operated dead-weight pressure tester is used for pressure system calibration, and flowmeter system calibration is achieved with an internal precision quartz clock which simulates a known flowrate.

All of the tests performed to date have been made with the rotor executing small motion about a centered position. A typical test begins by centering the seal rotor in the stator with the Zonic hydraulic shaker, starting airflow through the seal, setting the rotational speed of the rotor, and then beginning the shaking motion of the rotor. Data points are taken at rotational speeds of 200, 500, and 1000-8000 cpm, in 1000 cpm increments. At each rotational speed, the inlet pressure is varied and data points are taken at one unchoked flow and four choked flow conditions. For each test case (i.e., one particular running speed, shaking frequency, inlet pressure, and prerotation condition), the measured leakage, rotordynamic coefficients, axial pressure distribution, and entrance loss coefficient are determined and recorded.

This test sequence is followed for each of three different shaking frequencies, and for three inlet swirl directions (with rotor rotation, opposite rotation, and no rotation). Therefore, fifty data points are taken per test (i.e. one shaking frequency and inlet swirl combination),

with a total of nine tests (for small motion about a centered position) made per seal.

RESULTS

The test results reported here were developed as part of an extended, joint NASA-USAF funded research program for annular gas seal studies. Tests were carried out on a smooth-rotor/smooth-stator seal and a smooth-rotor/honeycomb-stator seal. The dimensions and pertinent data for each are included in Table 1. The honeycomb stator insert, provided by the Rocketdyne division of Rockwell International, is the turbine interstage seal of the HPOTP (High-Pressure Oxygen Turbopump) of the SSME (Space Shuttle Main Engine). Fig. 19 illustrates the honeycomb configuration.

The test program had the following objectives:

1) Acquire leakage, friction factor, and entrance-loss data for smooth and honeycomb seals.

2) Compare predictions from current theory to test results.

3) Compare the stability performances of a smooth-rotor/honeycomb-stator and a smooth constant-clearance annular seal.

The Hirs coefficients for both seals were determined in the manner described previously. The values of these coefficients are listed in Table 2. Relative roughness values based on measured Hirs coefficients as suggested by Colebrook [22] are also included. Colebrook's formulation,

$$(4\ nsR_a^{ms})^{-1/2} = -2 \log (((\varepsilon/2C) / 3.7) + (2.51 / (R_a\sqrt{4\ nsRams}))) \quad (23)$$

is a curve-fit of experimental data obtained for fluid flow through pipes with various wall roughnesses. The appropriate stator coefficients are substituted to obtain the relative roughness ($\varepsilon/2C$)

Table 1. Test seal specifications.

	Smooth-rotor/ smooth stator	Smooth-rotor/ honeycomb stator
Rotor		
Diameter:	15.136 cm (5.959 in)	14.453 cm (5.690 in)
Material:	304 Stainless steel	304 Stainless steel
Surface roughness:	0.102 μm (4 μin)	0.127 μm (5 μin)
Stator		
Diameter:	15.283 cm (6.017 in)	14.614 cm (5.754 in)
Material:	304 Stainless steel	6061-T6 Aluminum
Surface roughness:	0.140 μm (5.5 μin)	1.575 mm (0.062 in) Comb
Radial clearance:	0.7366 mm (29 mil)	0.8065 mm (31.8 mil)
Seal length:	5.080 cm (2.00 in)	2.540 cm (1.00 in)

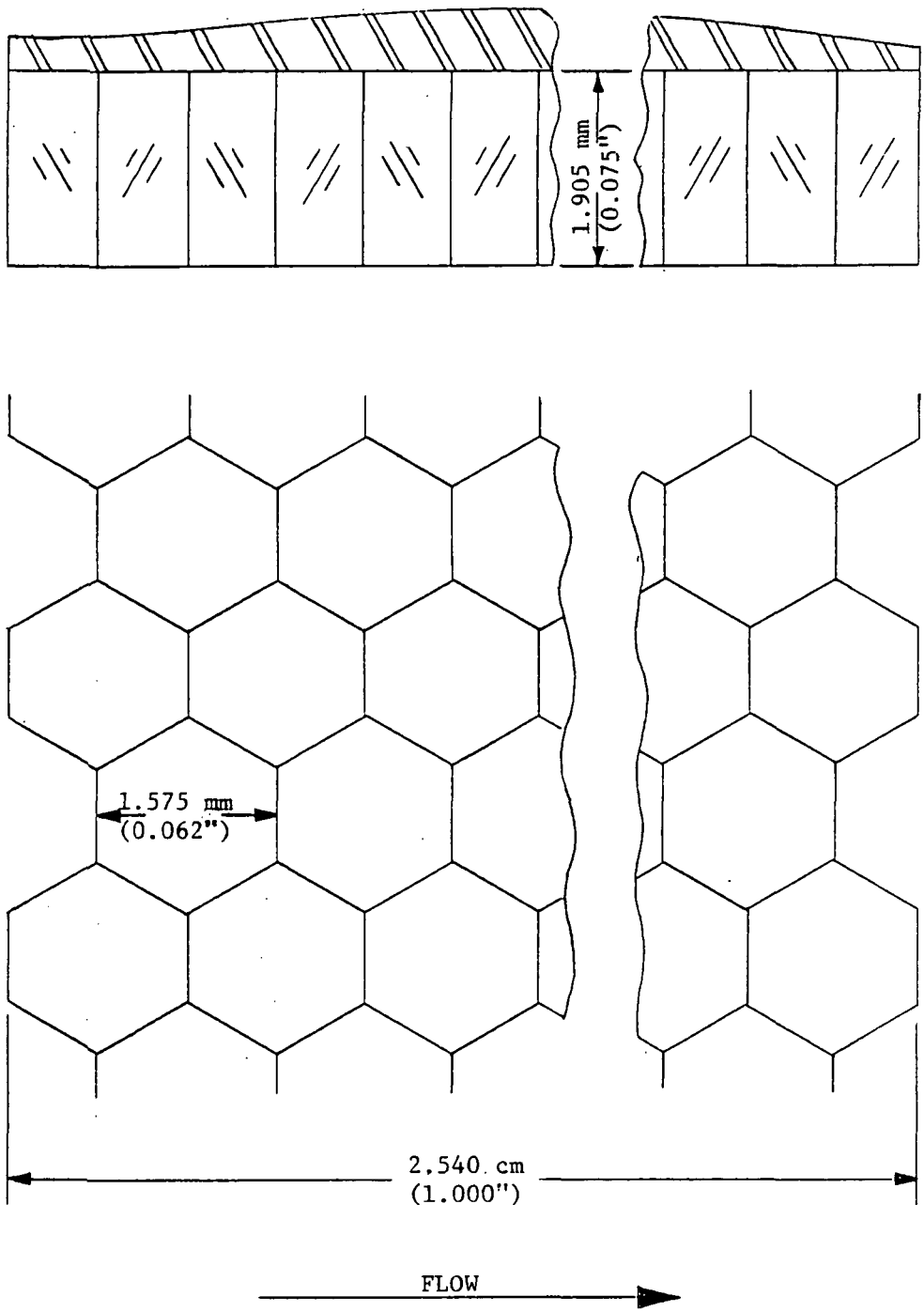

Fig. 19 Honeycomb stator insert detail.

Table 2. Friction-factor data.

	Smooth-rotor/ smooth-stator	Smooth-rotor/ honeycomb-stator
Hirs coefficients		
Rotor ns:	0.187	0.187
Rotor ms:	-0.333	-0.333
Stator ns:	0.187	0.187
Stator ms:	-0.333	-0.0778
Relative roughness $\varepsilon/2C$		
Rotor:	1.44×10^{-4}	1.44×10^{-4}
Stator:	1.44×10^{-4}	4.93×10^{-4}

(Note: The relative roughness values shown are averages over an axial Reynolds number range of 20,000 - 80,000.)

values. It should be noted that friction factor data for honeycomb seals have not been previously published.

The results provided here are grouped in static (leakage, pressure distribution, entrance loss coefficient) and dynamic (rotordynamic coefficient) sections. A one-to-one comparison of the smooth and honeycomb seal configuration is precluded, however, due to differences in seal length, nominal clearance, and inlet guide vane configuration, as illustrated in Figs. 12 and 14.

Static Results. Figs.20 and 21 and Table 3 show a comparison of the theoretical and experimental leakage through the seal for various fluid prerotation conditions. The figures show the leakage at various pressure ratios (reservoir pressure / sump pressure). In the table, the leakage has been averaged over all speeds and pressure ratios, and is presented in ratio form (Theory/Experiment). The comparison shows that for both the smooth and the honeycomb seal, leakage is underpredicted for the non-prerotated case. Conversely, for fluid prerotation either in or opposing the direction of rotor rotation, the leakage is overpredicted for both seals. The maximum error is approximately 7.5%, occurring for the smooth seal with prerotation in the direction of rotor rotation. Average error for the smooth seal is 1.7%, and for the honeycomb seal is 1%.

The pressure gradient plots are included in Figs.22-28. Fig. 22 illustrates the negligible effect of running speed on the pressure distribution in the seal. This plot has ten curves (corresponding to the ten rotational speed increments) plotted. This accounts for the heavy lines which appear in some cases. This particular plot is of the experimental data for the non-prerotated smooth seal case, however,

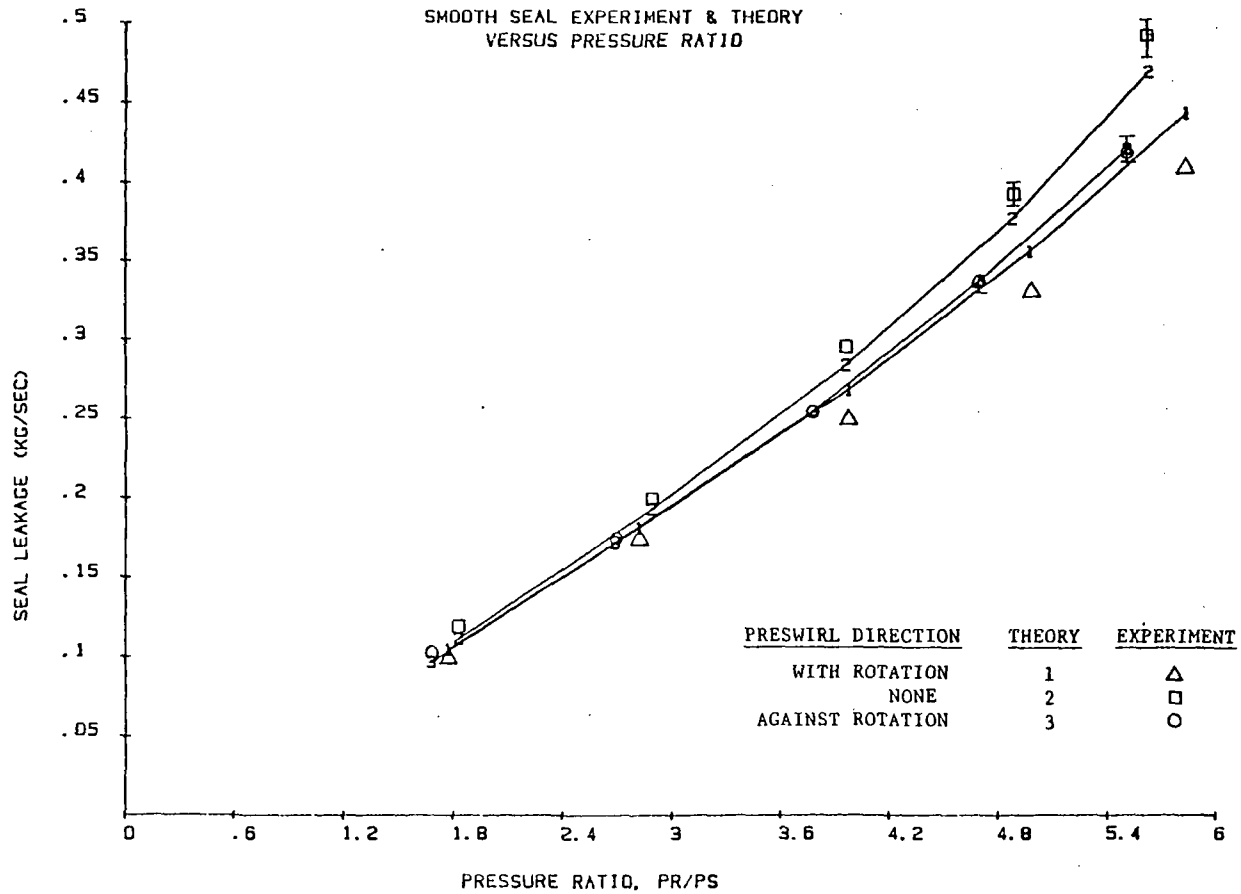

Fig. 20 Smooth seal leakage.

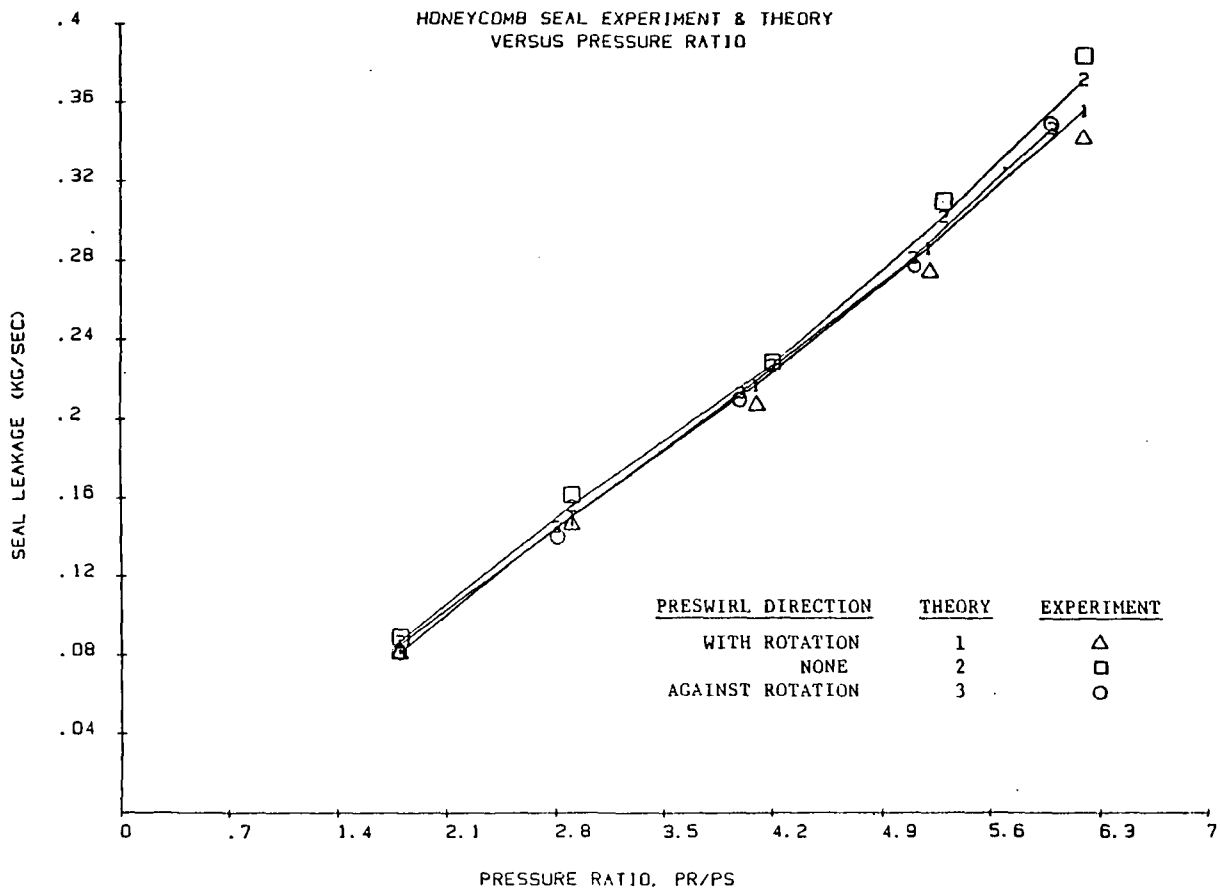

Fig. 21 Honeycomb seal leakage

Table 3. Theory versus experiment leakage comparison.
(Theory/Experiment)

Fluid prerotation direction	Smooth-rotor/ smooth-stator	Smooth-rotor/ honeycomb-stator
With rotor rotation	1.075	1.047
(standard deviation)	0.012	0.008
No prerotation	0.9684	0.9712
(standard deviation)	0.012	0.005
Opposite rotor rotation	1.007	1.013
(standard deviation)	0.012	0.004

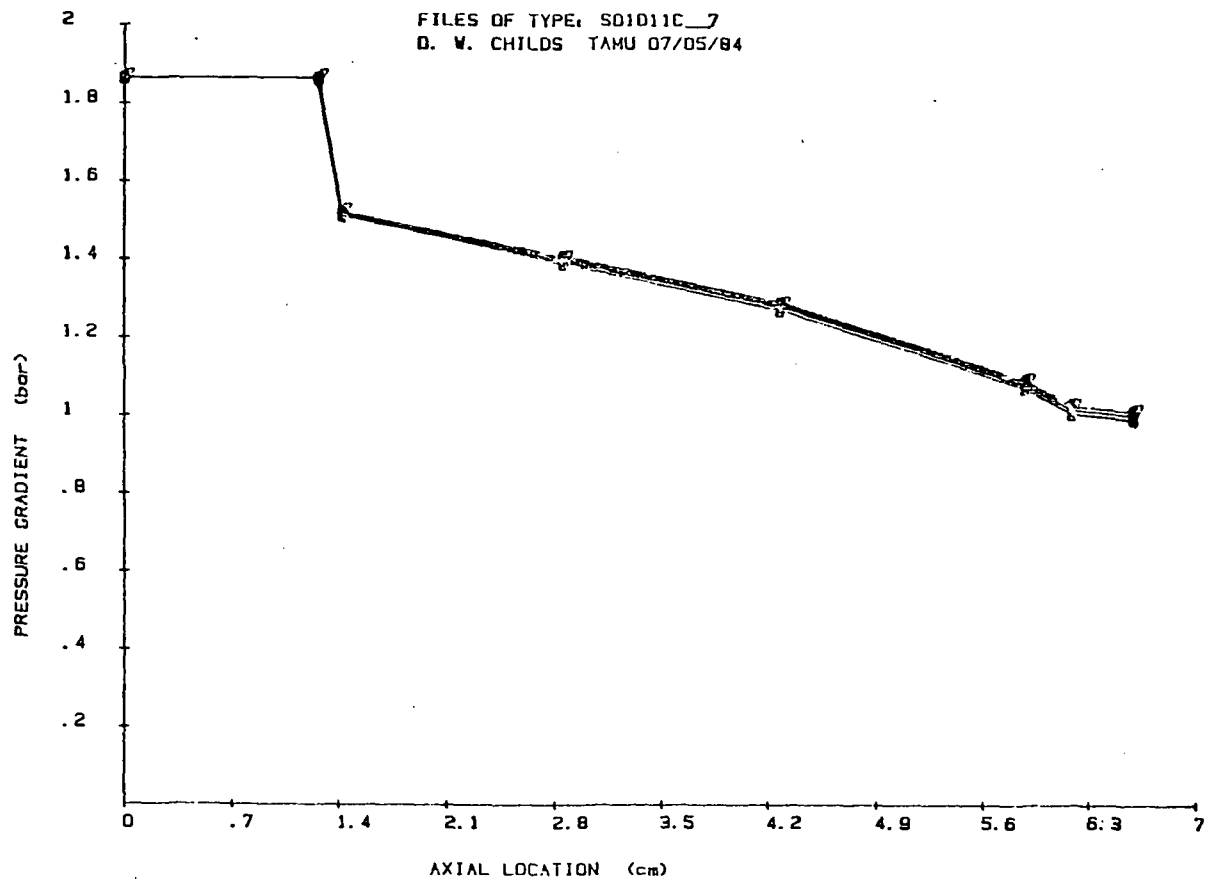

Fig. 22 Axial pressure gradient in smooth seal with no prerotation, unchoked flow, ten running speeds.

none of the pressure plots show any appreciable variation due to running speed.

Figs. 23-28 show the theoretical and experimental pressure data for each of the seals under various prerotation conditions. Due to the absence of running speed dependence, only one speed is plotted for each inlet pressure condition. The numbers on the plotted lines refer to the inlet pressure, where 1 corresponds to approximately 186.9 kPa (12.4 psig), and 2 through 5 correspond to 308.2 kPa (30 psig), 446.1 kPa (50 psig), 584.0 kPa (70 psig), and 721.9 kPa (90 psig), respectively. The lowest pressure corresponds to unchoked flow through the seal, while the others are choked. The shapes of the pressure-gradient plots show fairly good correspondence between theory and experiment. This to be expected, however, since the Hirs' coefficients used in the analysis come directly from the measured pressures. The best agreement occurs for the non-prerotated flow in both the smooth and honeycomb seals. For prerotated flow in either direction, the theoretical gradient is shifted up slightly for both seal configurations. This upward shift is partly due to a total pressure correction that is made. When the flow is prerotated by the guide vanes, it is accelerated as well as turned, and the measured static pressure at the vane exit decreases. This explains why the experimental plots show lower seal entrance pressures for either prerotated case than for the non-prerotated case. Nelson's analysis, however, assumes that the supply pressure upstream of the seal is the total pressure. Hence, the axial component of the fluid velocity as it leaves the guide vanes is used to calculate an effective total pressure, which is higher than the measured static pressure. This corrected pressure is then input as the reservoir pressure to Nelson's analysis.

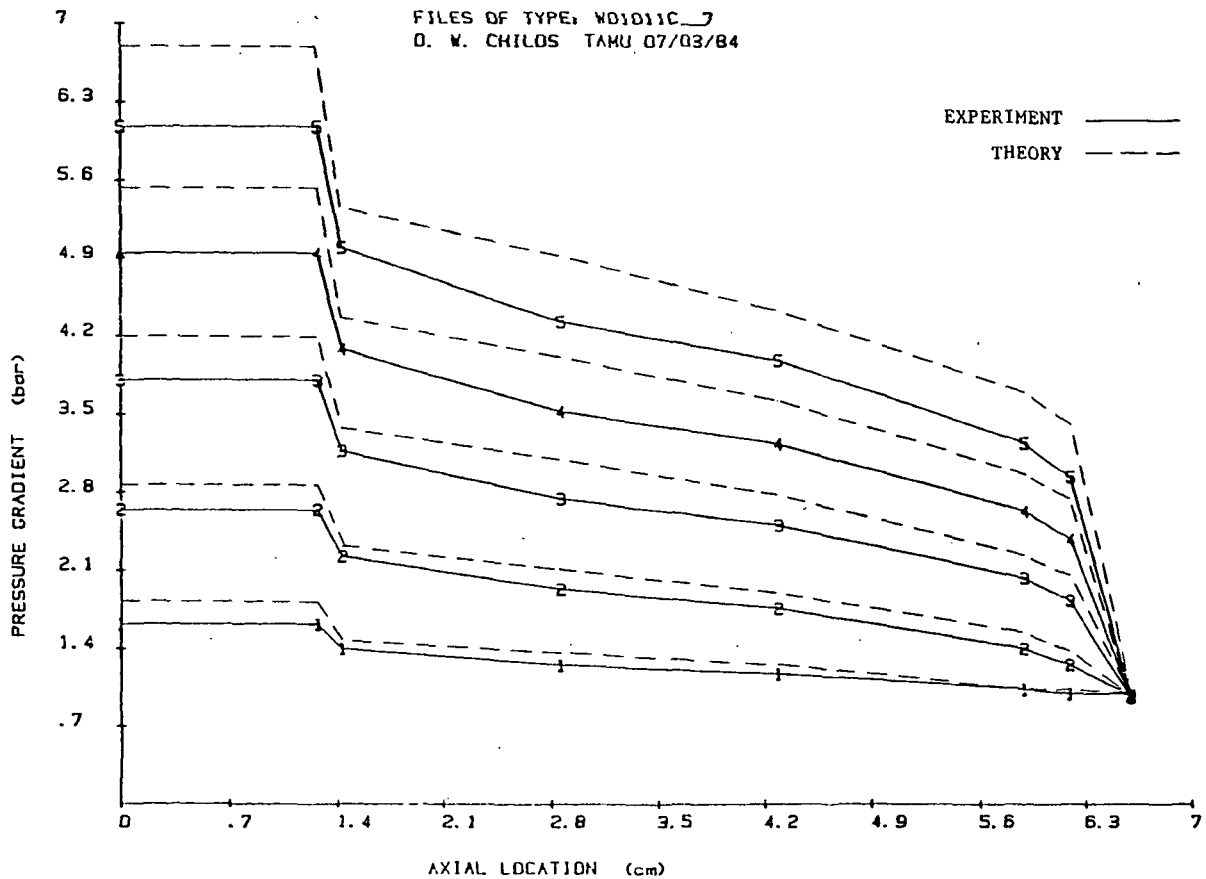

Fig. 23 Axial pressure gradient in smooth seal with prerotation in the direction of rotor rotation.

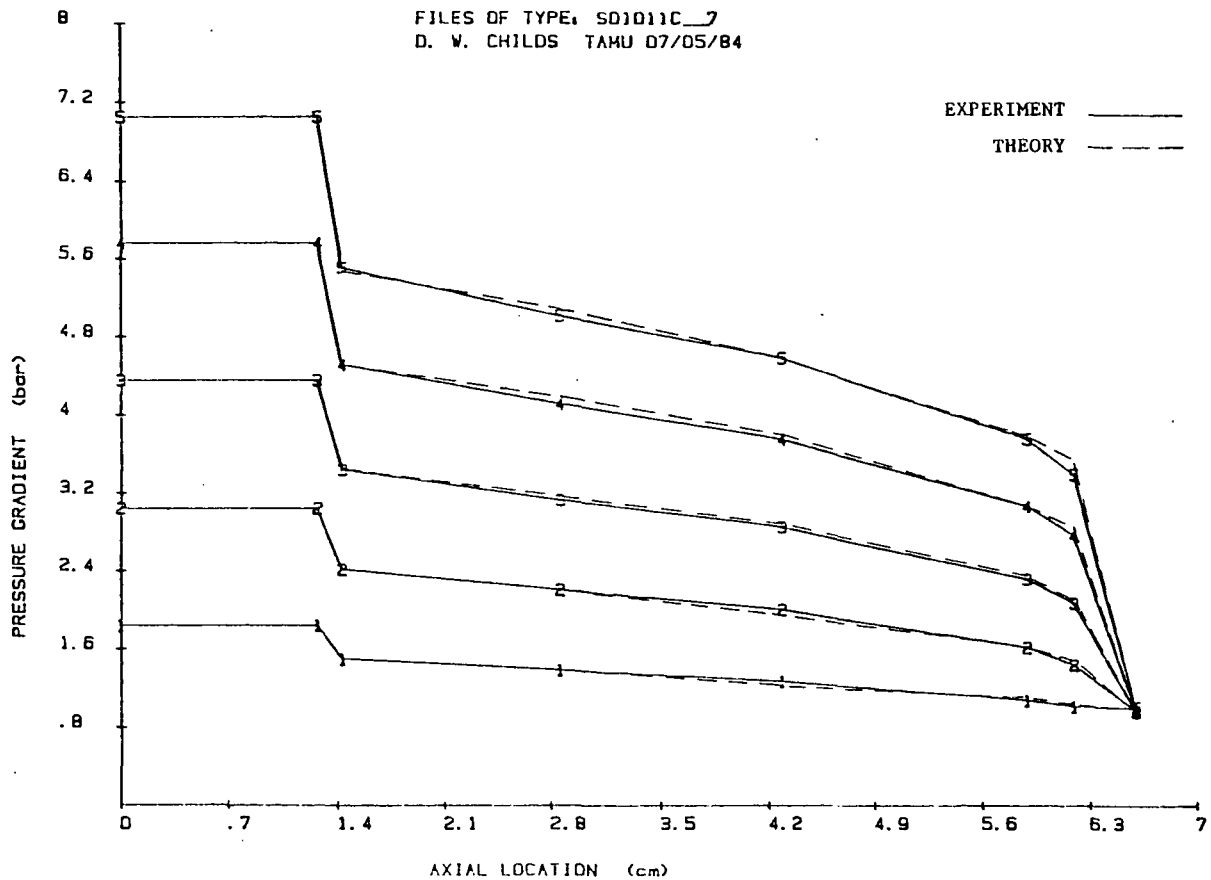

Fig. 24 Axial pressure gradient in smooth seal with no prerotation.

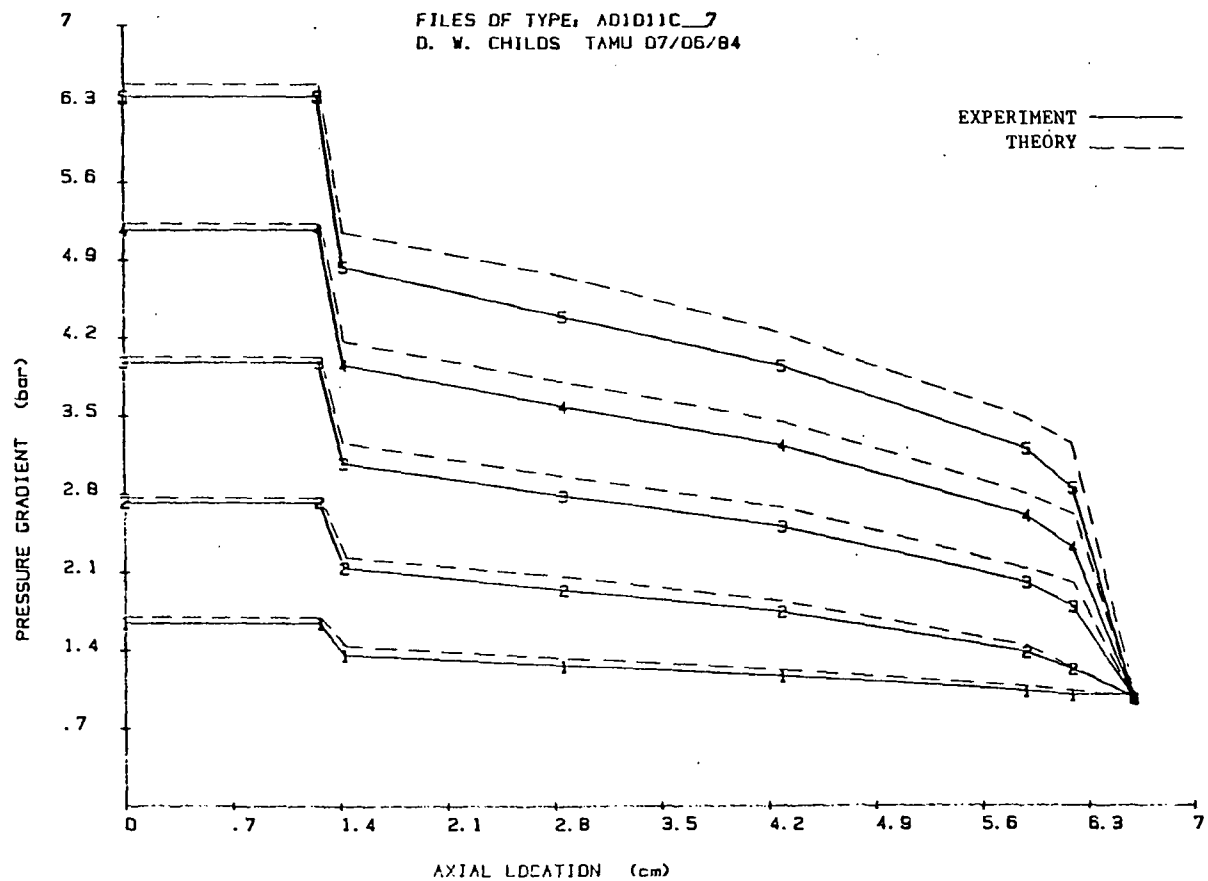

Fig. 25 Axial pressure gradient in smooth seal with prerotation opposing rotor rotation

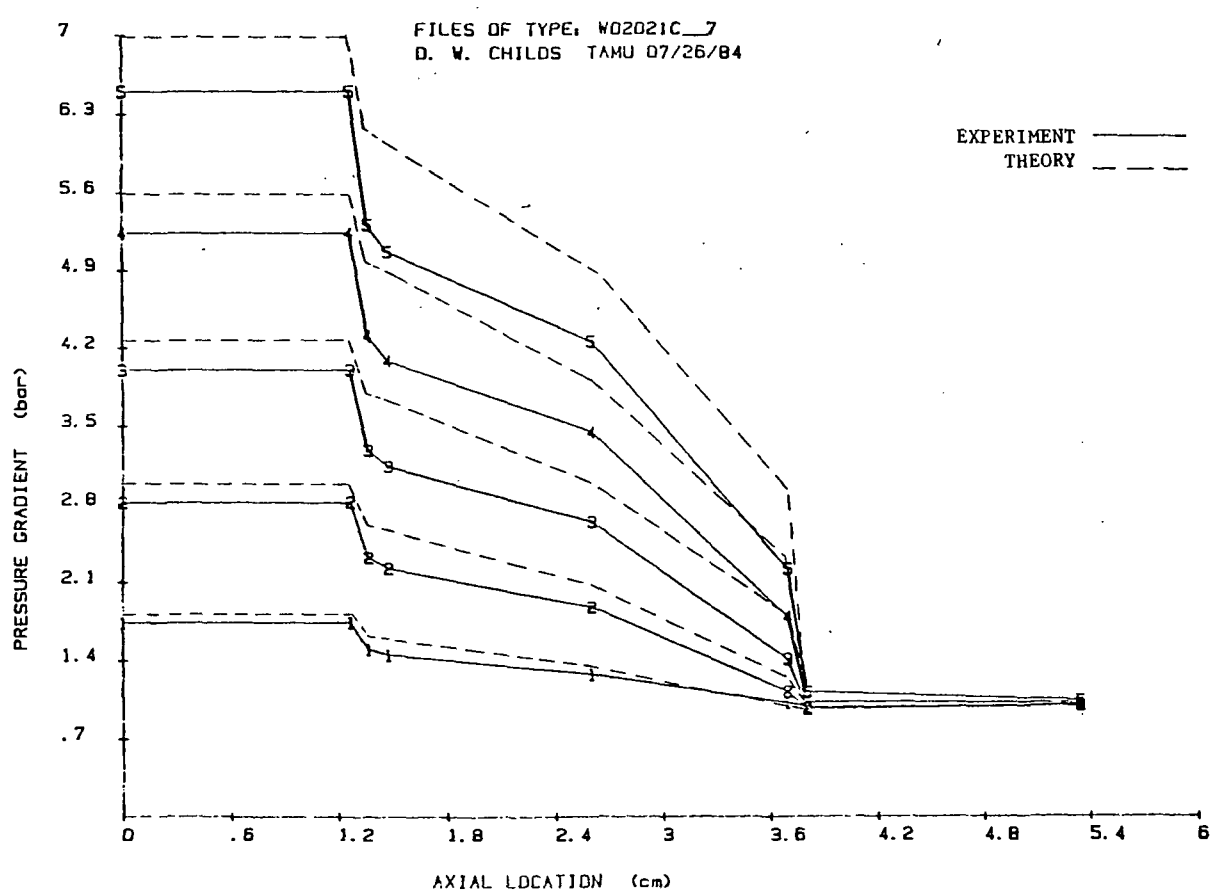

Fig. 26 Axial pressure gradient in honeycomb seal with prerotation in the direction of rotor rotation.

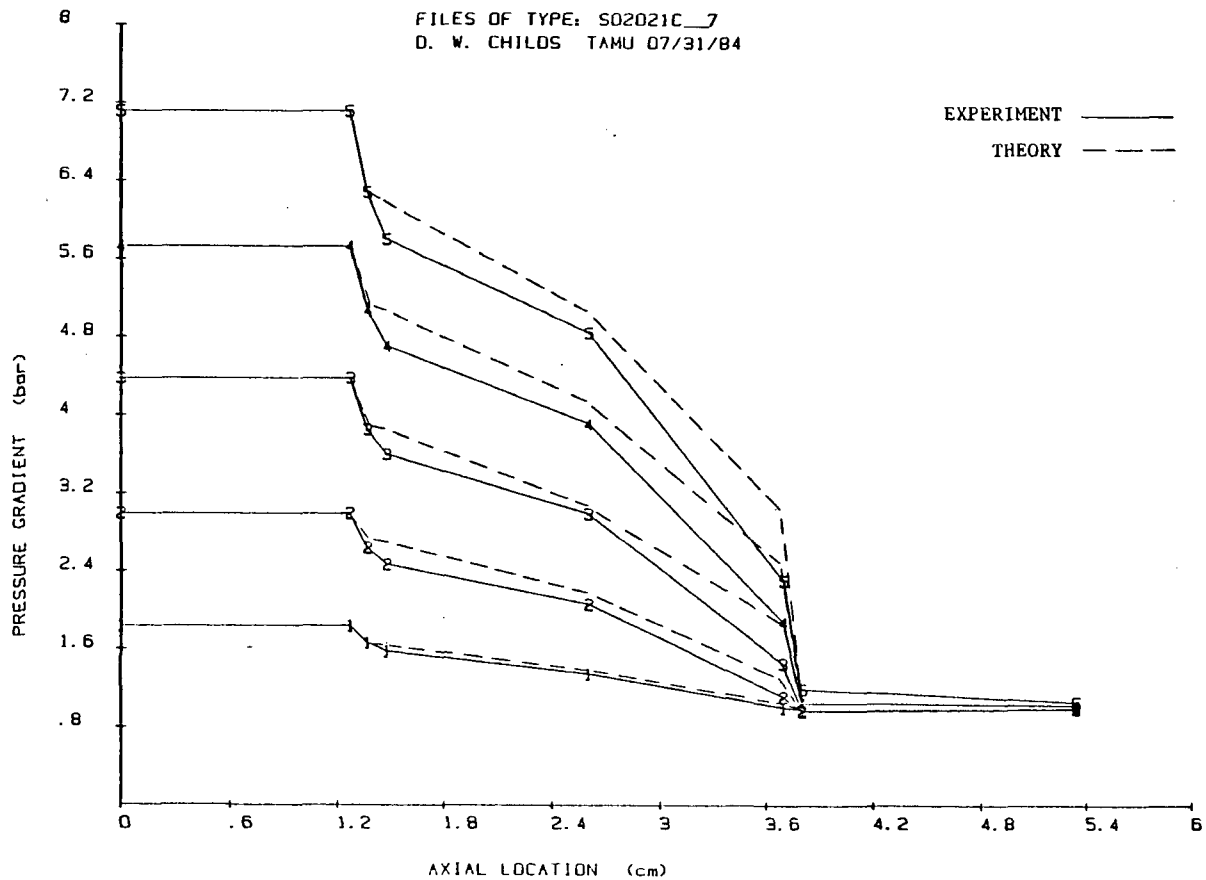

Fig. 27 Axial pressure gradient in honeycomb with no prerotation.

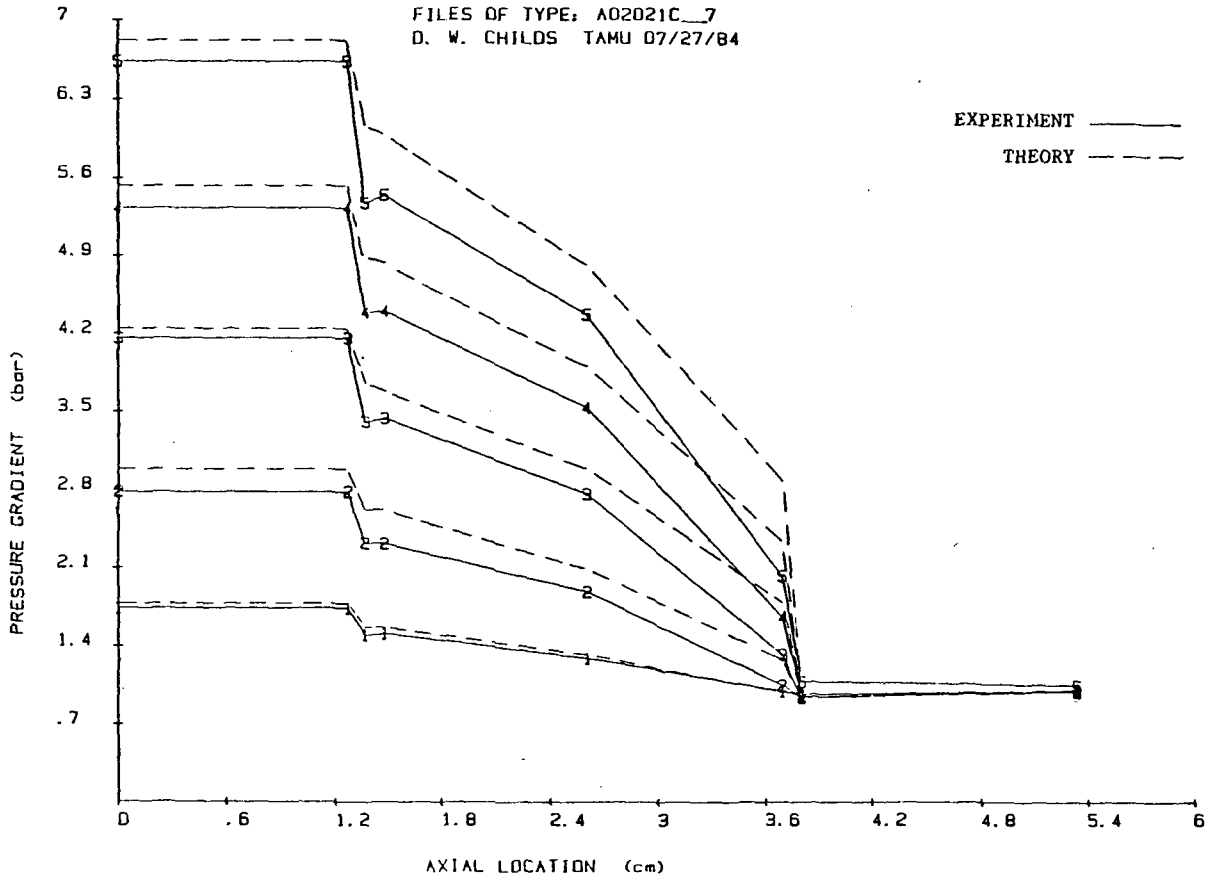

Fig. 28 Axial pressure gradient in honeycomb seal with prerotation opposing rotor rotation.

The entrance loss coefficient, $\bar{k}$, also may have some bearing on the upward shift seen in some of the pressure gradient plots. Plots of $(\bar{k}+1)$ versus axial Reynolds number are included in Figs. 29-34. Ten experimental curves, corresponding to running speed are plotted on each. Recalling Deissler's curve fit employed by Nelson and plotted in Fig.3, experimental results show loss terms $(\bar{k}+1)$ significantly higher than those predicted for both prerotated honeycomb seal cases. Agreement between theory and experiment is fairly good for the non-prerotated cases for both seals. For the smooth seal with prerotation in the direction of rotor rotation, the loss coefficient is overpredicted, with the experimental results indicating a negative $\bar{k}$.

Dynamic Results. Dynamic tests were performed at shaking frequencies of 58.8, 74.6, and 124.6 Hz. As was discussed in the Data Acquisition section of this report, these frequencies were chosen to provide the desired sample rate and a steady trigger signal. The dynamic coefficients obtained at the two lower frequencies are essentially the same. At the 124.6 Hz shaking frequency, however, correspondence of the data to that obtained at the lower frequencies is unsatisfactory. In seeking to explain the discrepancy, tests were run to determine the relative transfer function of the test apparatus. The plots in Fig. 35 show the results of these tests, and indicate a resonance of the apparatus occurring at approximately 25 Hz (the drop in phase difference at approximately 45 Hz corresponds to a resonance of the shaker support structure). As the shaking frequency is increased above this, the input force levels required to achieve a given motion amplitude increase rapidly. At the 124.6 Hz shaking frequency, attainable motion amplitude is about 50% of that achieved at the

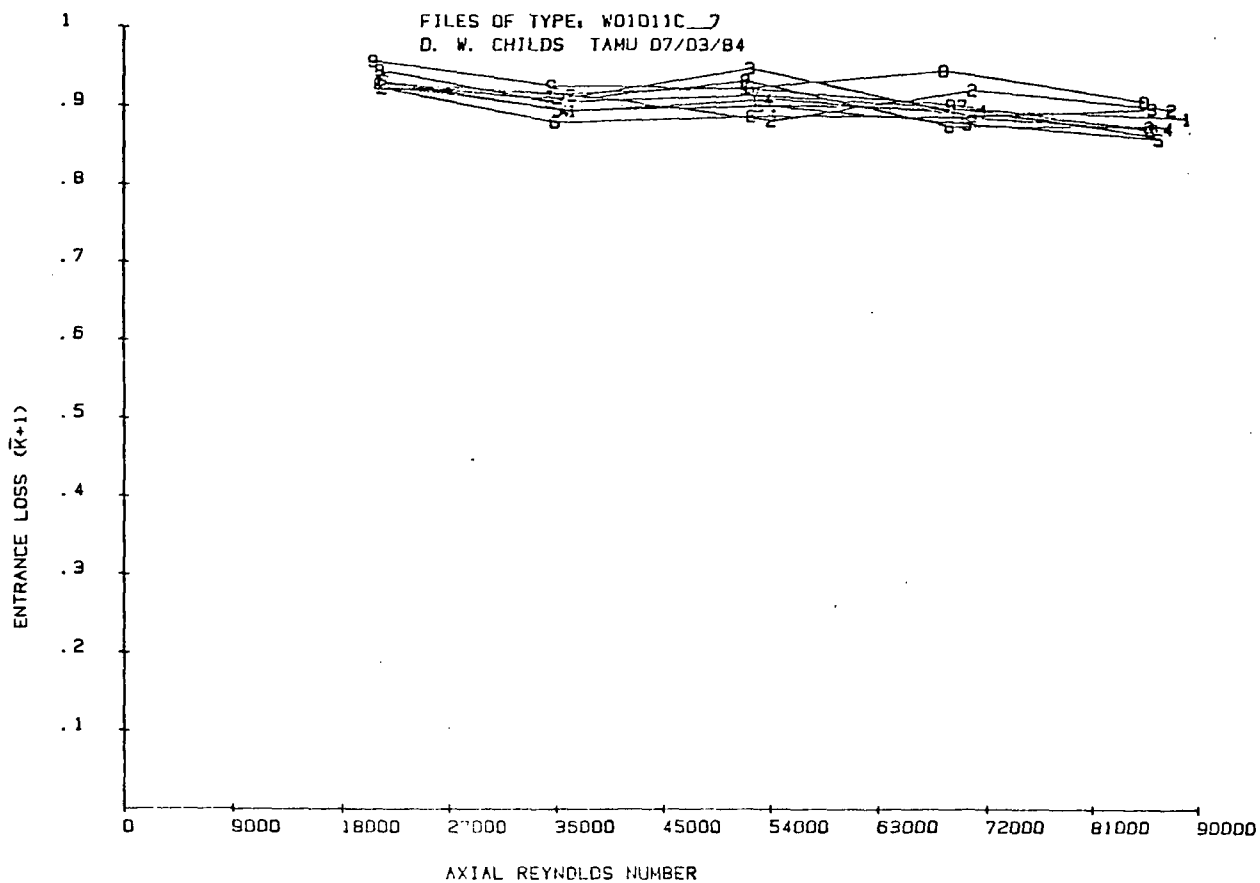

Fig. 29 Entrance-loss for smooth seal, prerotation in direction of rotor rotation.

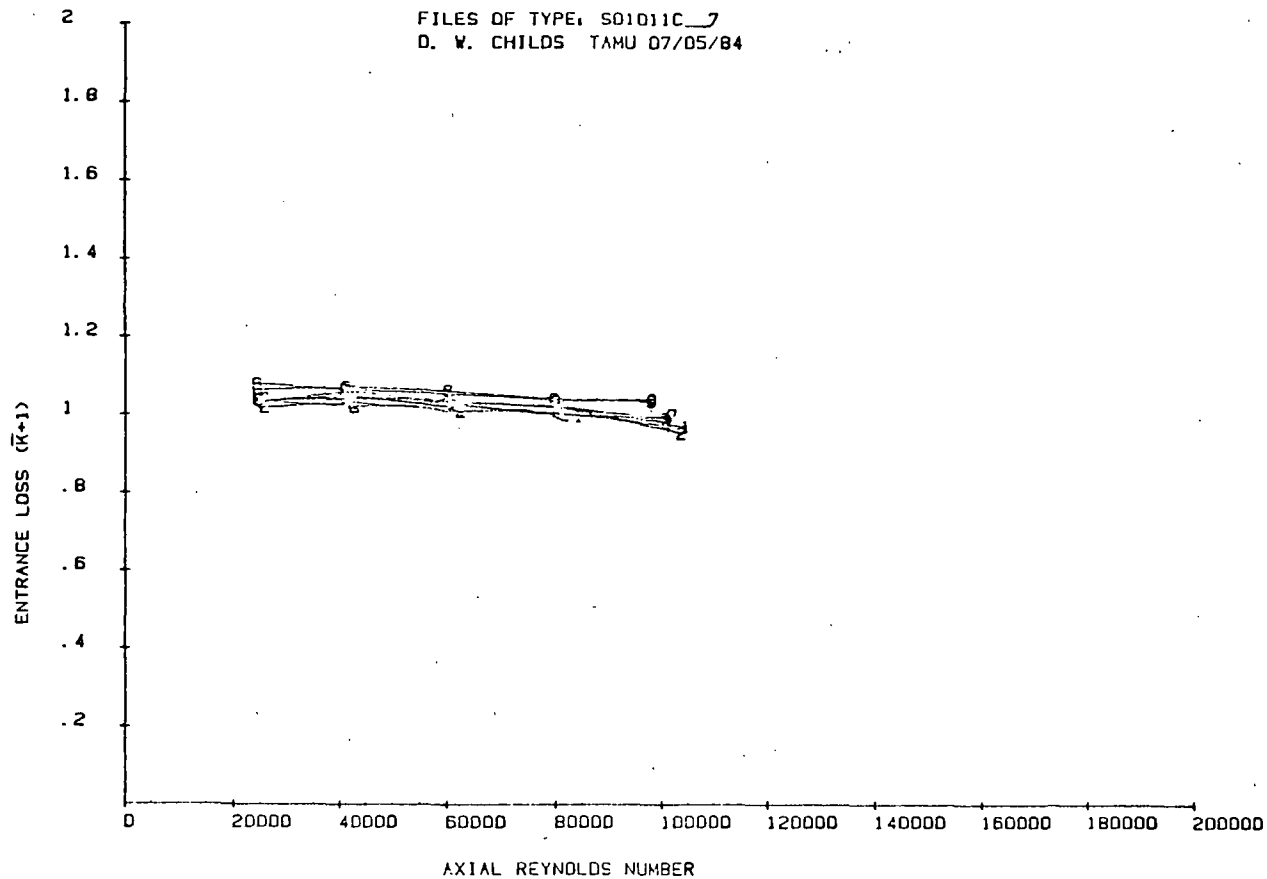

Fig. 30 Entrance-loss for smooth seal, no prerotation.

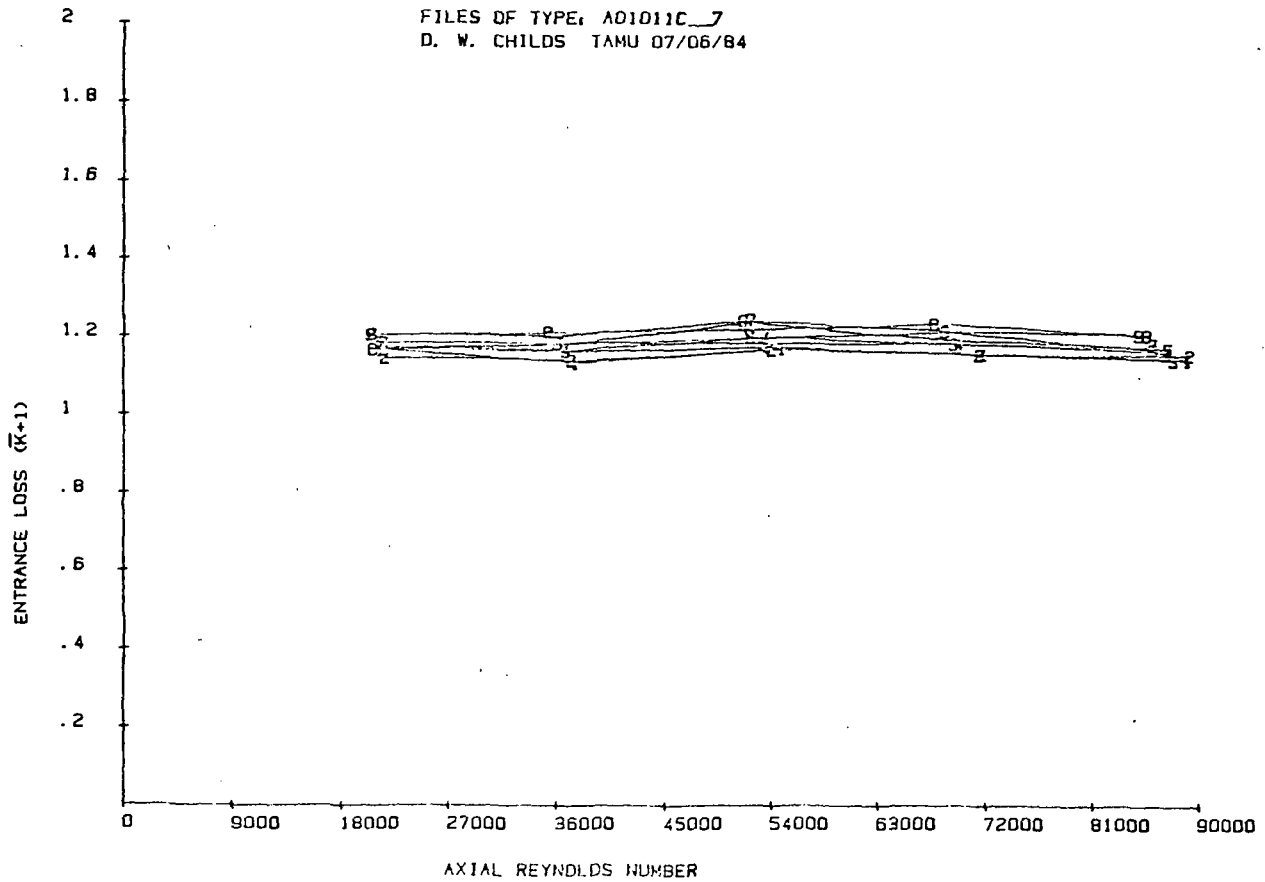

Fig. 31 Entrance-loss for smooth seal, prerotation opposing rotation.

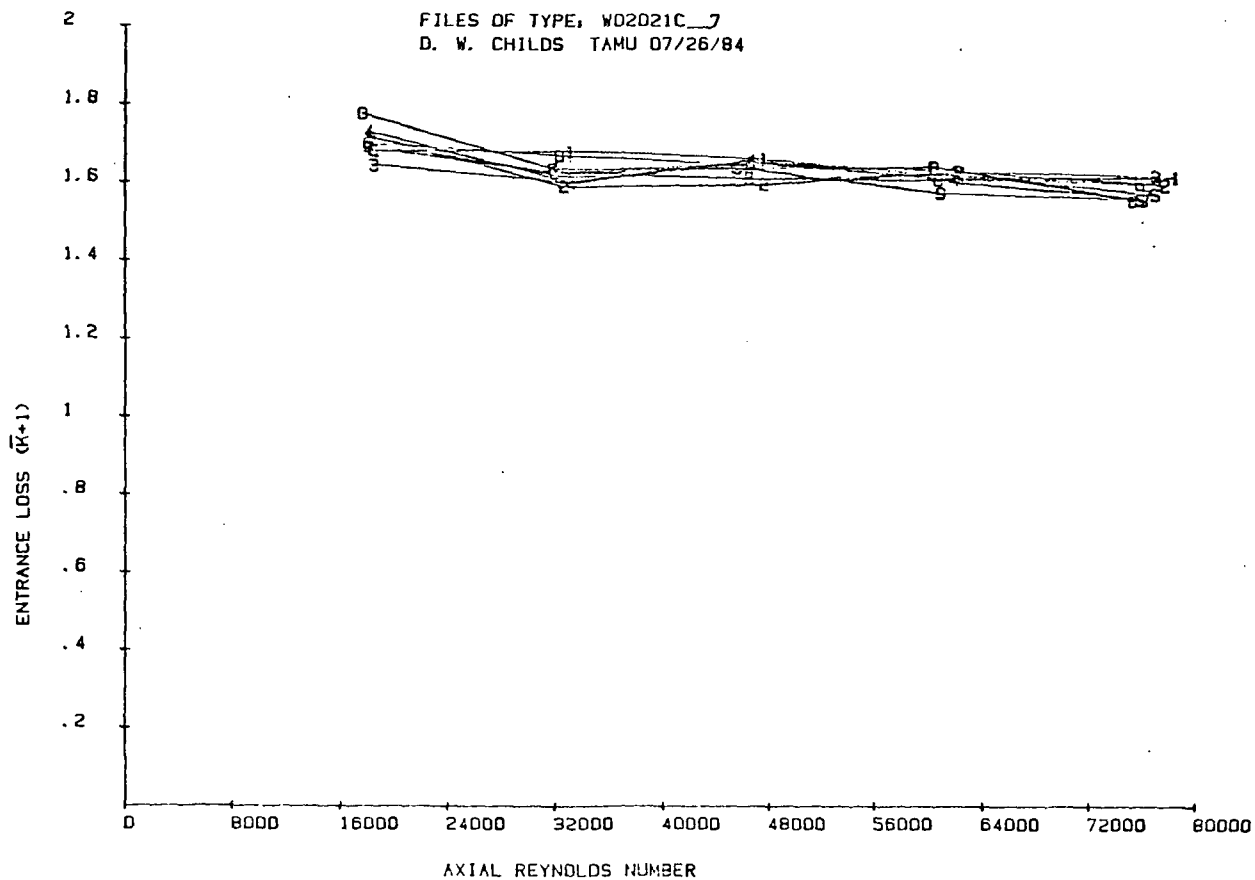

Fig.32 Entrance-loss for honeycomb seal, prerotation in direction of rotor rotation.

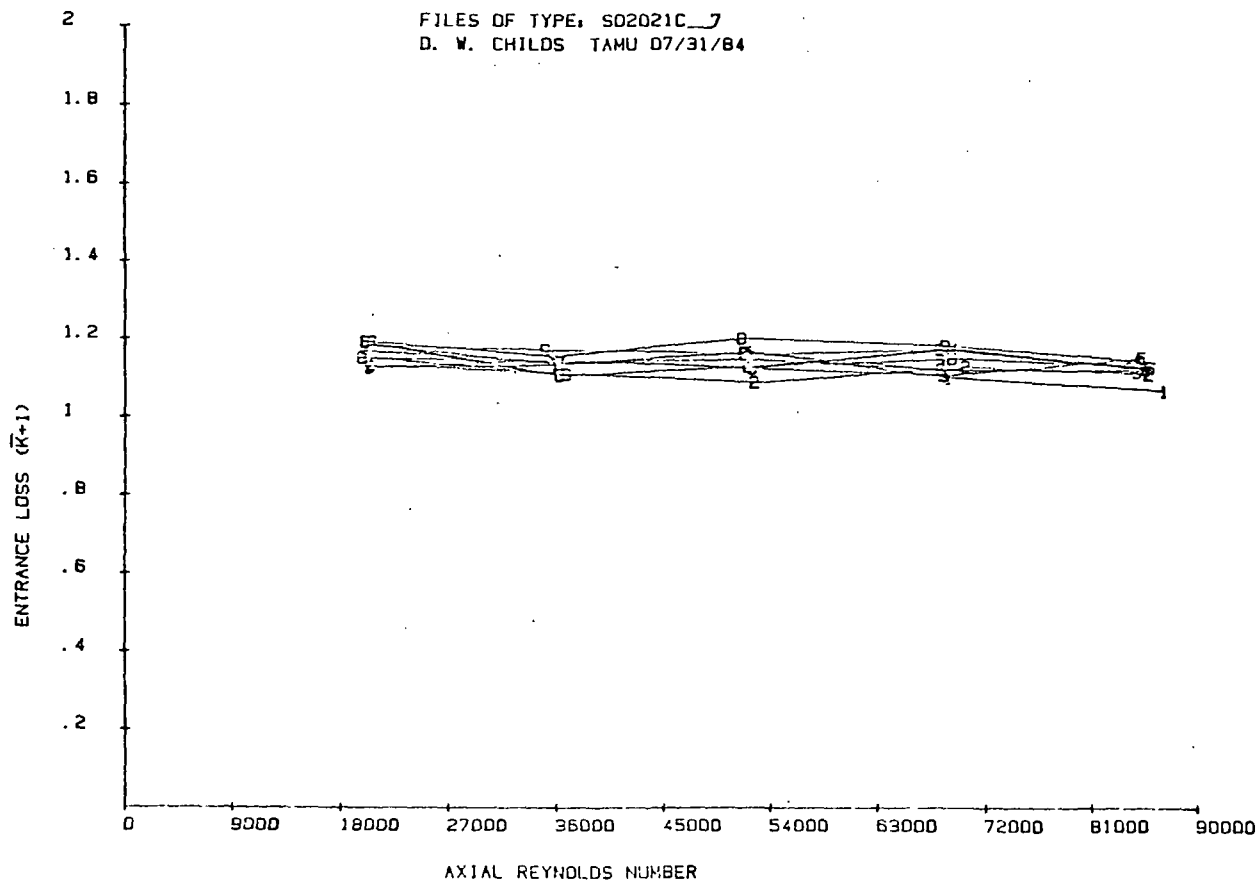

Fig. 33 Entrance-loss for honeycomb seal, no prerotation.

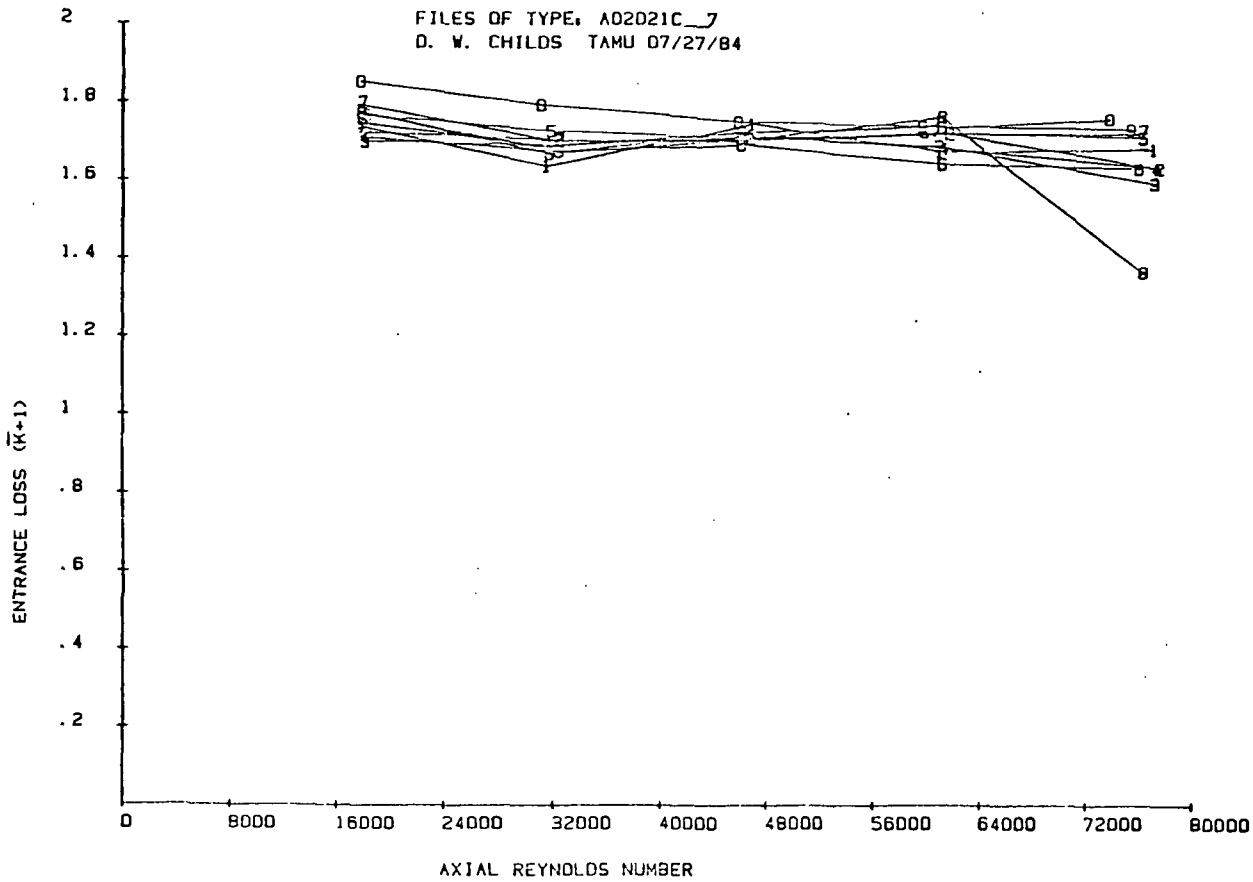

Fig. 34 Entrance-loss for honeycomb seal, prerotation opposing rotor rotation.

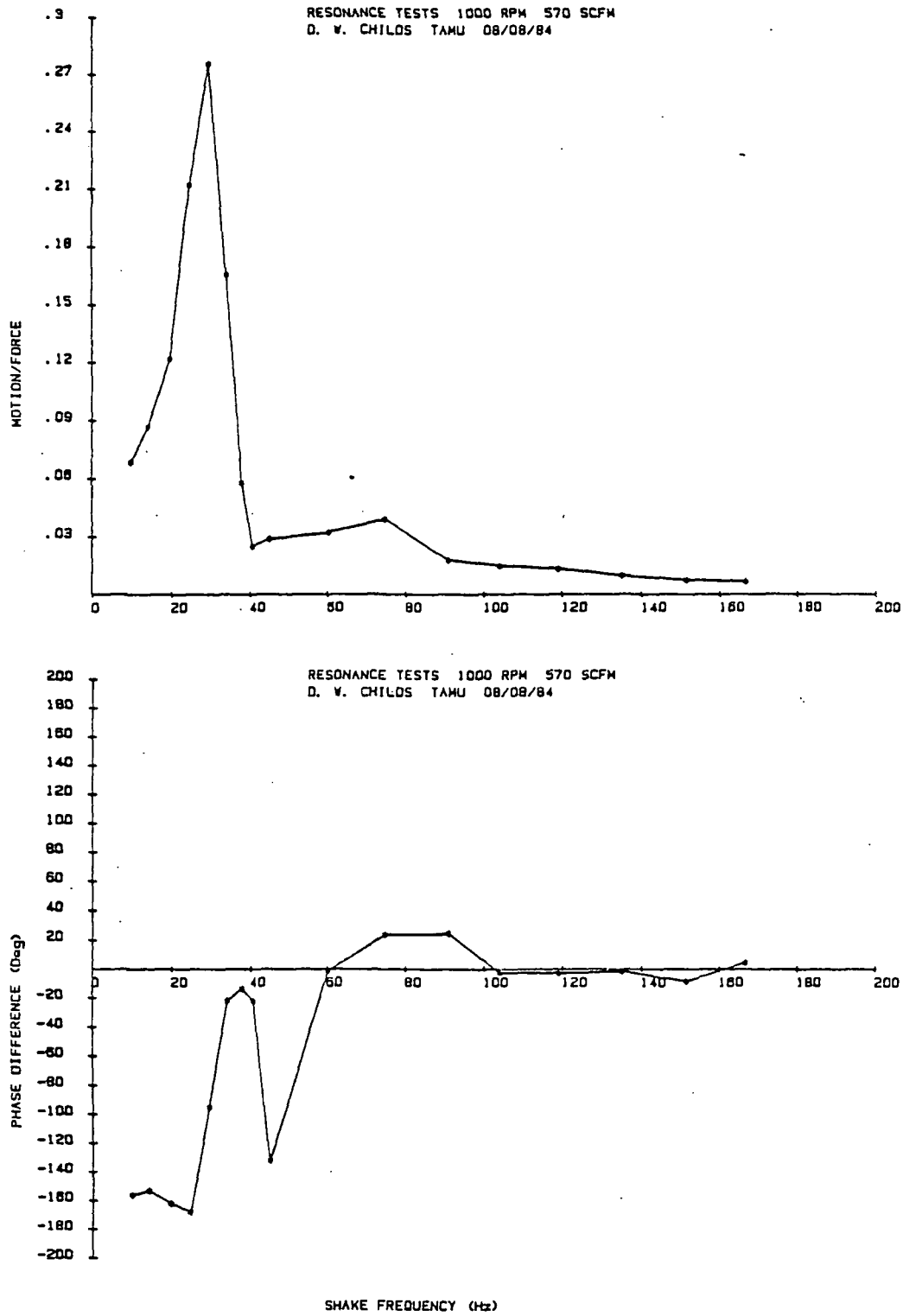

Fig. 35 Relative transfer function of test apparatus.

58.8 and 74.6 Hz frequencies. Therefore, one possible explanation for the poor agreement between the results is that as motion amplitude decreases, so does the force measured by the load cells, and the measurement system resolution suffers.

The plots of the rotordynamic coefficients are found in Figs. 36-43. These plots include both the theoretical and experimental data. The coefficients are plotted versus the reservoir / sump pressure ratio, and the solid lines correspond to the theoretical data. The experimental results are indicated by symbols. The location of the symbols represents the average value of the coefficient (averaged over all of the running speeds) at each particular inlet pressure condition, and the vertical lines drawn through the symbols signify the range over which they varied through the speed range. The test results plotted here were obtained by shaking the rotor with an amplitude of seven mils at 74.6 Hz.

Dynamic Results - Smooth Seal. For the smooth seal, direct stiffness (Fig.36) is overpredicted for the non-prerotated condition, and underpredicted for both prerotated conditions. Best agreement is seen in the case for prerotation opposite rotor rotation, and the trend of increasing stiffness with increasing pressure ratio compares favorably.

In the cross-coupled stiffness comparison for the smooth seal (Fig. 37), theory overpredicts for both prerotation conditions, and underpredicts for the straight flow case. In every instance, agreement becomes worse with increasing pressure ratio. The non-prerotated case shows a divergence both in magnitude and sign. It should be noted, however, that the magnitudes for this case are significantly smaller than for either of the prerotated cases.

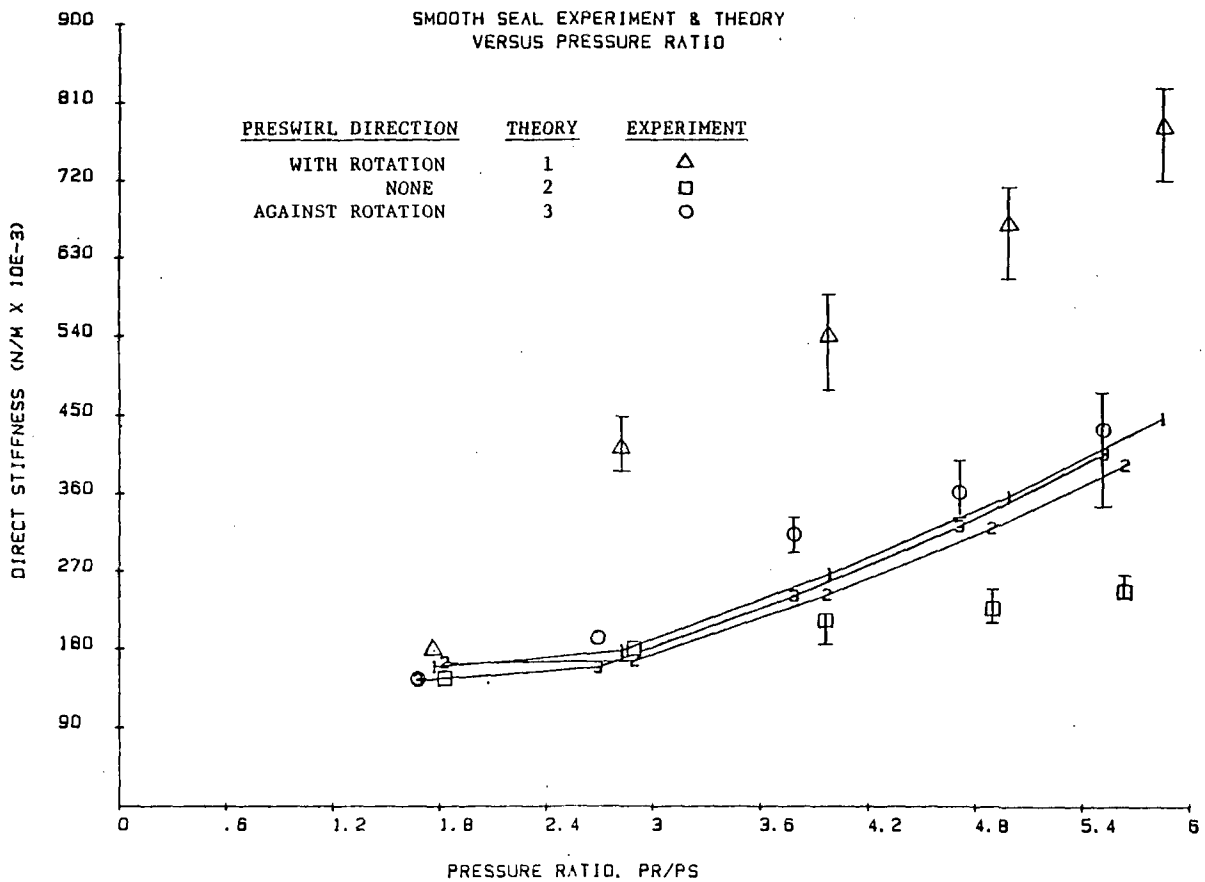

Fig. 36 Direct stiffness of smooth seal.

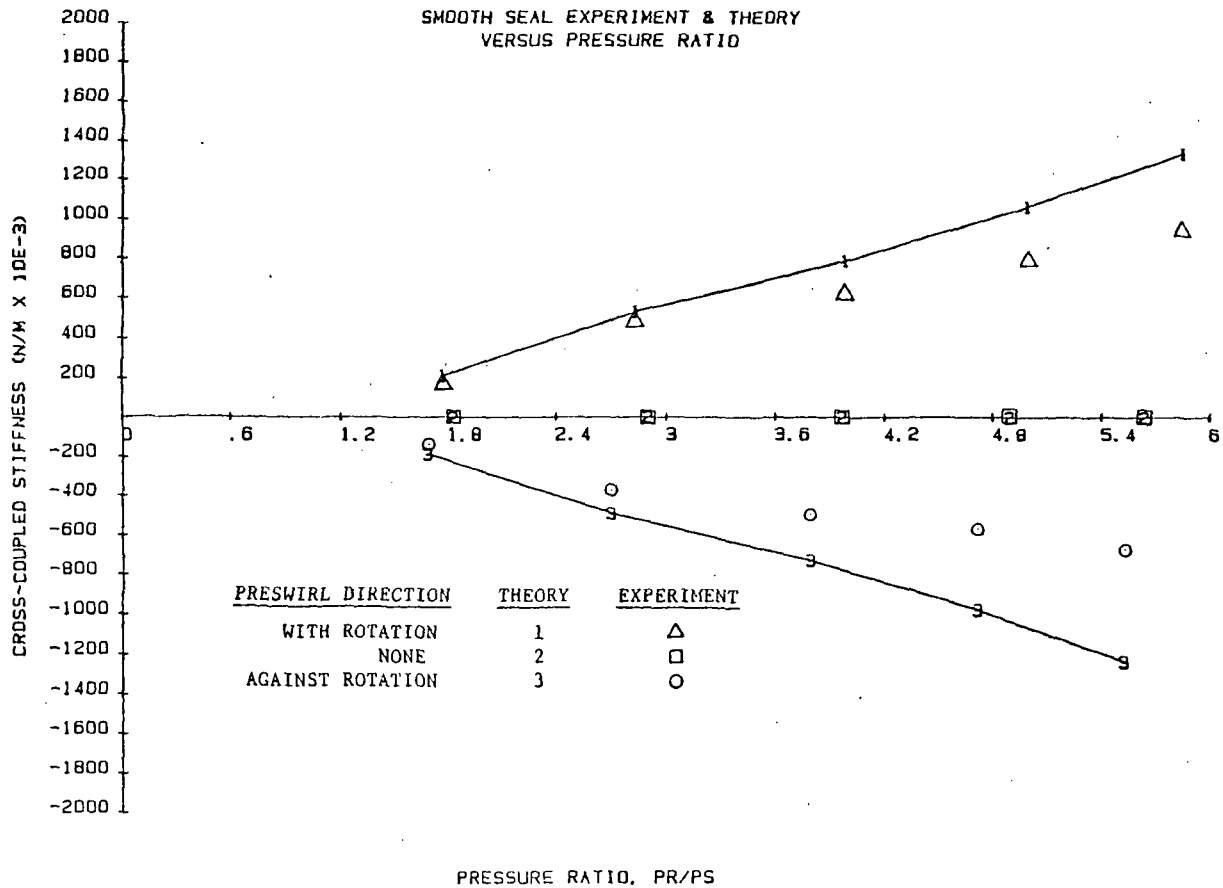

Fig. 37 Cross-coupled stiffness of smooth seal.

Agreement between theory and experiment for direct damping (Fig.38) is the most favorable of all the dynamic coefficients. Direct damping for the smooth seal shows an increase for increasing pressure ratio across the seal, with theory overpredicting slightly for the case of prerotation in the direction of rotor rotation. For the other prerotation conditions, the direct damping is slightly overpredicted at higher pressure ratios.

Cross-coupled damping (Fig.39) for the smooth seal generally shows agreement in the trends for the theoretical and experimental results. For prerotation in and opposing the direction of rotor rotation, the theory underpredicts cross-coupled damping magnitude by approximately 50%, but shows a sign consistent with the test data. For the non-prerotated case, the theory predicts coefficients so small as to be considered negligible. This is not inconsistent with the test results, however, as the magnitudes for this case are significantly smaller than for either prerotated case.

Dynamic Results - Honeycomb Seal. The honeycomb seal data, in general, shows the same correspondence between theory and experiment as the smooth seal. A notable exception, however, is in the direct stiffness coefficient (Fig.40). For both prerotated cases, the predicted stiffness decreases with increasing pressure ratio, while the measured stiffnesses increase. This same predicted decreasing trend is shown for the non-prerotated case at the lower pressure ratios.

In the cross-coupled stiffness comparison (Fig.41), the theory underpredicts the magnitudes, but correctly predicts the signs of the coefficients. For the non-prerotated case, the predicted stiffnesses are essentially zero. The relative magnitudes of the experimental

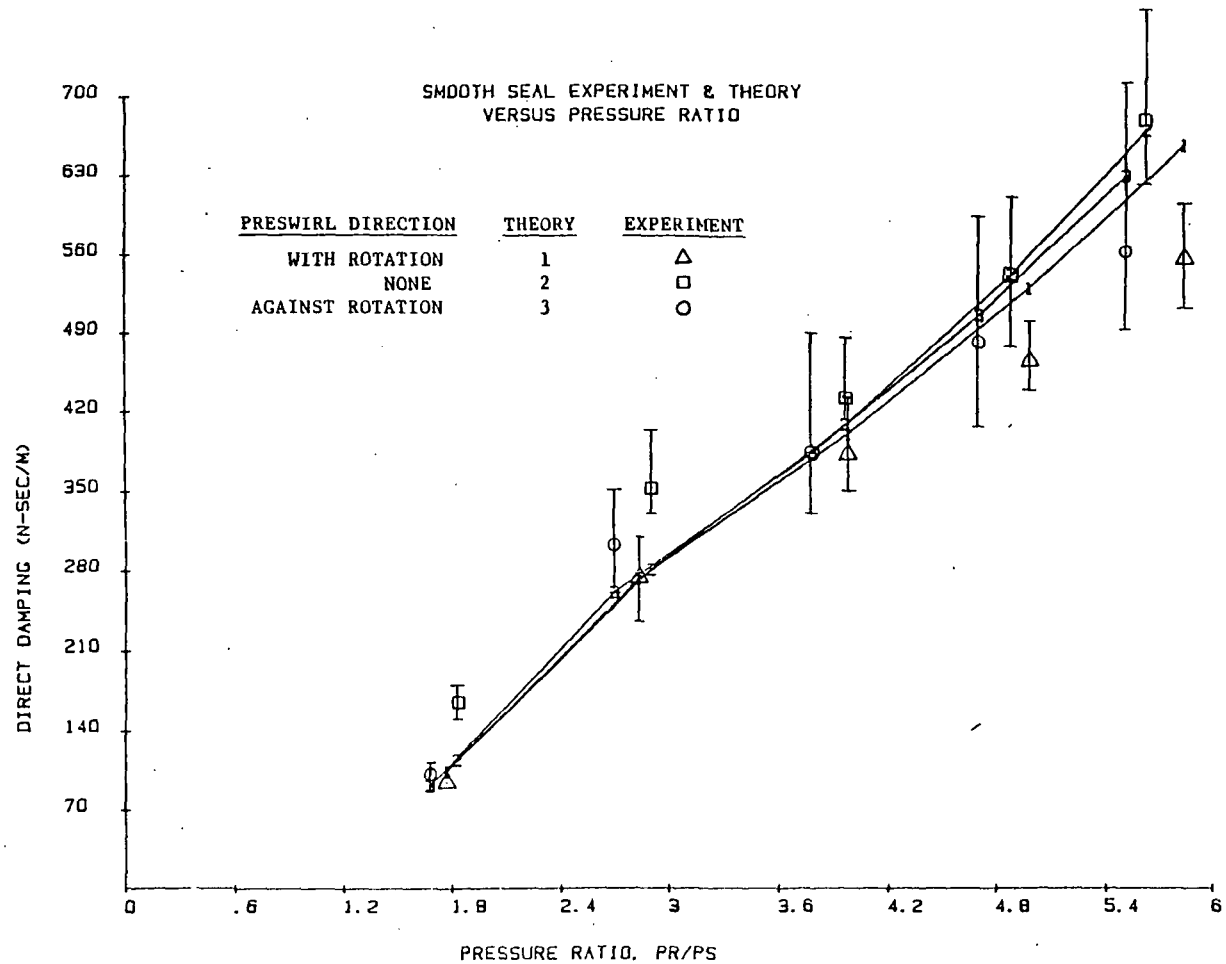

Fig. 38 Direct damping of smooth seal.

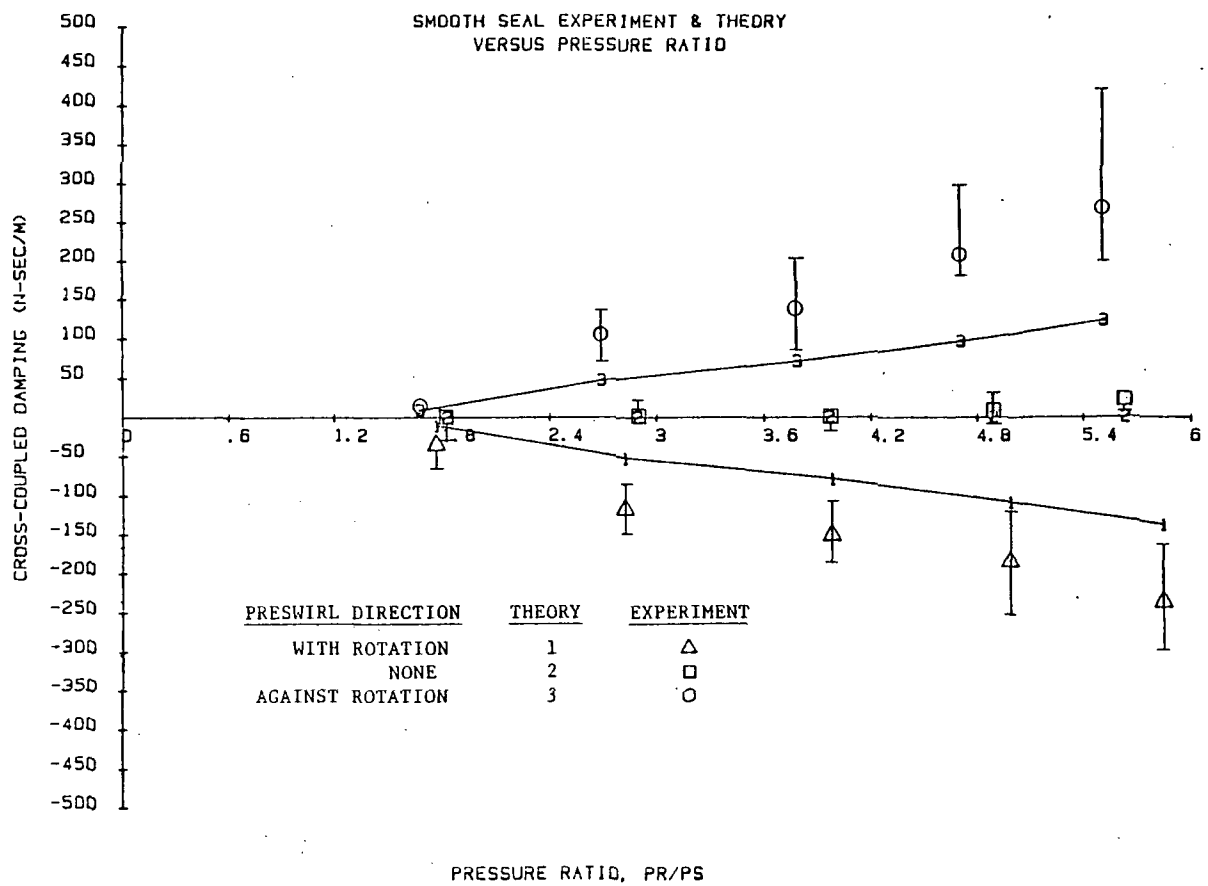

Fig.39 Cross-coupled damping of smooth seal.

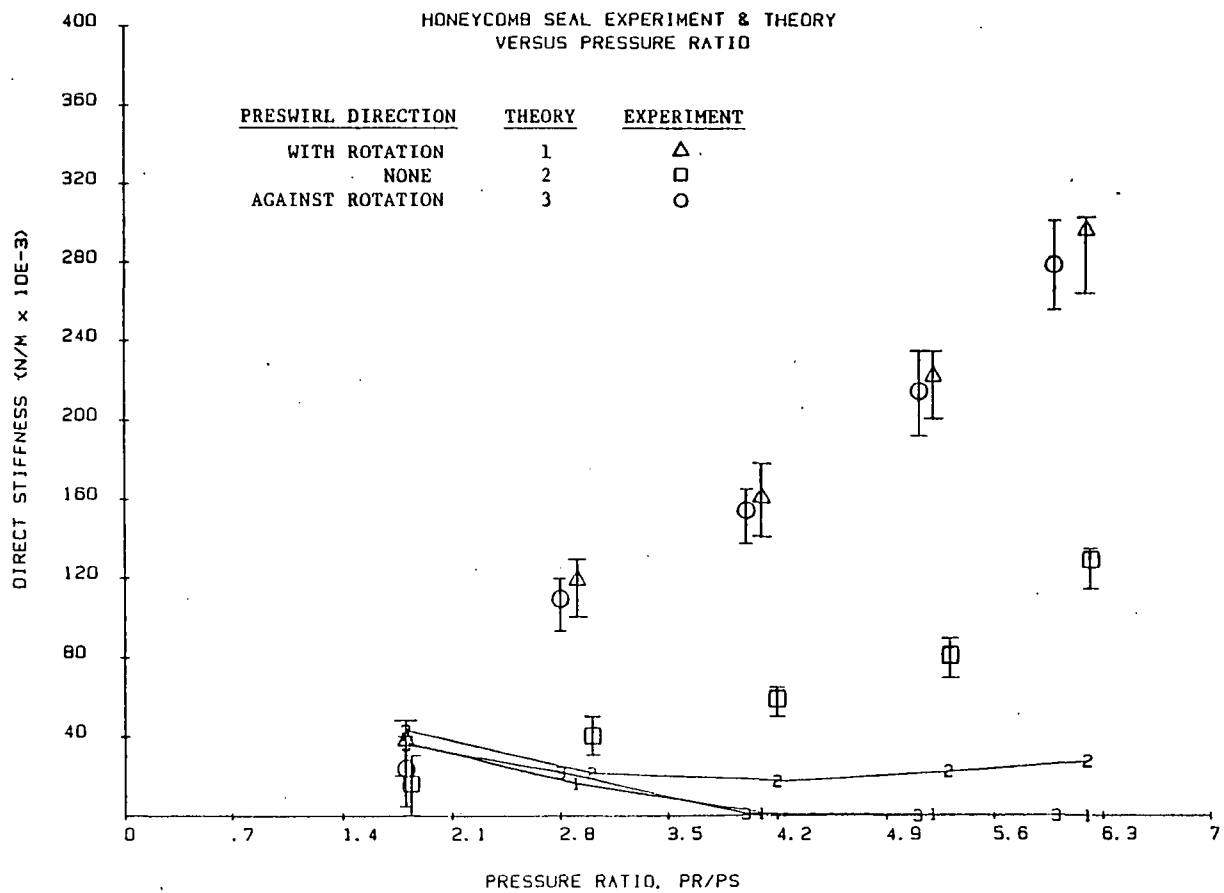

Fig. 40 Direct stiffness of honeycomb seal.

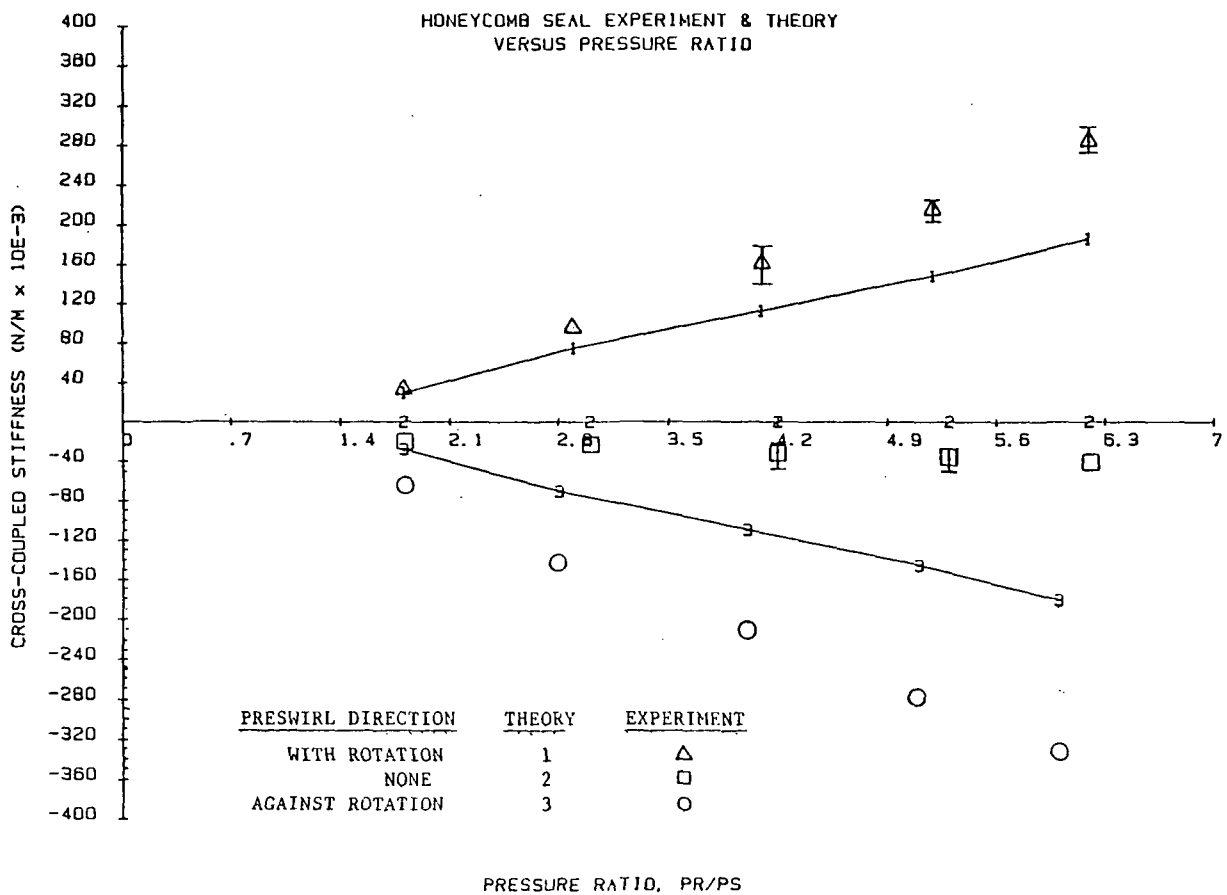

Fig. 41 Cross-coupled stiffness of honeycomb seal.

results for this same case in comparison to either prerotated case are also quite small, however. For prerotation in the direction of rotor rotation, theoretical cross-coupled stiffnesses are approximately 25% less than experimental ones. For counter prerotation, theory underpredicts by about 50%.

With the exception of the non-prerotated case, agreement between theory and experiment is fairly good for the direct damping coefficients (Fig.42) of the honeycomb seal. In the non-prerotated case, theory underpredicts the coefficients by approximately 46%. The prerotated cases show agreement to within approximately 10%.

Theoretical results for the cross-coupled damping coefficients (Fig.43) of the honeycomb seal are small enough to be considered negligible. In every case, the theory underpredicts the coefficients by a wide margin. However, the trend of increasing magnitude with increasing pressure ratio, as well as the signs of the coefficients, agree.

One method in which the dynamic coefficients of the smooth and honeycomb seals can be directly compared is through their respective non-dimensional whirl frequency ratios. Whirl frequency ratio is defined

$$\text{Whirl frequency ratio} = k / C\Omega ,$$

where Ω is the shaking frequency. This ratio is a measure of the destabilizing influence of the cross-coupled stiffness with respect to the stabilizing influence of direct damping. Plots of whirl frequency ratio versus running speed are included in Fig.44. The smooth seal plot shows a small, positive whirl frequency ratio over most of the running speed range. The honeycomb seal plot, however, shows a negative whirl frequency ratio. The negative sign arises due to a

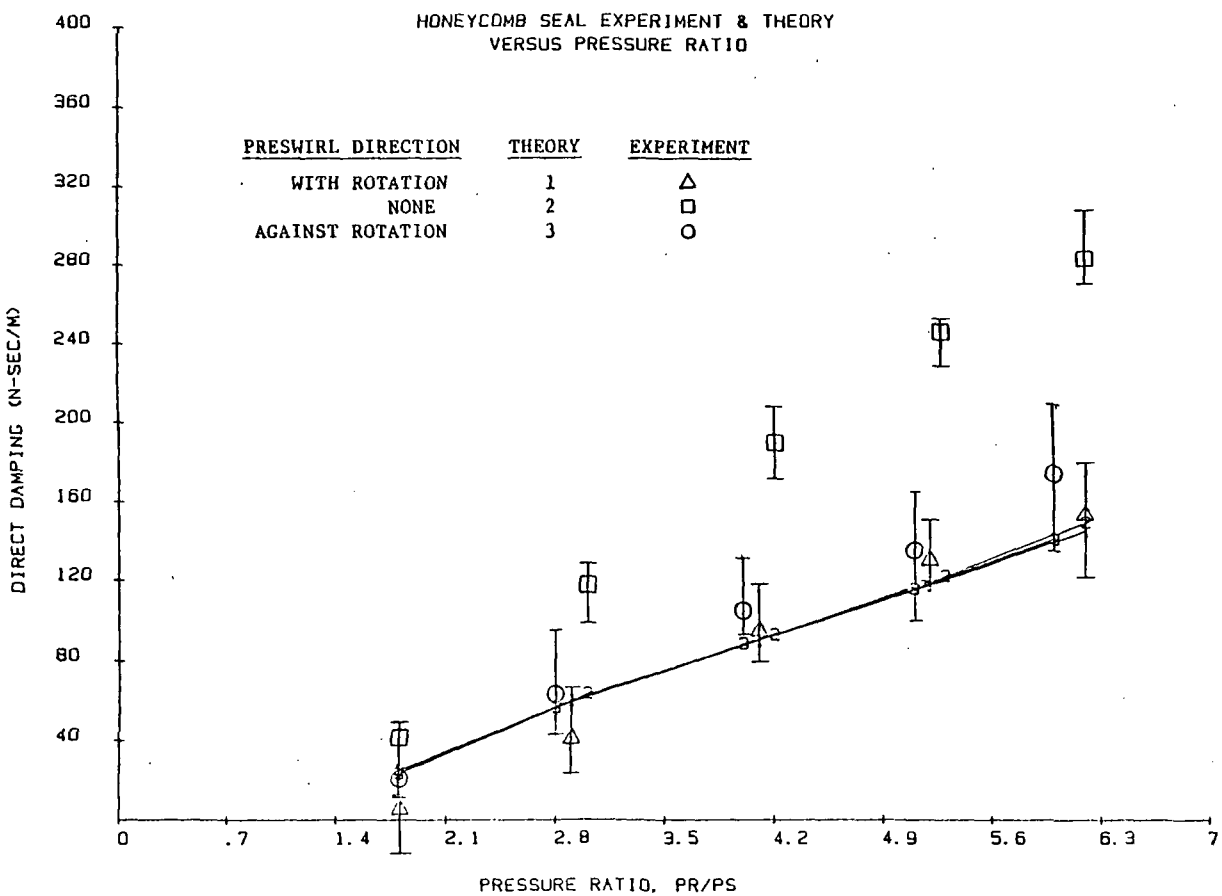

Fig. 42 Direct damping of honeycomb seal.

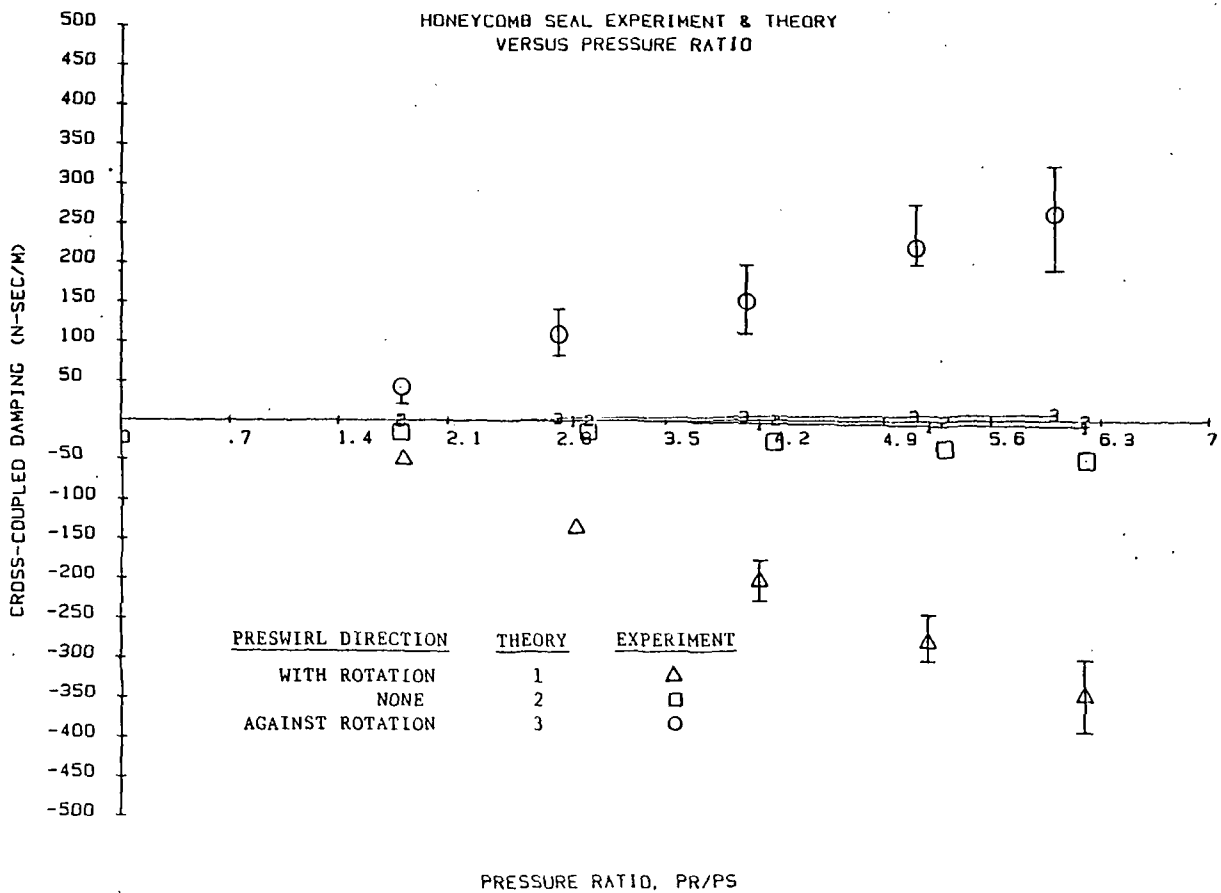

Fig. 43 Cross-coupled damping of honeycomb seal.

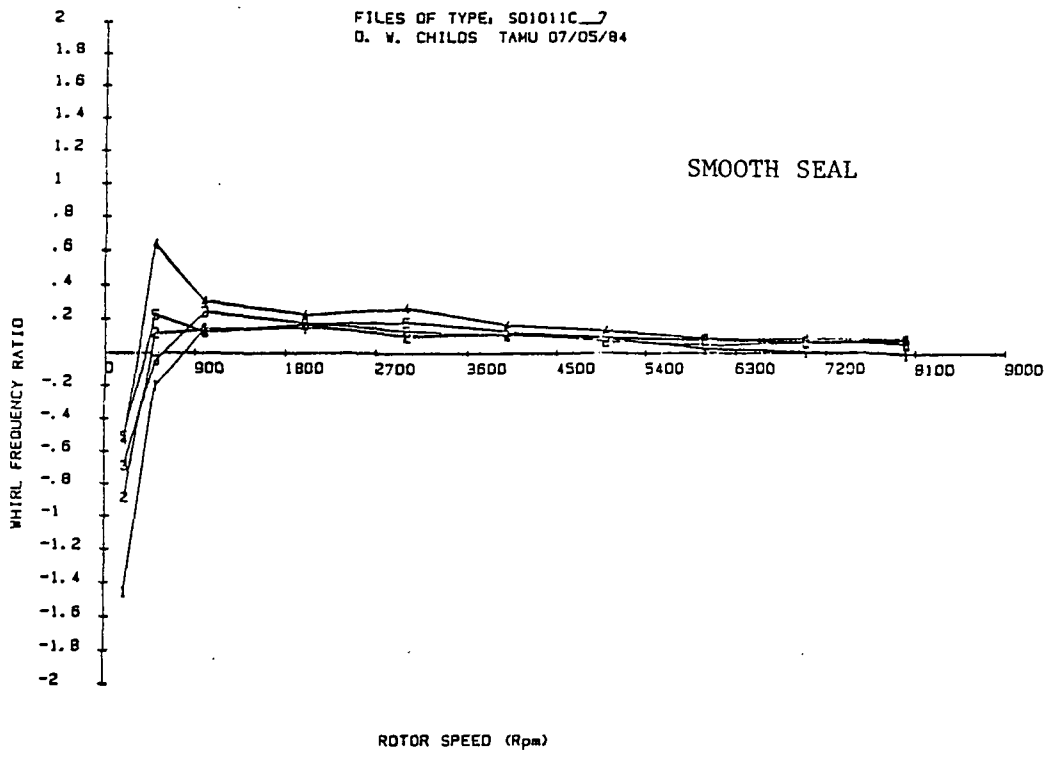

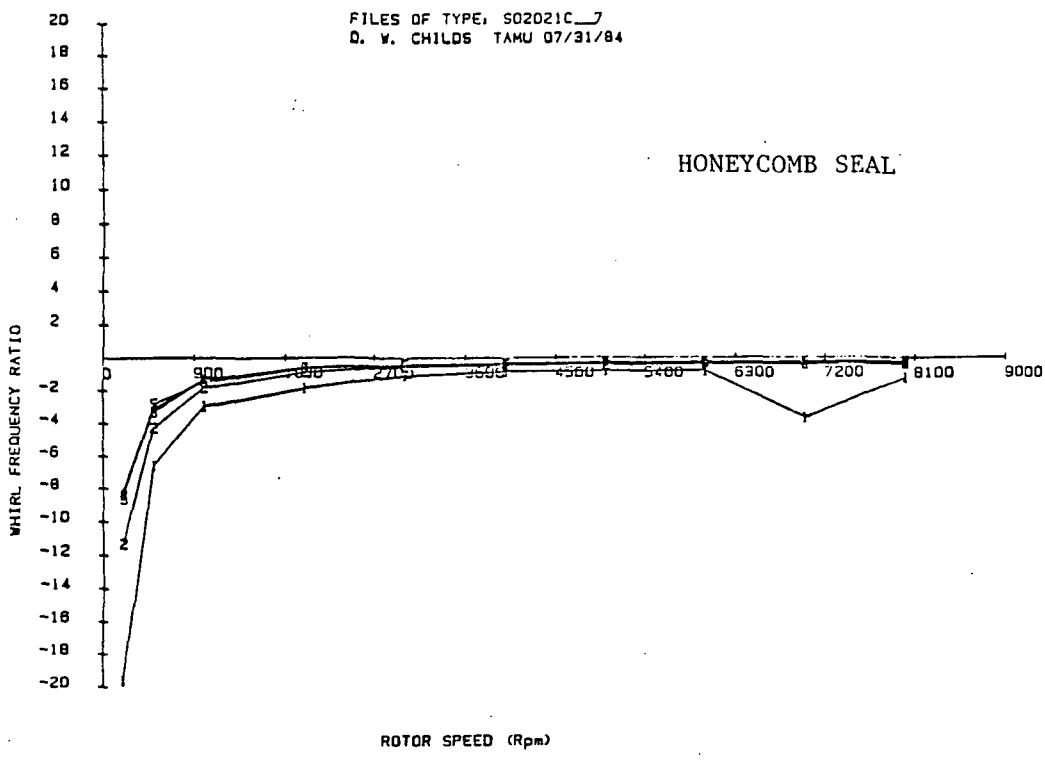

Fig. 44 Whirl frequency ratio for smooth and honeycomb seals.

negative cross-coupled stiffness. This negative k exerts a stabilizing influence, resulting in a force which acts in the same direction as the direct damping force.

CONCLUSIONS

A seal-test facility has been developed for the study of various types of gas seals. A method of determining rotordynamic coefficients has been established, and consistent, repeatable results have been obtained. After some initial failures in the test apparatus, reliability has been satisfactory, and a complete set of experimental results can be acquired in a matter of days.

The experimental and theoretical results of the preceding section support the following conclusions:

(a) Theoretical results for leakage are consistent with test results. Slightly higher leakage occurs for cases where the flow is not prerotated. Agreement between theory and experiment is satisfactory, with a maximum error of approximately 7.5%.

(b) Experimental and theoretical results for the pressure distributions and entrance-loss coefficients are relatively insensitive to running speed for the ranges (0-8500 cpm) and seals tested to date.

(c) The entrance-loss relationship (Deissler [13]) employed by Nelson is inconsistent with the test results for cases where the fluid is prerotated. For all such cases except one, the entrance-loss coefficient is underpredicted.

(d) In the test results for the honeycomb seal, the steep entrance pressure-loss seems to extend partially inside the seal. Also, the measured pressure at the exit of the seal generally equals the back pressure, rather than being greater, as is predicted by compressible flow theory for choked flow. These same phenomena do not occur for the smooth seal, implying that perhaps the effective length of the honeycomb

seal is less than its actual physical length.

(e) Test results for the direct stiffness of both the smooth and honeycomb seals show much greater sensitivity to fluid prerotation than predicted by theory. Prerotation of the fluid (in either direction) results in measured direct stiffnesses which are significantly larger than for no prerotation. Theory predicts the direct stiffness to be relatively insensitive to fluid prerotation.

(f) Theoretical predictions of the influence of fluid prerotation on cross-coupled stiffness and damping are consistent with the test results. In general, theory underpredicts the magnitudes of these cross-coupled coefficients, while correctly predicting their trends with respect to prerotation.

(g) Agreement between theory and test results for the direct damping coefficients is favorable. For both the smooth and honeycomb seal, direct damping is largest for no fluid prerotation.

(h) Over the speed range tested, none of the rotordynamic coefficients show appreciable sensitivity to the rotational speed of the rotor. This may be due to the lack of development of significant shear forces in the seal. It appears that running speeds above those attained to date may be necessary to produce significant shear force effects.

(i) For the non-prerotated case, the smooth seal has a positive cross-coupled stiffness, while k for the honeycomb seal is negative. This negative cross-coupled stiffness, and hence negative whirl ratio, indicates that the stability performance of the honeycomb seal is more favorable than that of the smooth seal.

REFERENCES

1 Black, H.F., and Jenssen, D.N., "Dynamic Hybrid Properties of Annular Pressure Seals," Proc. J. Mech. Engin., Vol. 184, pp. 92-100, 1970.

2 Jenssen,D.N., "Dynamics of Rotor Systems Embodying High-Pressure Ring Seals," Ph.D. dissertation, Herriot-Watt Univ., Edinburgh, Scotland, July 1970.

3 Black, H.F., and Jenssen, D.N., "Effects of High-Pressure Ring Seals on Pump Rotor Vibrations," ASME Paper No. 71-WA/FF-38, 1971.

4 Childs, D.W., "The Space Shuttle Main Engine High-Pressure Fuel Turbopump Rotordynamic Instability Problem," ASME Trans. J. of Engineering for Power, pp. 48-57, Jan. 1978.

5 Childs, D.W., and Moyer, D.S., "Vibration Characteristics of the HPOTP (High-Pressure Oxygen Turbopump) of the SSME ("Space Shuttle Main Engine)," ASME Paper No. 84-GT-31, 29th International Gas Turbine Conference and Exhibit, Amsterdam, 1984.

6 Black, H.F., Allaire, P.E., and Barrett, L.E., "The Effect of Inlet Flow Swirl on the Dynamic Coefficients of High-Pressure Annular Clearance Seals," Ninth International Conference in Fluid Sealing, BHRA Fluid Engineering, Leeuwonhorst, The Netherlands, Apr. 1981.

7 Childs, D.W., "Finite-Length Solutions for Rotordynamic Coefficients of Turbulent Annular Seals," ASME J. of Lubrication Technology, Vol. 105, pp.437-444, July 1983.

8 Hirs, G.G., "A Bulk-Flow Theory for Turbulence in Lubricant Films," ASME Journal of Lubrication Technology, Vol. 95, pp. 137-146, April 1973.

9 Fleming, D.P., "Stiffness of Straight and Tapered Annular Gas Path Seals," ASME Journal of Lubrication Technology, Vol. 101,pp. 349-355, July 1979.

10 Fleming, D.P., "Damping in Ring Seals for Compressible Fluids," NASA CP 2133, Rotordynamic Instability Problems in High-Performance Turbomachinery, proceedings of a workshop held at Texas A&M University, 12-14 May 1980, pp.169-188, 1980.

11 Nelson, C.C., "Rotordynamic Coefficients for Compressible Flow in Tapered Annular Seals," Mechanical Engineering Dept., Texas A&M University.

12 Nelson, C.C., "Analysis for Leakage and Rotordynamic Coefficients of Surface-Roughened Tapered Annular Gas Seals," ASME Paper No. 84-GT-32, 1984. Texas A&M University.

13 Deissler, R.G., "Analysis of Turbulent Heat Transfer and Flow in the Entrance Regions of Smooth Passages," NACA TN 3016, 1953.

14 Benckert, H., and Wachter, J., "Flow Induced Spring Coefficients of Labyrinth Seals for Application in Rotor Dynamics," NASA CP 2133, Rotordynamic Instability Problems in High-Performance Turbomachinery, proceedings of a workshop held at Texas A&M University, 12-14 May 1980.

15 Childs, D.W., and Dressman, J.B., "Testing of Turbulent Seals for Rotordynamic Coefficients," NASA CP 2250, Rotordynamic Instability Problems in High-Performance Turbomachinery, proceedings of a workshop held at Texas A&M University, 10-12 May 1982.

16 Chameih, D.S., Acosta,A.J., Brennen, C.E., Caughey, T.K., and Franz, R., "Experimental Measurement of Hydrodynamic Stiffness Matrices for a Centrifugal Pump Impeller," NASA CP 2250, Rotordynamic Instability Problems in High-Performance Turbomachinery, proceedings of a workshop held at Texas A&M University, 10-12 May 1982.

17 Shoji, H., and Ohashi, H., "Lateral Fluid Forces Acting on a Whirling Centrifugal Impeller in Vaneless and Vaned Diffuser," presented at the Third Workshop on Rotordynamic Instability Problems in High-Performance Turbomachinery, 28-30 May 1984.

18 Adams, M.L., and Makay, E., "Measurement of Interstage Fluid-Annulus Dynamical Properties," NASA CP 2250, Rotordynamic Instability Problems in High-Performance Turbomachinery, proceedings of a workshop held at Texas A&M University, 10-12 May 1982.

19 Iino, T., and Kaneko, H., "Hydraulic Forces Caused by Annular Pressure Seals in Centrifugal Pumps," NASA CP 2133, Rotordynamic Instability Problems in High-Performance Turbomachinery, proceedings of a workshop held at Texas A&M University, 12-14 May 1980.

20 Bowen, W.L., and Bhateje, R., "The Hollow Roller Bearing," ASME Paper No. 79-Lub-15, ASME-ASLE Lubrication Conference; Dayton, Ohio, 16-18 October 1979.

21 Cohen, H., Rogers, G.F.C., and Saravanamuttoo, H.I.H., Gas Turbine Theory, Longman Group Limited, 1972.

22 White, F.M., Fluid Mechanics, McGraw-Hill, 1979.

VITA

Name: Colby Oran Nicks

Permanent Address: 4501 Elm Branch Drive
Arlington, Texas 76017

Birthdate: 1/10/60

Higher Education: B.S., Mechanical Engineering, 1983,
Virginia Polytechnic Institute and State University